Development of functional nanoparticle-biomolecule conjugates based biosensors

Yue Zhang

Submitted in accordance with the requirements for the degree of
Doctor of Philosophy

The University of Leeds
School of Chemistry

July, 2013

The candidate confirms that the work submitted is his/her own, except where work which has formed part of jointly authored publications has been included. The contribution of the candidate and the other authors to this work has been explicitly indicated below. The candidate confirms that appropriate credit has been given within the thesis where reference has been made to the work of others.

Chapter 2 is based on work from the following jointly-authored publication:
Yue Zhang, Haiyan Zhang, Jeff Hollins, Michael E. Webb & Dejian Zhou, “Small-molecule ligands strongly affect the Förster resonance energy transfer between a quantum dot and a fluorescent protein”. *Phys. Chem. Chem. Phys.*, 2011, 13(43), 19427-19436.
Author contributions:
Yue Zhang (the candidate): performed all QD-Mcherry FRET experiments (except those outlined below), including static, and time-dependent FRET, QD characterisation, data analysis and drafting the paper.
Haiyan Zhang: provided small-ligand capped QDs.
Jeff Hollins and Michael E. Webb: provided His-tagged Mcherry protein and helped on FPLC analysis.
Dejian Zhou, designed and supervised the whole experiments

Chapter 3 is based on work from the following jointly-authored publication:
Yue Zhang & Dejian Zhou, "Magnetic particle-based ultrasensitive biosensors for diagnostics". *Expert Rev. Mol. Diagn.*, 2012, 12(6), 565-571.
Author contributions:
Yue Zhang (the candidate): drafted the review.
Dejian Zhou, modified and revised the review.

Chapter 5 is based on work from the following jointly-authored publication:
Yue Zhang, Yuan Guo, Philip Quirke, Dejian Zhou, “Ultrasensitive single-nucleotide polymorphism detection using target-recycled ligation, strand displacement and enzymatic amplification”. *Nanoscale*, 2013, 5(11), 5027-5035.
Author contributions:

Yue Zhang (the candidate): performed all the experiments including MNP synthesis and modification, DNA detection and SNP discrimination, data analysis and drafting the paper.
Yuan Guo, performed some relevant work which are not included in this paper and provided helps on designing the experiments.
Philip Quirke, provided some disease related mutant DNA samples.
Dejian Zhou, provided guidance on designing the sensing platform and supervised the whole experiments.

Acknowledgements

First and foremost, I would like to offer my gratitude to my primary supervisor Dr Dejian Zhou. Of the many things that I have learned from him, I hold in high regard his rigorous scholarship and passion for science. I would like to thank him for the academic guidance he provided, and for the insightful advice and help he offered to my future career.

I also want to thank my second supervisor Dr Terry Kee, my internal assessor Dr Julie Fisher and previous postgraduate tutor Prof. Andy Wilson for their comments and suggestions on my reports, PhD progression and future career planning. I would like to thank Mr Dave Fogarty for offering instruction and help on using fluorimeter and Dr Christopher Empson for the help and suggestions on using Envision plat reader. More importantly, I want to acknowledge the University of Leeds and China Scholarship Council for offering me scholarship.

I had the pleasure of interacting with many intelligent and friendly co-workers within the Zhou group. I would like to thank Dr Yuan Guo either in providing massive knowledge on biological aspect of my project and insightful guidance regarding the development of the magnetic nanoparticle-based biosensor. I would like to thank Ms Haiyan Zhang and Mr Lei song who offered me a lot of support and help both on research and daily life. I want to thank Mr Yifei Kong both for the insightful discussions in research and for company in conferences. Moreover, I would like to thank Mr Josep Garcia and Dr Chailermchai Pilapong with whom I co-developed the magnetic nanoparticle-based biocatalysts and biosensors. In addition, I want to say thank you to Dr Zhenlian Ling, Mr Weili Wang, Dr Shunlong Pan, Mr Xiaochuan He, Dr Lin Wu and Prof Guoqiang Feng for the help and advice they provided on my work and career planning. I also want to thank the research groups of Dr Michael Webb and Dr Bruce Turnbull for their help

and support. Especially, thanks to Dr Jeff Hollins for providing fluorescent proteins for my project and guidance for FPLC usage.

Thanks to my closest friends and house mates, who provided happy daily life and facilitated my PhD adventure, especially Feng Cheng, Zhengyang Ling, Leigang Cao, Wei Jiang, MingFu Guan. They not only provided an incredible opportunity for me to experience other academia but also made my stay in Leeds so enjoyable.

Last but not least, I would like to extend my deepest gratitude to my family: mum and dad, sister and her family for unwavering support through the whole PhD adventure. I could not have done it without your understanding and encouragement. Very special thanks to you!

Abstract

This thesis is composed of two parts: Part I is focused on studying how quantum dot (QD) surface small-molecule capping ligands affect its Förster resonance energy transfer (FRET) with a fluorescent protein (FP); Part II is focused on developing an ultrasensitve DNA sensing technology by combining magnetic nanoparticle (MNP) and enzymatic signal amplification.

Part I

The FRET between a CdSe/ZnS core/shell QD capped with three different small-molecule ligands and a hexa-histidine (His_6)-tagged FP (mCherry) has been studied. Results show that small-molecule ligands strongly affect the FRET behaviours between QD and FP. The QD-FP self-assembly process is fast (complete in minutes at low nM concentration), strong (with K_d ~ 1 nM), suggesting that the QD-His_6-tagged biomolecule self-assembly is an effective approach for making compact QD-bioconjugates which may have a wide range of sensing and biomedical applications.

PART II

I have developed a facile, rapid, and sensitive DNA sensor by combining the efficient MNP-based target capture with the highly efficient signal amplification power of enzymes to achieve ultra-sensitivity. This sensor works efficiently in both pure buffer and complex media (such as 10% human serum in buffer). Moreover, this developed approach is able to quantitate two distinct DNA strands in a homogenous phase at the same time with a detection limit of ~5 pM.

Second, I have developed a novel, highly sensitive and selective approach for label-free DNA detection and single-nucleotide polymorphism (SNP) discrimination by combining target-recycled ligation (TRL), MNP assisted target capture/ separation, and efficient enzymatic amplification. This

approach possesses a detection limit of 600 fM unlabelled DNA targets and offers exquisitely high discrimination ratio (up to > 380 fold) between a perfect-match mutant and its single-base mismatch DNA target. Furthermore, it can quantitate the rare cancer mutant in large excesses of coexisting wild-type DNA down to 0.75%.

Table of Contents

List of Tables

List of Figures

List of Abbreviations

Ab	antibody
ABTS	2,2'-azino-bis(3-ethylbenzothiazoline-6-sulphonic acid)
ALP	alkaline phosphatase
APTES	(3-aminopropyl)triethoxysilane
BSA	bovine serum albumin
CL	chemiluminescence
DAB	3,3-diaminobenzidine
DHLA	dihydrolipoic acid
DLS	dynamic light scattering
dsDNA	double stranded DNA
ECL	electrochemiluminescence
EDTA	ethylene Diamine Tetraacetic Acid
ELISA	enzyme linked immunosorbent assay
FAM	Fluorescein amidite
FDP	fluorescent diphosphate
FP	fluorescent protein
FRET	Förster (fluorescent) resonance energy transfer
GMR	giant magnetoresistive

GNP	gold nanoparticle
GSH	glutathione (tripeptide Glu-Cys-Gly)
HRP	horseradish peroxidase
LCR	ligation chain reaction
LOD	limit of detection
MBP	maltose binding protein
MMP	magnetic microparticle
MNP	magnetic nanoparticle
MP	magnetic particle
MPA	3-mercaptopropionic acid
MRS	magnetic relaxation switch
NAV	neutravidin
OG	Oregon Green fluorescent dye
PBS	phosphate-buffered saline PBS
PCR	polymerase chain reaction
PL	photoluminescence
QD	quantum dot
QY	quantum yield
RCA	rolling circle amplification
SM	single molecule
SNP	single-nucleotide polymorphism

SPR	surface plasmon resonance
ssDNA	single stranded DNA
TCCD	two-colour coincidence detection
TEM	transmission electron microscopy
TEOS	tetraethyl orthosilicate
TMB	tetramethylbenzidine
TOPO	trioctylphosphine oxide
TRL	target recycled ligation
VSM	vibrating sample magnetometer

Part I

Quantum dots (QDs) -based Fluorescent resonance energy transfer (FRET) studies

Chapter 1
Quantum dot (QD) based fluorescent techniques for biological applications

The investigation of many fundamental biological processes and disease diagnostics largely relies on the ability to detect biomolecule interactions and quantify small amount of disease biomarkers by some ultra-fast, sensitive, reliable and reproducible techniques. In this regard, fluorescence based techniques are well-suited to meet such requirements and challenges. Fluorescence analysis techniques encompass several unique experimental parameters such as excitation/emission wavelength, intensity, fluorescence lifetime and anisotropy).[1] Among which, Förster resonance energy transfer (FRET) is one of the most powerful techniques for biomolecule structure analysis[2], enzymatic activity assays[3-4], and biosensors[5-6].

Particularly, FRET analysis at single molecule (SM) level is leading a revolution in the real-time visualization and ultra-sensitive detection of biomarkers by providing previously unobtainable information on fundamental molecular processes. [2, 7-8] A unique advantage for SM fluorescence analysis is that it has the capabilities of detecting static conformational heterogeneity and dynamic conformational changes of single biological molecules that are not detectable at the bulk level both in solution and immobilized to surfaces.[9-11] In addition, SM fluorescence analysis also offers the possibility for ultrasensitive detection of low abundant species because it can probe single-fluorophore-labelled biomolecules in solution under biological conditions. In addition to FRET, two-colour coincidence detection (TCCD) is another favourite SM fluorescent approach which relies on coincidence event counting.[12-13]

In this chapter, the intrinsic properties of QD in comparison with organic dyes and/or fluorescent proteins (FPs) will be discussed first. Then several representative strategies for the preparation, modification and bioconjugation of QD will be introduced. Following on that, the principle and applications of FRET based on QDs will be illustrated. Then after discussion of the TCCD approach, an overview of the first part of my project will be discussed.

1.1 Distinct properties of QDs as fluorophores

In fluorescence spectroscopy, a fluorescent label, *i.e.* fluorophore, is of critical importance for fluorescence imaging or sensing applications. Fluorophore properties (such as size, stability, chemical and optical nature, and biocompatibility) could affect their detection limit and dynamic range, the reliability of the result for a particular target or event, and the suitability for parallel detection of different targets.[1]

When a fluorophore is attached to a biological molecule, it can send back a report about its host molecule in a stream of photons when excited. An ideal fluorophore should: (a) be easy to excite and detect with conventional instrumentation; (b) soluble in relevant buffers; (c) posses high fluorescence quantum yield (QY); (d) show steady emission and be reproducible; (e) be stable and not perturb the properties and conformation of the host molecule; (f) and maintain photo-activity over a sufficiently long time under relevant conditions.[1, 14]

The optical properties of organic dyes/ FP (Figure 1.1A) are determined by the inherent electronic transition(s) involved. Thus their optical properties are tunable *via* careful structural design, which can be done, but in practice this is often limited by synthetic capabilities and therefore difficult to achieve.[15] Generally speaking, conventional fluorophores (for instance, organic dyes, FPs, and fluorescent polymers) tend to have narrow excitation bands and broad emission spectra. Moreover, many conventional fluorophores have relatively low QYs. In addition, they can be sensitive to environmental changes, such as pH, temperature and local environmental hydrophobicity, and often liable to chemical and photo-degradations. [16]

QDs are fluorescent semiconductor nanocrystals with a size of ~ 1-10 nm. QDs have a number of unique attractive electronic and optical properties which deviate substantially and cannot be extrapolated from those of the bulk materials. These unique electronic and optical properties are determined not only by the constituent materials, but also particle size, and size distribution (dispersity), and surface chemistry and coating.[17]

Compared to organic dyes or FPs, QDs have several unique advantageous properties which make them well-suited for analytical and imaging applications.[18] By varying the nanocrystal size and composition, QDs' emission can cover a wide range of wavelengths, from the near UV to the near IR regions of the optical spectrum.[18-20] Besides, the emission spectrum of QDs is typically narrow and symmetric (see Figure 1.1B). Furthermore, QDs possess a broad absorption (excitation) which allows the simultaneous and efficient excitation of different coloured QDs with a single wavelength light source far from their respective emissions; this makes QDs excellently suited for multiplexing

applications. QDs are also extremely photostable and are hundreds of times more resistant to photobleaching than conventional organic fluorophores, making them extremely useful in long term bio-imaging, cell-tracking and trafficking applications. Additionally, QDs have a comparatively long fluorescence lifetime (typically 5 to 100 nanoseconds) which enables significant and selective reduction of the fluorescence background from cellular auto-fluorescence by using time-gated excitation measurement, thereby enhancing the sensitivity.[21]

QDs are considerably larger than organic dye molecules which can make them inefficient for FRET based applications (to be discussed in the section 1.3), especially at low target: QD copy number situations, because of the resulting large donor-acceptor distance. Their hydrodynamic radius (5 - 50 nm) could be affected by surface ligands which is dependent on a combination of factors, such as the inorganic core (or core-shell) dimension, shape, and the type of hydrophilic surface capping.[24] In comparison to organic dyes, the large surface area of QD can offer multiple binding sites so that several biomolecules could be simultaneously immobilized onto a single QD to increase the target: QD copy numbers (n) and improve the FRET efficiency for a single-donor-multiple acceptor FRET system. This offers significant advantages for applications where high FRET efficiency is required.[23]

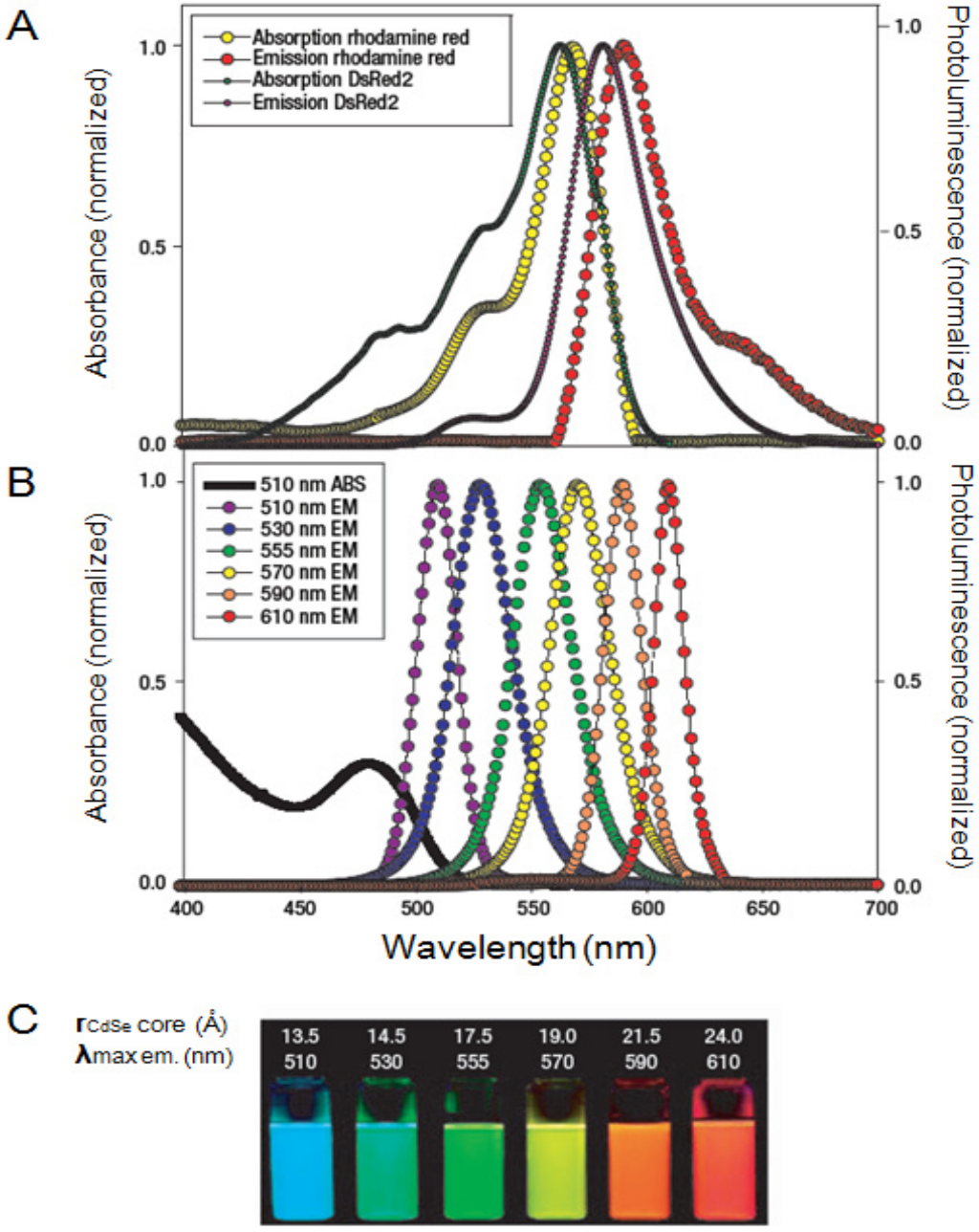

Figure 1.1 Comparison of absorption and emission spectra for different fluorophores and photo for different sized QDs.

Absorption (ABS) and Emission (EM) spectra for organic dyes (**A**, rhodamine red), genetically encoded FP (A, DsRed2)[22] and QDs (**B**, six different QD dispersions). **C**, Photo demonstrating the size-tunable fluorescence properties and emission spectral peak of the six QD dispersions plotted in B versus CdSe core size. All samples were excited at 365 nm with a UV source. (Reprinted by permission of the Nature Publishing Group)[23]

1.2 Preparation, modification and bioconjugation of QD

The synthesis of monodisperse QDs, such as CdSe, CdS, or CdTe, can be achieved by high-temperature (~300 °C) thermal decomposition means.[25] Generally, uniform nanocrystals are obtained by rapidly injecting organometallic reagents into a hot coordinating solvent to generate homogeneous nucleation followed by the slow growth and annealing.[25] This approach requires inert atmosphere and appropriate organic solvents. By adjusting the concentration of precursors and reaction time, different sized nanocrystals could be obtained.[25-26] Furthermore, in order to achieve higher QY and improve resistance against chemical-/ photo- oxidation, the synthesized core-only QDs are usually coated with an inorganic shell surrounding it.[27] For instance, ZnS, a high band-gap semiconductor material, was used to coat a CdSe QD core and the QY increased up to 80%.[28-29] The high temperature synthetic route is capable of producing highly crystalline and uniformly sized QD with narrow size distribution. And this approach allows the facile core/shell growth control, which is significantly important for improvement of QY.

Nevertheless, the semiconductor nanocrystals synthesized as above are coated with hydrophobic surface layer and only soluble in non-polar solvents, which severely hamper their biorelated applications which require working in aqueous media. In this regard, the aqueous synthetic approaches have attracted researchers' attentions widely. The aqueous synthetic method not only uses the biocompatible solvent (water), but also offers versatile functionalization possibilities during the synthetic process. Usually in the aqueous strategy, metal ions or their complexes react with chalcogen containing precursors forming nuclei, which then grow to nanocrystals in the presence of appropriate capping

ligands. This method has been employed to yield stable nanocrystals such as CdS[30], CdTe[31], CdSe[32], ZnSe[33], ZnCdSe[33], *etc*.[34] Moreover, although a little bit difficult, core/shell QDs could also be yielded by this means.[35-36] The QDs prepared by this low temperature aqueous route are readily water soluble and so no post synthesis modifications are needed. However, the quality of the QDs is poorer than those prepared by the high temperature method.[27, 34] Thus in order to obtain mono-disperse QDs with improved stability and higher QY, the most often used synthetic method is the high temperature approach.

Consequently, to facilitate the bio-applications of hydrophobic QDs, post synthesis modifications are critical to render them water-soluble and biocompatible. The hydrophobic ligands of QDs could be exchanged by excess bifunctional molecules such as mercaptocarbonic acid[37] and bidentate dihydrolipoic acid derivatives[38]. These ligand exchange methods are easy to conduct and the yielded QDs are small-sized, which is important for efficient FRET. Nevertheless, the QDs subjected to ligand exchange procedures suffer a decreased fluorescent QY and lack long term stability. Silane shells[39-40] and box dendrimers[41] around QDs can also be achieved through metal-thiol bonds. In addition, the hydrophobic QDs can be coated with amphiphilic polymers such as poly(acrylic acid)-octadecyl- amine polymers[42-43] or amphiphilic saccharides[44], or can be encapsulated within PEGylated lipid micelles[42]. These coating methods make highly stable and biocompatible QDs while maintaining their high QY. Unfortunately, the QDs modified by these macromolecules are not preferred for bioapplications because of their big hydrodynamic sizes, which lead to poor FRET efficiency and low permeability into cells. Several representative surface capping approaches to make hydrophobic QDs hydrophilic are listed in Table 1.1.

Table 1.1 A list of the representative approaches for QD surface-capping

Surface-capping approaches	Interaction mechanism	Examples
Monothiolated caps	Dative thiol bond	Mercaptocarbonic acids[37] Alkylthiol terminated DNA[48] Thioalkylated oligo-ethyleneglycols[56]
Bidentate thiols	Two interactions/ligand	Dihydrolipoic acid derivatives[38, 57]
Silane shell or Box dendrimer	Cross-linked shell	Mercaptopropyl silanols[39-40] Amine box dendrimers[41]
Amphiphilic polymer	Hydrophobic interactions	Phospholipid micelles[42] Modified acrylic acid polymer[42-43] Amphiphilic triblock copolymer[58] Amphiphilic poly-saccharides[44]

To explore the bio-applications of QDs in live cells or tissue imaging, drug delivery, and biosensing and so on, QDs need to be conjugated to bioactive molecules (such as oligonucleotides, peptides, proteins or drugs) without hampering the biological functions of these molecules. Several strategies have been employed to conjugate biological molecules to QDs, including adsorption, electrostatic interaction, mercapto (-SH) exchange, metal affinity, and covalent

linkage.[45] The adsorption method is simple but nonspecific.[46-47] The electrostatic interactions are usually used to conjugate positively charged proteins to negatively charged surfaces of QDs. The QD-protein conjugates obtained by this method are stable and maintain high fluorescence yield.[38] Mercapto exchange can conjugate thiol group containing biomolecules directly to the QD surface. Nevertheless, the yielded conjugates are not quite stable due to the weak bond between Zn^{2+} ion and thiol group resulting in the easy detachment of the biomolecules.[48-49]

Metal affinity coordination enables direct attachment of the peptides and proteins with polyhistidine groups onto QDs.[50-53] This self-assembly interaction is very strong with a dissociation constant (K_d) of nanomolar level.[52-53] Thus this metal affinity induced self-assembly strategy can be utilized as an effective way for preparing functional QD-bioconjugates. Nevertheless, the tricky issue of this approach is that polyhistidine group needs to be introduced to the biomolecules first prior to their conjugation with QDs.

In addition, the covalent linkage method is a more reliable way to make stable QD-biomolecule complexes. QDs subjected to versatile surface chemistries (see Table 1.1) can bear various functional groups such as –OH, -COOH, -SH, or $-NH_2$. If the biomolecules to be conjugated with QDs also possess these functional groups, it is easy to covalently link QDs and biomolecules through chemical reactions.[6, 39-41, 54-55]

1.3 Förster resonance energy transfer (FRET)

1.3.1 FRET principle

FRET is a process that involves non-radiative energy transfer from a photo-excited donor to an acceptor in close proximity (*i.e.* typically < 10 nm). Absorbing a photon excites the donor, which can then transfer the excitation energy to the acceptor, and the acceptor subsequently relaxes to its ground state by emitting a lower energy photon (Figure 1.2).

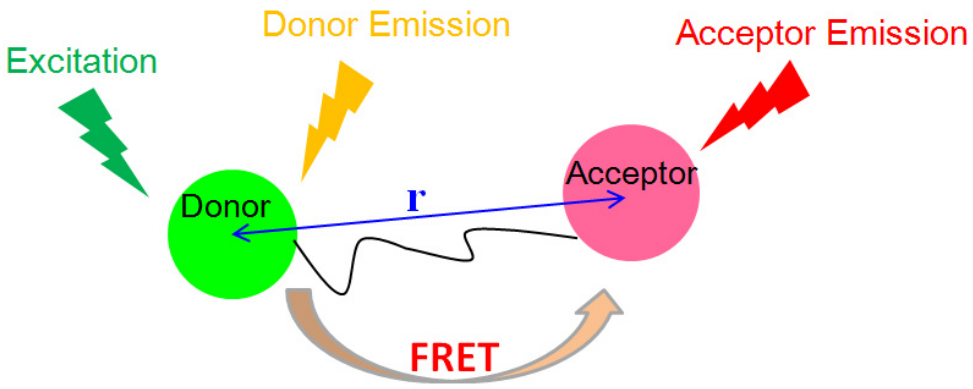

Figure 1.2 Schematic diagram of the FRET interaction between a donor fluorophore and an acceptor fluorophore.

The donor and acceptor are brought into close proximity by a linker (black line). Upon photo-excitation of the donor, energy is transferred to the acceptor non-radiatively, leading to donor sensitized acceptor emission.

This process is strongly dependent on the separation distance between donor and acceptor. It also requires finite spectral overlap between donor emission and acceptor absorption profiles.[59] Elaborate selection of an appropriate donor-acceptor pair could lead to improved FRET efficiency.

The FRET efficiency, *E*, represents the fraction of photon energy that is transferred from the donor to the acceptor non-radiatively. In a typical single-donor-single-acceptor FRET system, *E* is defined as:

$$E=R_0^6/(R_0^6 + r^6) \quad (1.1)$$

Where *r* is the donor-acceptor distance and R_0 is the Förster radius of the FRET pair under which *E* = 50% FRET.

If enhancement of the energy transfer is required, multiple acceptors may be brought close to the same donor so that one donor can transfer energy to several acceptors. In this regard, the above analysis can be modified to account for these complicated energy transfers, and the increased efficiency can be expressed as:

$$E = n\times R_0^6/(n\times R_0^6 + r^6) \quad (1.2)$$

In this expression, *n* is the average number of acceptor molecules interacting with one donor. From the equation, it is easy to figure out that the presence of several acceptor fluorophores should increase the FRET efficiency. Such efficiency enhancement may be attributed to an effective proportional enhancement of the energy transfer cross section (the overlap integral) between a donor and several acceptors around its centre.

The FRET between two different coloured QDs,[60] QD and dye-labelled biomolecule,[61-62] QD and gold nanoparticle,[63] and QD and dye-labelled polymers[64] have been reported. Figure 1.3 depicts the spectral overlap profiles for some QD→organic dye, organic dye→QD, and QD→QD photo energy transfer pairs.[65]

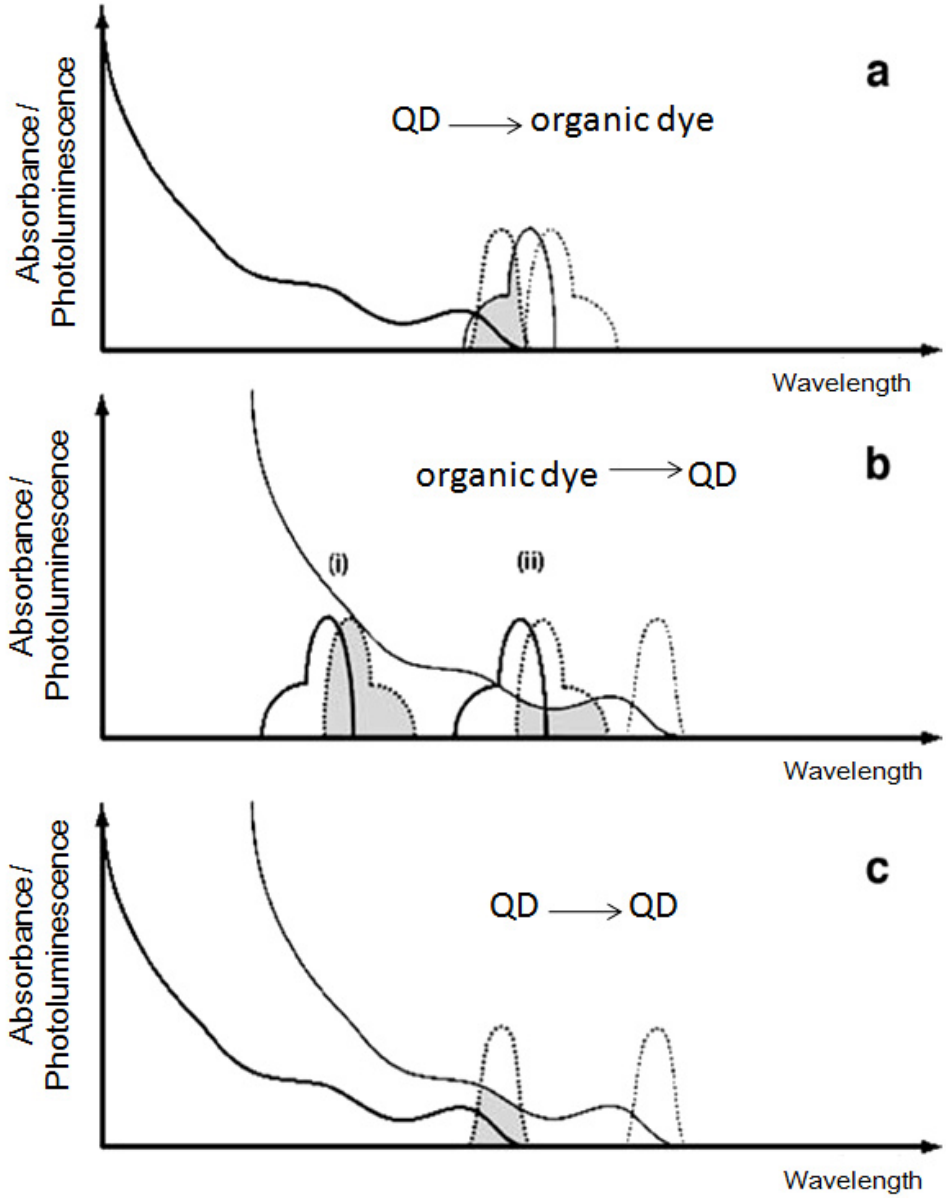

Figure 1.3 Spectral overlap profiles for three possible FRET scenarios with QD. **a)** a QD donor and an organic fluorophore acceptor; **b)** an organic fluorophore as donor and a QD as acceptor; **c)** one coloured QD as donor and the other coloured QD as acceptor. In **b)**, two fluorophores, (I and ii), are shown as potential donors. Absorption spectra are shown as solid lines; luminescence spectra are shown as broken lines. Thick lines represent the donor and thin lines represent the acceptor. (Reprinted by permission of the Springer)[65]

As shown in Figure 1.3, it is possible to excite the QD donor without directly exciting the acceptor dye fluorophore (a). However, in both b) and c), it is impossible to only excite the donor without directly exciting the acceptor QD, and hence there will always be strong background emission. Therefore, although all three combinations shown above can produce efficient FRET, only the FRET between a QD donor and organic dye acceptor is most suitable for ultra-sensitive detection. In other words, a QD is naturally not a good acceptor because of its broad absorption spectral profile which will always lead to direct acceptor excitation even in the absence of FRET.

1.3.2 Nucleic acid sensing

FRET in SM level has been applied to detect DNA targets by the Wang group. Sandwiched hybrids labelled with organic dyes are conjugated onto the QD surface *via* streptavidin-biotin interaction (Figure 1.4).[7]

This DNA nanosensor consists of two target-specific oligonucleotide probes, which are designed to possess complementary sequences to two different segments of a target DNA. These two probes are a ‘reporter probe’ labelled with an organic dye acceptor and a ‘capture probe’ labelled with biotin respectively. In addition, a QD conjugated with several streptavidins is the central part of the nanosensor (Figure 1.4a). Target DNA strands present in the solution could be sandwiched by a pair of reporter-capture probes and several sandwich structures could then be captured by a single QD through the biotin–streptavidin interaction. Thus, multiple acceptor dyes are brought into close proximity to the QD donor and the FRET efficiency is enhanced. In this design, the QD functions as both a FRET energy donor and a target concentrator (Figure 1.4b). The

solution was then injected into a glass microcapillary and flowed through a small excitation spot. The fluorescence signals from individual bioconjugates could be monitored as they traverse the laser confocal volume (Figure 1.4c).

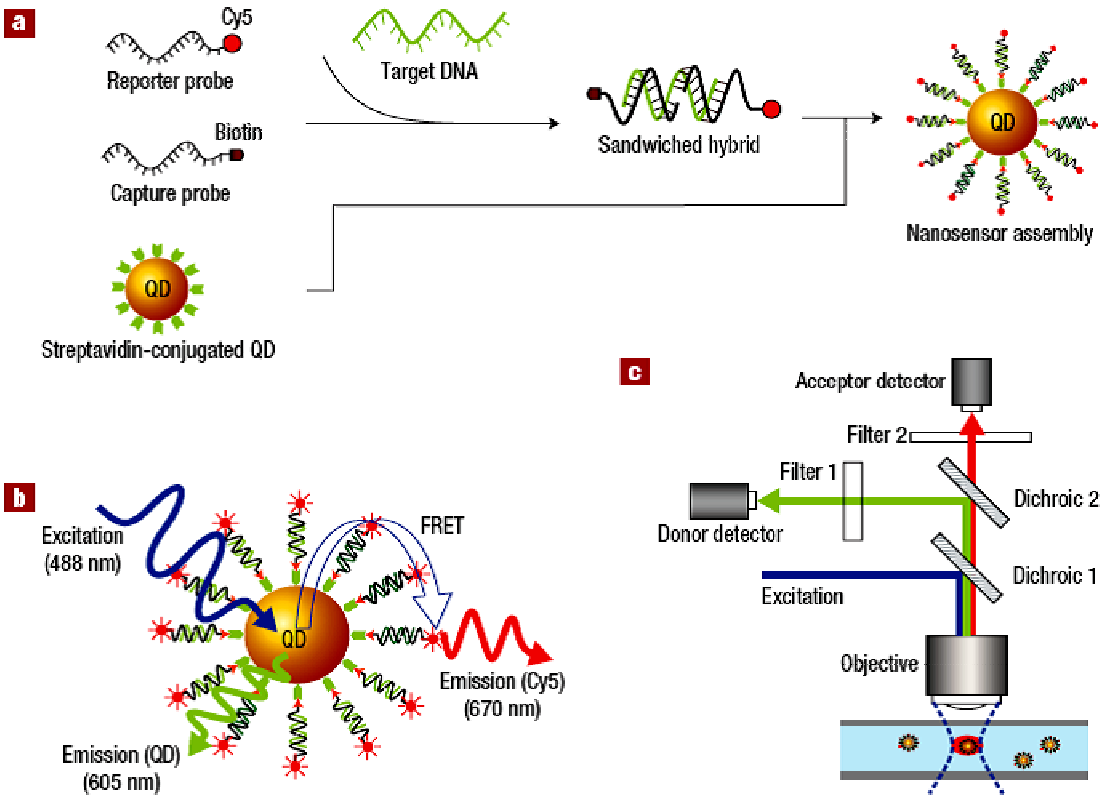

Figure 1.4 Schematic of single-QD-based DNA nanosensors.

a, Conceptual scheme showing the formation of a nanosensor assembly in the presence of targets. **b**, Fluorescence emission from Cy5 on illumination on QD caused by FRET between Cy5 acceptors and a QD donor in a nanosensor assembly. **c**, Experimental setup. (Reprinted by permission of the Nature Publishing Group)[7]

This assay format requires no separation of the sample, as the unhybridized probes do not participate in FRET and are non-fluorescent. This system provides much higher sensitivity in detecting the hybridization of DNA due to the dual roles of the central QDs. It should be noted however, this design only works well in situations of multiple target:QD copy number (*e.g.* n > 20), it is

inefficient at the low target:QD ratios (*e.g.* 1:1) because of the small FRET efficiency obtainable due to the large donor-acceptor distance.

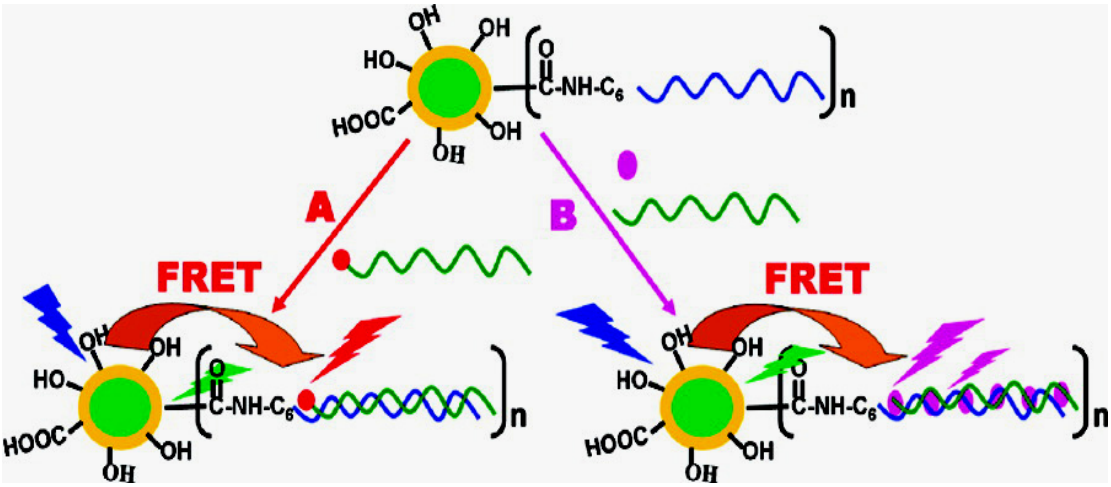

Figure 1.5 Schematic principle of the approach for label-free DNA detection.

The DNA detection assay is based on a covalently coupled QD-DNA probe via QD sensitized FRET signal. (Reprinted by permission of the American Chemical Society)[6]

Besides biotin-streptavidin interactions, functional thiols have also been demonstrated to be a very useful QD coating and/or linkers between the QD donors and dye acceptors, because QDs have a high affinity for thiolated ligands. In this regard, a thiolate linker has been used to directly couple a dye-labelled double-stranded DNA (dsDNA) acceptor to a 3-mercaptopropionic acid (MPA) capped QD donor.[66] Although the above design was very efficient in producing high FRET, however the strong nonspecific adsorption of the DNA on the MPA-capped QD has prevented it from being useful for specific DNA sensing application. To overcome the problem of nonspecific adsorption, our group has developed another compact, functional QD-DNA conjugate (see Figure 1.5) where a tri(ethylene glycol) linker, EG_3, which is well known for its

ability to resist non-specific adsorption, has been introduced in between the QD and the functional DNA in this configuration.[6]

The advantages of introducing the EG_3 linker are: (1) it can eliminate the strong, nonspecific adsorption of DNA onto the QD surface, and (2) it allows control of the separation distance between the QD donor and dye acceptor within the range of the Förster radius by tuning the number of the repeat units. Moreover, this study provides a model system for both label and label-free detection of nanomolar complimentary DNA at low DNA probe/QD copy numbers.

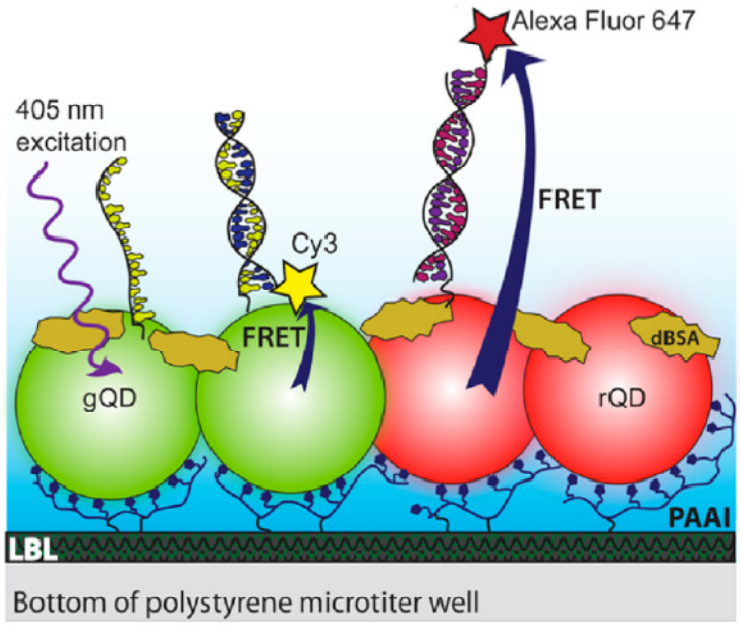

Figure 1.6 Schematic illustration of multiplexed DNA detection.

DNA hybridization brought the FRET donor-acceptor pairs (QD donors and dye accepters) together. Thus by examining the FRET behaviors of the donor-accepter pairs, quantifications of DNA were realized correspondingly. (Reprinted by permission of the American Chemical Society)[5]

More recently, multiplex DNA detection has been performed by employing different coloured QDs donors based FRET.[5] In this developed system, two different coloured QDs (green- and red- emitting) were capped with thioalkyl acid ligands and immobilized on the polystyrene microwells using multidentate imidazole linkers. As presented in Figure 1.6, QDs are modified with two different capture-DNA strands (c1 and c2) which are complementary with two different DNA targets (T1 and T2), respectively. In the presence of Cy3-labelled T1, FRET between green-emitting QD and Cy3 accepter happens upon DNA hybridization. Likewise, hybridization of Alexa Fluor 647-labelled T2 and C2 would induce FRET process between Alexa Fluor 647 and the red- emitting QDs. Consequently, DNA quantifications have been effectively achieved *via* the FRET efficiency analysis. This assay demonstrates excellent resistance to the nonspecific adsorption of DNA, associated with the detection limit of 4 nM. Furthermore, this strategy is able to discriminate the single base-pair mismatched sequences with a discrimination ratio >2.

1.3.3 FRET between QD and dye-labelled protein or FP

The Mattoussi group has investigated the FRET between fluorescent QD donor and dye-labelled protein (see Figure 1.7).[50] In this research, the maltose binding protein (MBP) is engineered appended with a polyhistidine tag and labelled with a dye (Cy3). The dye-labelled MBP self assembled on to the QD *via* metal affinity interaction between Zn^{2+} ions and the polyhistidine tag. Thus the QD donor and dye acceptor are in close proximity providing a good model system to explore FRET phenomena. By carefully choosing donor-acceptor pairs (different QD donors with the same Cy3 acceptor), this designed QD-MBP configuration offers the possibility for adjustment of the degree of spectral overlap between

donor and acceptor. Moreover, more than one acceptor could be accommodated around one single QD donor *via* self-assembly. In other words, FRET efficiency can be delicately controlled either by tuning the emission peak of QDs or by adjusting the copy number of dye-labelled proteins around the QD donor.

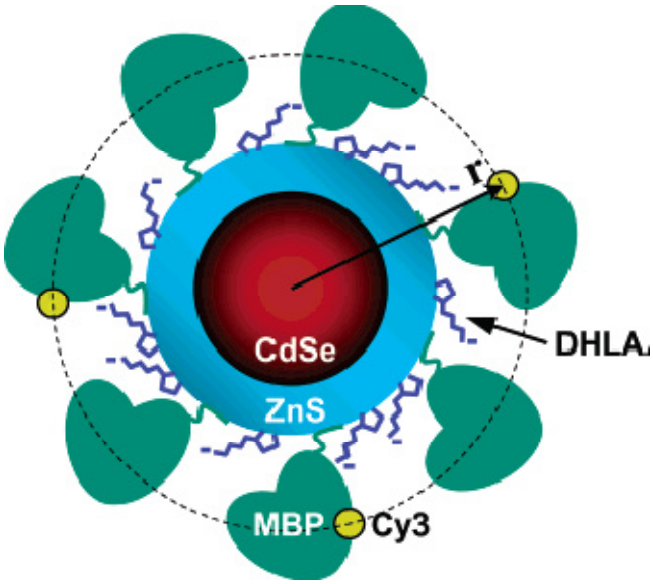

Figure 1.7 Schematic representation of the QD-MBP-dye nanoassembly (not drawn to scale).

The total number of proteins immobilized on each QD surface is ~15. The distance r represents the radius or average distance between the QD centre and location of the Cy3-labeled residue on MBP. (Reprinted by permission of the American Chemical Society)[50]

On the basis of the above designed QD–protein assemblies, a competitive sensing format has been developed by the same group.[67] As demonstrated in Figure 1.8A, MBP self assembles onto QD and functions as a sugar receptor and each QD-MBPs conjugate is bound with a β-cyclodextrin-QSY9 dark quencher in the MBP saccharide binding site to quench QD photo-luminescence *via* FRET. Upon addition of maltose, which can effectively substitute the β-cyclodextrin-QSY9 dark quencher, the QD photoluminescence recovers gradually. Thus the quantification of maltose is realized by monitoring

the QD emission increase. Another maltose sensor developed in this research consists of self assembled QD, Cy3-modified MBP and Cy3.5-labelled β-cyclodextrin (Figure 1.8B).

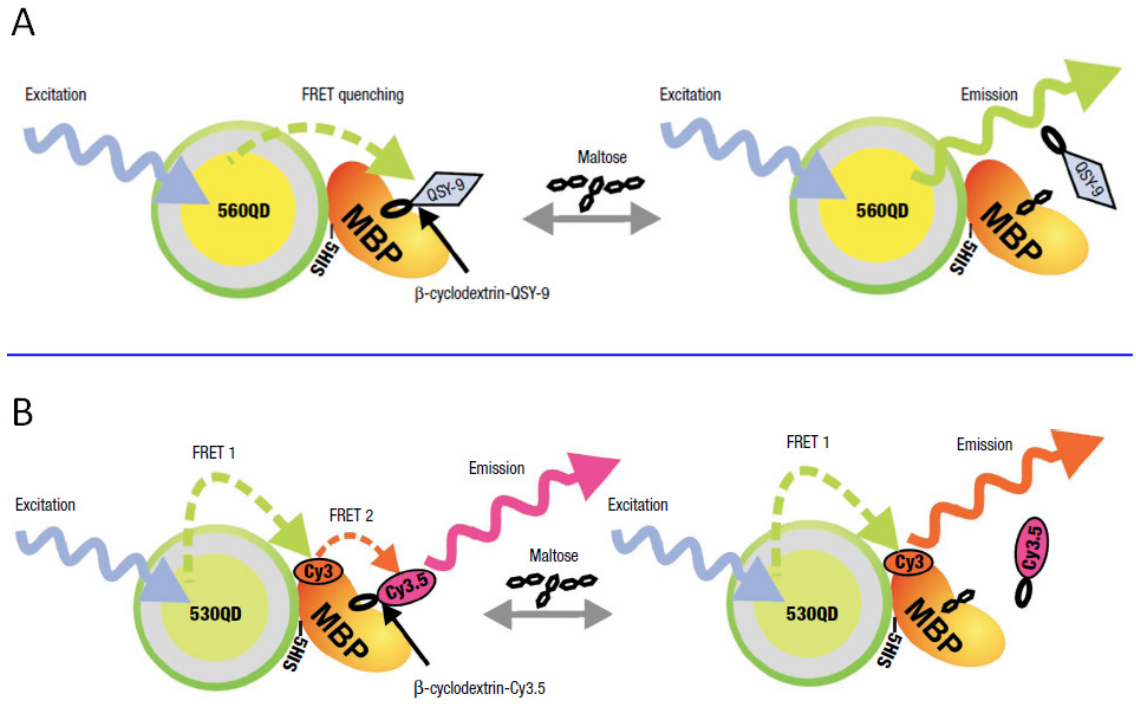

Figure 1.8 Schematic illustration of the QD-MBP nanosensor for maltose detection.

Each QD is surrounded by multiple copies of MBP (~10) but only a single MBP is shown for clarity. (A) QD emission at 560 nm is quenched by QSY9 (maximum absorption ~565 nm) labelled β- cyclodextrin in the absence of maltose. As the maltose is added, and displaces the β-cyclodextrin-QSY9, the QD emission increases schematically. (B) 530 nm-emitting QD is self assembled with Cy3-labelled MBP and Cy3.5-labelled β- cyclodextrin. Upon excitation, two step FRET happens from QD to Cy3 and from Cy3 to Cy3.5. Added maltose substitutes β- cyclodextrin-Cy3.5 hampering the second FRET process. Thus by carefully examine the fluorescent signal change, the detection of maltose is realized. (Reprinted by permission of the Nature Publishing Group)[67]

In the absence of maltose, the complex undergoes two-step FRET (QD→Cy3→Cy3.5). Added maltose displaces the β-cyclodextrin-Cy3.5, resulting in the suspension of the second-step FRET in a systematic manner. This sensing protocol by employing two-step FRET overcomes the distance limitations between donor and acceptor and thus leads to enhanced sensitivity.

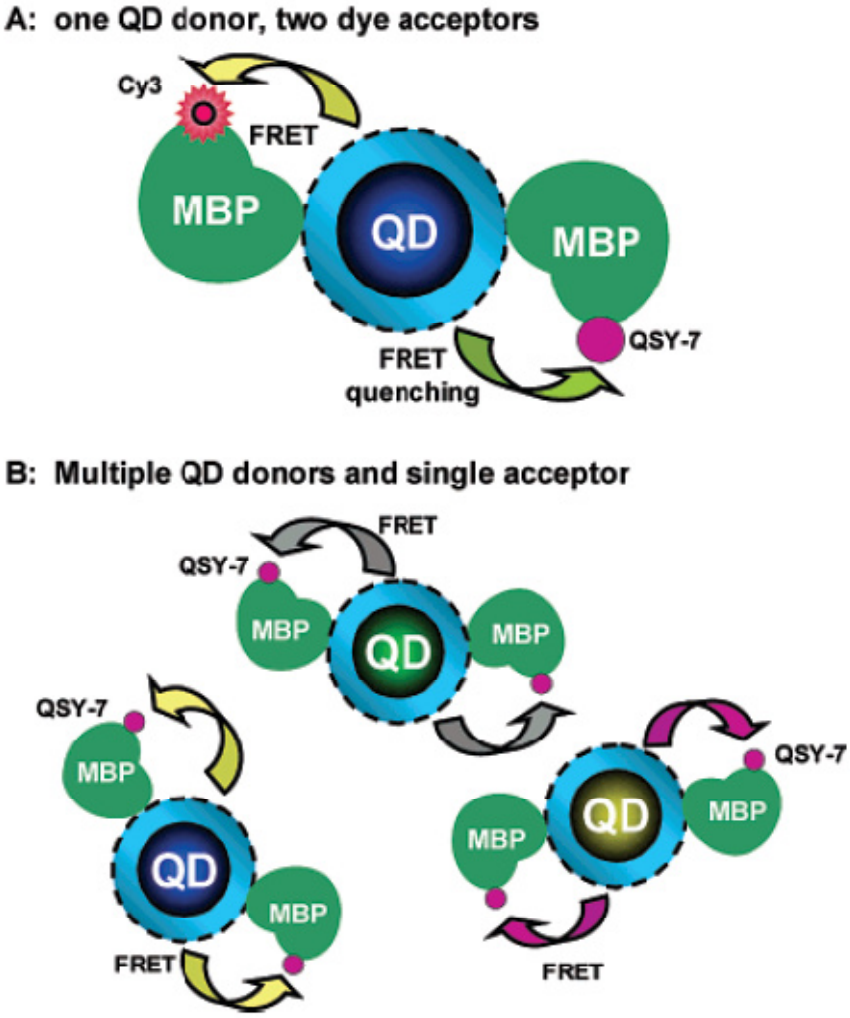

Figure 1.9 Principle of QDs conjugated to dye-labelled MBP acceptors for FRET in a multiplexed format.

(A) a single colour QD interacts with multiple distinct acceptors (Cy3 and QSY7) (B) three different coloured (blue, green and yellow emitting) QD donors interact with one type of acceptor (QSY7). (Reprinted by permission of the American Chemical Society)[68]

Subsequently, QD-based multiplexed FRET to dye-labelled MBP has been demonstrated.[68] Figure 1.9A shows that two distinct dyes labelled MBP interact with a single QD donor leading to two simultaneous FRET processes between the two donor-acceptor pairs (QD-Cy3 and QD-QSY7). Furthermore, FRET assay between various QD donors and one type of acceptor has been investigated. Due to different degrees of spectral overlap and various donor-to-acceptor ratios, FRET behaviours of the assemblies are versatile. This provides guidance in designing QD-based sensors especially for multiplexing detection. [5]

Later on, FRET between QD and Cy3-labelled MBP at the SM level has been also demonstrated by the same group.[69] The same QD-MBP-dye configuration is achieved by employing the same polyhistidine mediated self-assembly interaction. Direct correlation between single-particle and ensemble FRET has been obtained in terms of donor-acceptor separation distances and FRET efficiencies. Compared with ensemble FRET measurement, the single-particle FRET not only offers higher FRET efficiency because a threshold is applied, which only counts brighter particle and disregards the dim ones, but also reveals distribution information about FRET efficiency.

Encouraged by the success in FRET studies on QD and organic dye labelled protein, there has been a growing interest in evaluating FRET between QD and FPs. Since these studies use FP as the acceptor, replacing organic dyes, post-synthesis dye-labelling of protein is not necessary.

FRET characteristics based on QD-FP pairs (Figure 1.10) including the efficiency, donor-acceptor distance and the self-assembly binding strength have

been studied by the Bao group.[52] In this research, polyhistidine- appended FPs self assemble onto PEGylated lipid encapsulated QDs. Different QD donors (520, 540, 560 nm-emitting) and different FP acceptors (mOrange, tdTomato and mCherry) are paired to tune the degree of spectral overlap, and thus to control FRET behaviours. By using the Forster dipole-dipole interactions formalism, the FRET results are analyzed and discussed. These results demonstrate that FPs are efficient acceptors for QD donors with up to 90% FRET efficiency obtained.

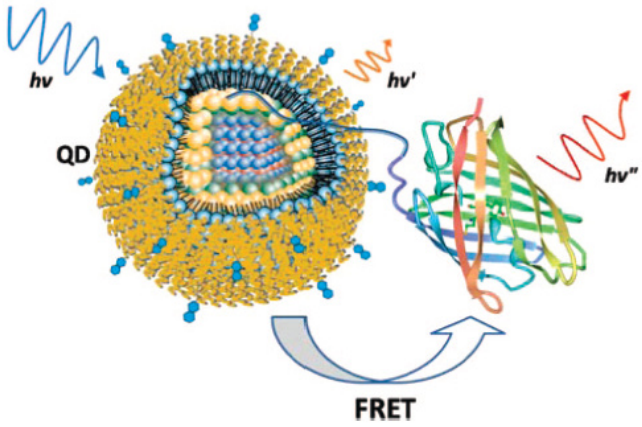

Figure 1.10 Schematic diagram of the FRET interaction between a QD and a FP.

FP is self assembled onto the QD *via* the poly-histidine tail, bringing the donor and acceptor together, and allowing the FRET to happens upon excitation. (Reprinted by permission of the American Chemical Society)[52]

Further development of this configuration has been conducted by the Niemeyer group where the FP was used as a relay in between the QD-dye FRET.[70] As demonstrated in Figure 1.11A, single stranded DNA (ssDNA) -FP conjugate (termed as 1) is attached onto QD *via* a polyhistidine tag to form a QD-FP-ssDNA conjugate (2). Then organic dye (Atto647)- labelled complementary ssDNA (3) hybridizes with the DNA strand on **2** forming QD-FP- dsDNA-Atto

647 complex (4), which enables two-step FRET. By varying the dye-labelling sites on the DNA2 sequence, the separation distance between FP donor and Atto 647 acceptor of the second FRET interaction could be tuned delicately allowing the FRET to happen in a controllable manner (Figure 1.11B).

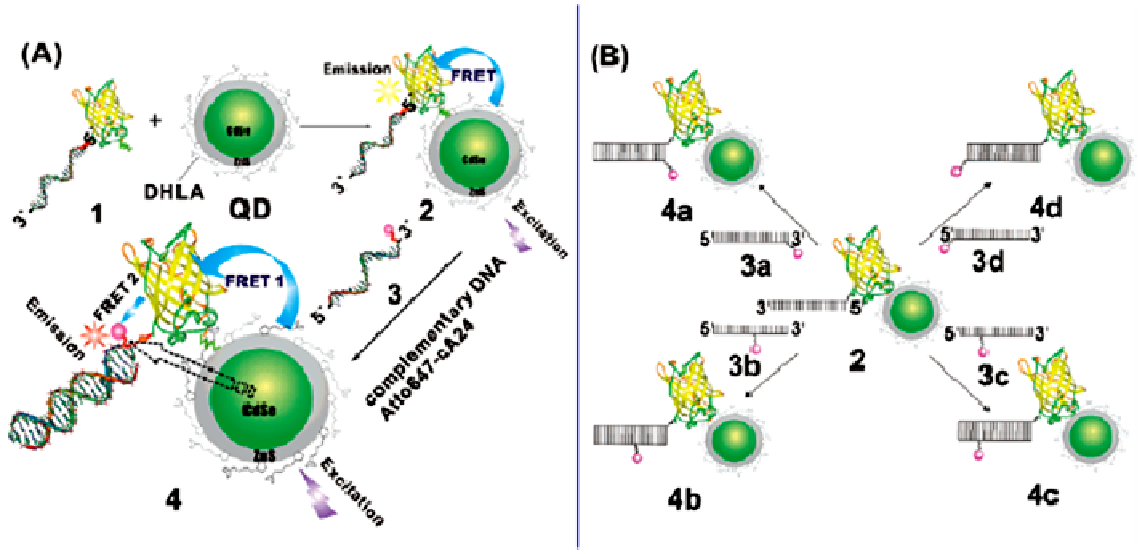

Figure 1.11 Schematic illustration of the two-step FRET system based QD-FP-Atto647 configurations.

(A) Initially, ssDNA1-FP conjugate (termed as 1) is assembled onto QDs forming QD-FP conjugate (2). Atto647- labelled DNA(3) is attached with (2) through DNA hybridization forming the final two-step FRET conjugate (4); **(B)** four different dye-labelled DNA conjugates (3a-d), which have different dye-labelling sites are attached onto 2 to generate versatile FRET behaviours. (Reprinted by permission of the American Chemical Society)[70]

Based on the above QD-FP system, a proteolytic activity sensing platform has been developed by using peptide substrates.[3] As demonstrated in Figure 1.12, this sensing system utilizes specific cleavable peptide substrates as the linker between QD donor and FP (mCherry) acceptor. In the presence of the target protease (Caspase 3), the peptide substrate is cleaved resulting in the detachment of FP from the QD. As the rate of proteolytic activity (peptide

cleavage) is a kinetic process, it will rely on the caspase 3 concentration and this can be tracked by monitoring the QD emission recovery following substrate cleavage. Several inherent advantages of this sensing strategy include bacterial expression of the protease substrate with FP as FRET acceptor and polyhistidine tail for facile self-assembly to QDs, and the potential to target other proteases of interest by delicate modification of the substrate.

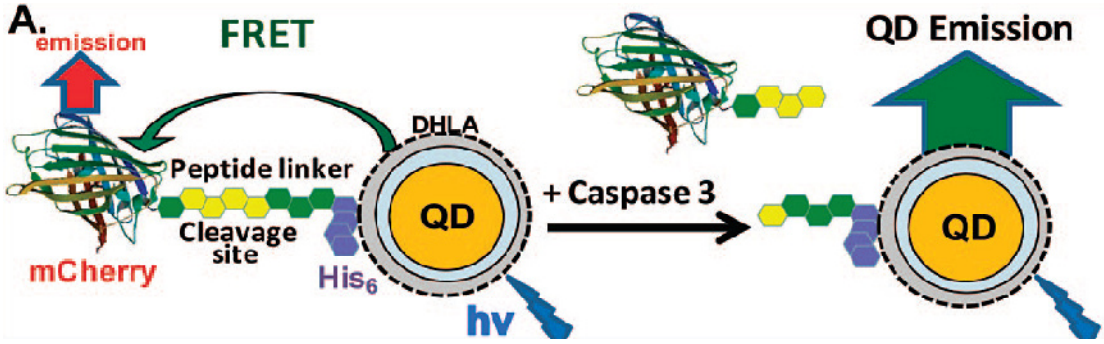

Figure 1.12 Peptide substrate-mCherry conjugate is assembled *via* metal affinity interaction between polyhistidine (His6) and Zn^{2+} on QD surface.

This configuration allows FRET to happen from QD donor to mCherry. Addition of Caspase 3 leads to the cleavage of peptide linker resulting in the release of mCherry from QD. Thus the detection of the Caspase 3 could be represented by QD emission changes in a systematic manner. (Reprinted by permission of the American Chemical Society)[3]

Inspired by this sensing format for an enzymatic activity assay, other FRET-based strategies have also been reported using QD-dye-labelled peptides/ oligonucleotides as substrates.[4, 71] In addition, multiplexed protease activity sensing is also possible by adapting multiple distinct dye-labelled peptides as FRET acceptors and substrates.[72-73]

1.4 Two-colour coincidence detection (TCCD)

Although FRET can provide accurate donor-acceptor distance information that has been demonstrated to be very powerful in studying the structure and conformation of complex biomacromolecules, as well as for sensing applications, an essential requirement for FRET to happen is that the donor-acceptor pair should be brought into close proximity, *i.e.* < 10 nm, which is often impossible for large molecular complexes, limiting its areas of application. This limitation can be overcome by TCCD, another SM fluorescence technique that relies on coincidence event counting. In this regard, the sample is simultaneously excited by two focused, overlapped laser beams (a typical setup is depicted by Figure 1.13). It could obtain the quantitative information through the fraction of coincident fluorescent bursts from the overall fluorescent signals.[12] It is worth to mention that if both of the two fluorophores used are QDs, only one laser is required.

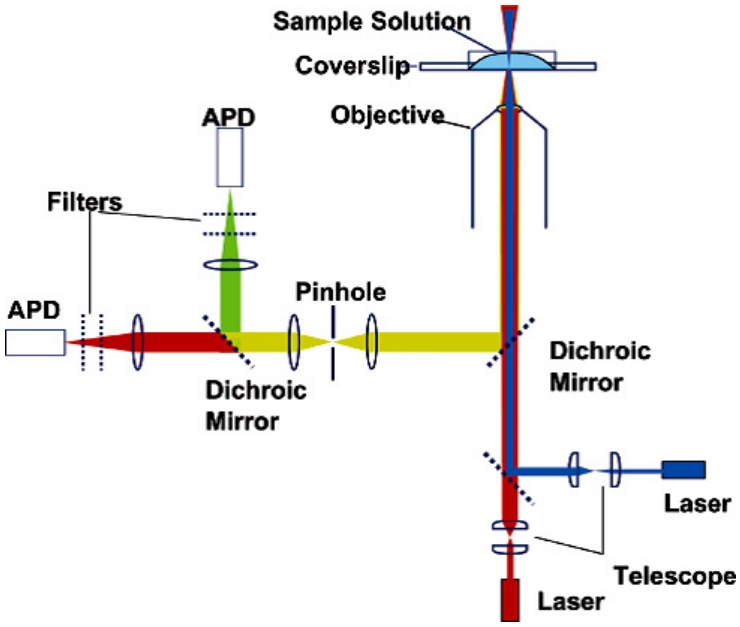

Figure 1.13 Schematic representation of the apparatus setup used for dual-colour excitation and two-colour coincidence detection. (Reprinted by permission of the American Chemical Society)[74]

TCCD has been shown to be less sensitive to background fluorescence than single-colour excitation and capable of detecting femtomolar levels of individual DNA molecules labelled with two different fluorophores.[74] In order to achieve high sensitivity, selection of a proper fluorescence counting threshold is very important: on one hand, it should be high enough to exceed the background fluorescence; on the other hand, it should also ensure a low rate of chance coincident events to achieve high reliability. More recently, automatic determination of optimized thresholds for SM analysis in TCCD has been reported.[75] This new development has enabled the detection of a small fraction (<1%) of dual-labelled duplex DNA molecules within a large excess of single-labelled single- stranded DNAs.

TCCD has also been used to direct counting of individual protein G-antibody complexes with red- and blue-excited fluorophore labelled antibodies (Figure 1.14).[76] The advantages for this method include, being sensitive (femtomolar sensitivity), being label-free (no target labelling required), requiring simple sample preparation (no separation); and being able to make measurements in complex media such as diluted serum. This method offers an opportunity for ultra sensitive detection and quantitation of proteins of interest. Besides, it is also possible to measure the stoichiometry, equilibrium constant, and dissociation rate of protein- protein complexes by TCCD. However, it should be noticed that despite its general applicability, TCCD can only work with target analytes with two or more accessible, independent binding sites because two different antibodies are required to form the protein complex.

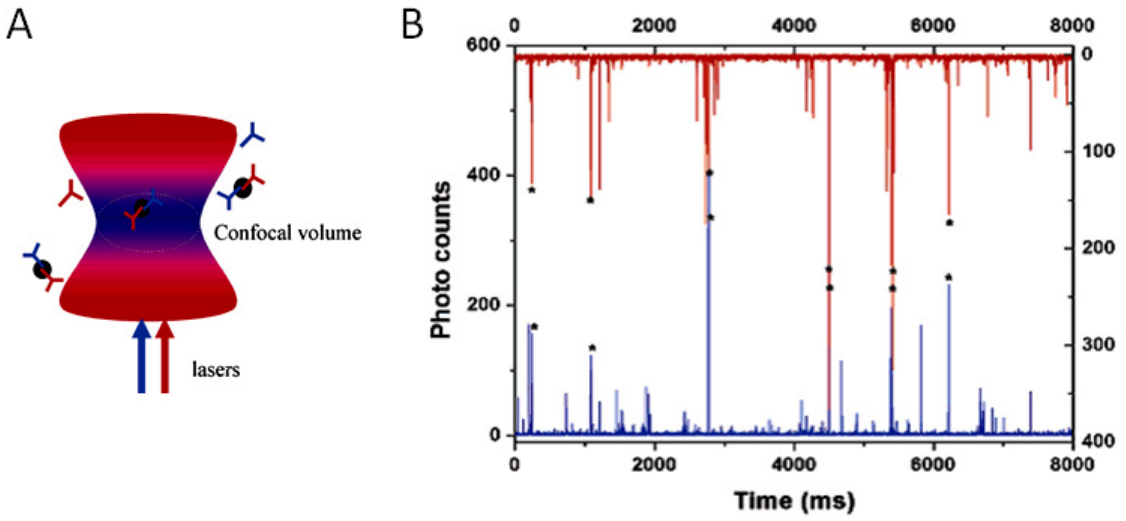

Figure 1.14 The principle of TCCD.

(A) Coincidence events are detected when a protein molecule labelled with a red-excited and a blue-excited antibody enters the probe volume. There are also coincident events when unbound red-excited and blue-excited antibodies enter the probe volume at the same time. This constitutes a statistical background below which it is not possible to detect dual-labelled proteins. **(B)** Fluorescence bursts on both the blue- and red-excited channels for protein G/IgG complexes in PBS buffer formed in solution at initial concentrations of 50 pM protein G, 50 pM IgG labelled with Alexa 647 and 50 pM IgG labelled with Alexa 488. Coincident bursts on both channels are marked with an asterisk. (Reprinted by permission of the American Chemical Society)[76]

While most TCCD approaches rely on using two overlapped excitation lasers as depicted in Figure 1.14, it is also possible to use only one laser to achieve TCCD by adapting the unique absorption and fluorescence properties of QDs. For instance, a new genotyping method based on TCCD has been demonstrated with only one laser.[77] The method is based on bioconjugates of oligonucleotide ligation and a QD-mediated TCCD scheme (see Figure 1.15).

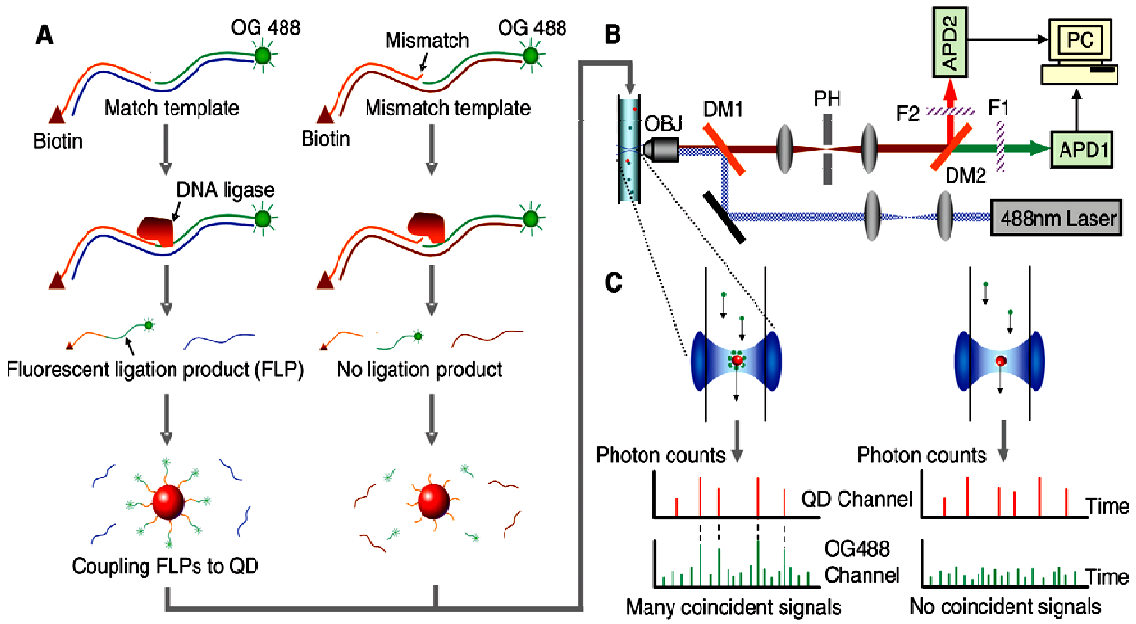

Figure 1.15 Schematic illustration for homogeneous point mutation detection using QD-mediated TCCD analysis using a single excitation laser.

(A) Process flow for OG488 (a dye): QD-FLPs nanoassemblies are formed in the presence of match templates (left). No QD-FLPs nanoassemblies are formed in the presence of the mismatch templates (right). **(B)** Detection of ligation products is carried out using a single wavelength-excitation, dual wavelength-emission confocal LIF spectroscopic system. OBJ, objective; DM(1 and 2), dichroic mirrors; PH, pin hole; F(1 and 2), filters; APD(1 and 2), avalanche photodiodes. **(C)** Left: When a QD-FLPs nanoassembly flows through the detection volume, simultaneous burst signals, or coincident signals (marked by dash lines), are detected in the two detection channels. Right: QDs are bound only with nonfluorescent probes in the mismatch experiments so no coincident signals will be seen. The coincident signals therefore serve as indicators of perfect match targets. (Reprinted by permission of the Oxford University Press)[77]

The sample preparation is started from two probes, which are complementary parts for two different sections of the template target. The two probes are the recognition probe and reporter probe conjugated with biotin and organic dye, respectively. Consequently, a DNA ligase is introduced to link the two probes in the hybrids. After denaturing the duplex by heat, the reporter probes or the fluorescent ligation products could be captured by streptavidin coated QDs *via*

the extremely strong streptavidin-biotin interaction. The fluorescence signals could be monitored as the conjugates flow through the laser confocal volume. When the mismatch templates were present in the solution, the two probes could not be covalently linked together. Thus no coincident events could be detected. This approach is able to detect zeptomoles of targets associated with an allele discrimination selectivity factor $>10^5$ offering a possibility for sensitive and specific detection of homogeneous point mutations in separation-free format.

Another example is a homogenous sensitive detection of nucleic acids using two-colour QDs based on SM coincidence detection (Figure 1.16).[78] Similarly, one target DNA is captured by two complementary biotinylated probes to form sandwiched hybrids. Then the hybrids are captured by streptavidin-coated 606QDs and 525QDs through specific steptavidin-biotin interactions sequentially. Here, the QDs function as both a nano-scaffold and as a fluorescence pair for TCCD. Only in the presence of target DNA, the 605QD/DNA hybrid/525QD complexes could form and the coincidence fluorescence events could be detected. This QD-based single-molecule coincidence detection offers a simple, highly efficient and ultra sensitive (with detection limit of 5 fM) approach for DNA analysis in a homogenous format. This assay offers a model system for the detection of DNA hybridization, single nucleotide polymorphisms, proteins and RNA.[78]

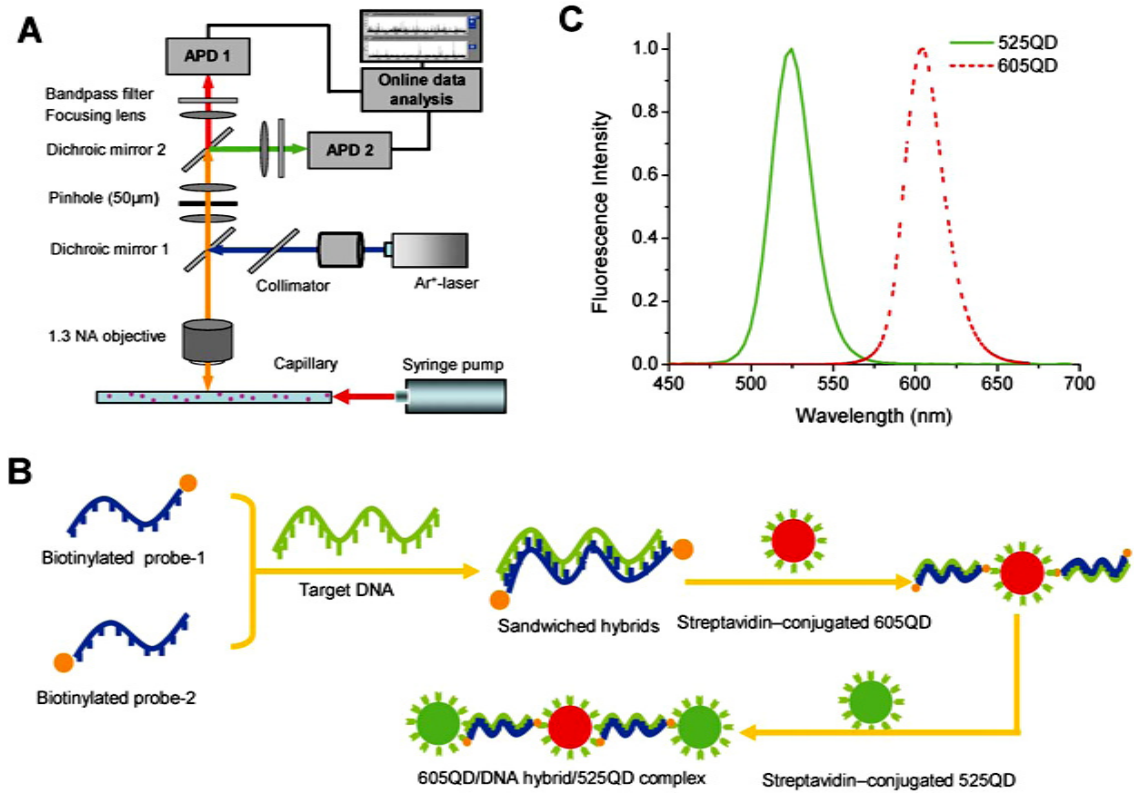

Figure 1.16 The principle of QD-based SM coincidence detection.

(A) The experimental setup for QD-based single-molecule coincidence detection. The sample was passed through a laser-focused detection volume using the pressure-driven flow of a syringe pump. A 488 nm argon ion laser was used to excite both 525QD and 605QD. The fluorescence emissions from 525QD and 605QD were separated and detected in green and red channels, separately. (B) The conceptual schematic for QD-based single-molecule coincidence detection. Two biotinylated oligonucleotide probes were used to recognize and detect specific complementary target DNA through a sandwich hybridization reaction. The DNA hybrids were first caught and assembled on the surface of 605QDs through specific streptavidin–biotin binding; then the second 525QDs were added to bind the other end of DNA hybrids to form the 605QD/DNA hybrid/525QD complex. C, The normalized emission spectra of 525QD and 605QD. (Reprinted by permission of the Royal Society Chemistry)[78]

1.5 Overview of the project (part I)

The unique optical properties (broad absorption and narrow emission, and excellent stability against photobleaching) of the QDs make them highly attractive for FRET based applications although most biolabels are still dye- or FP- based. Moreover, their promising applications in imaging, therapy and biosensing are attracting more and more researchers' attention. One of the trickiest issues hindering their effective biomedical applications is their surface chemistry. As discussed above, amphiphilic polymers (or PEGylated lipids micelles) encapsulated QDs suffer from large overall sizes that are mostly coming from the thick surface coatings. In FRET-based biosensors, the big-sized QD leads to large distances between the QD and dye labelled biomolecules, which can severely limit their sensitivity because FRET efficiency decreases dramatically with the increasing donor-acceptor distance. Furthermore, the oversized QDs might be unsuitable to target specific intracellular sites[79] which will hamper their applications in therapy, imaging or sensing in cells.[80] In this regard, small-molecule ligands capped QDs appear to be better-suited for situations requiring compact sizes. As a result, significant efforts have been devoted to prepare stable, compact QDs with specifically designed small-molecule ligands.[6, 66]

Consequently, in the first part of my project, the optical properties of QDs capped by three different small-molecule ligands, 3-mercaptopropionic acid (MPA), glutathione (GSH), and dihydrolipoic acid (DHLA), are investigated. Then the metal affinity induced self-assembly interaction between the QD and His_6-tagged FP is employed to conjugate the QD and FP. Following that, the FRET studies between QD and FP are carried out to elucidate how different QD

surface small-molecule capping affects their FRET behaviours (see Figure 1.17 for illustration). The experimental results are carefully analyzed and possible QD-FP interaction models are proposed to explain the observed FRET differences.

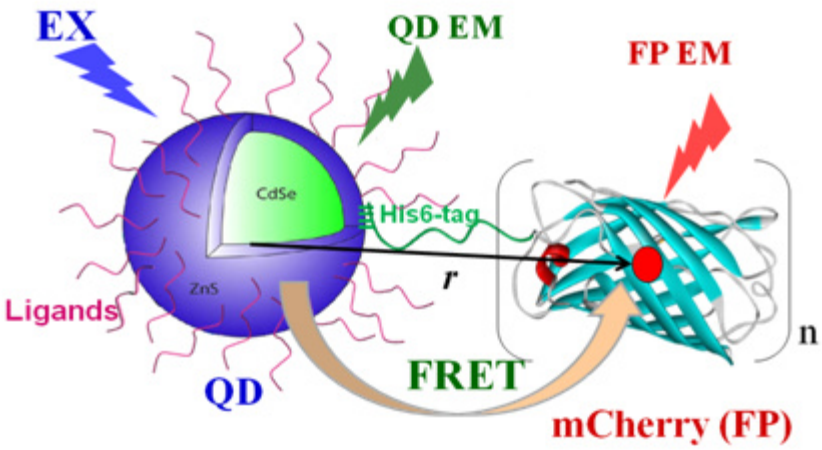

Figure 1.17 Schematic diagram of the FRET interaction between a QD donor and FP acceptors.

A His6-tag at the N-terminus of the mCherry (FP) coordinates to the Zn^{2+} ions on the QD ZnS shell which brings the two into close proximity. Upon photo-excitation of the QD, energy is transferred to the FP non-radiatively, leading to QD sensitized FP emission.

1.6 References

1. U. Resch-Genger, M. Grabolle, S. Cavaliere-Jaricot, R. Nitschke and T. Nann, *Nat. Methods*, 2008, **5**, 763-775.
2. A. Gansen, A. Valeri, F. Hauger, S. Felekyan, S. Kalinin, K. Toth, J. Langowski and C. A. M. Seidel, *Proc. Natl. Acad. Sci. USA*, 2009, **106**, 15308-15313.
3. K. Boeneman, B. C. Mei, A. M. Dennis, G. Bao, J. R. Deschamps, H. Mattoussi and I. L. Medintz, *J. Am. Chem. Soc.*, 2009, **131**, 3828-3829.

4. K. E. Sapsford, J. Granek, J. R. Deschamps, K. Boeneman, J. B. Blanco-Canosa, P. E. Dawson, K. Susumu, M. H. Stewart and I. L. Medintz, *Acs Nano*, 2011, **5**, 2687-2699.
5. E. Petryayeva, W. R. Algar and U. J. Krull, *Langmuir*, 2013, **29**, 977-987.
6. D. J. Zhou, L. M. Ying, X. Hong, E. A. Hall, C. Abell and D. Klenerman, *Langmuir*, 2008, **24**, 1659-1664.
7. C. Y. Zhang, H. C. Yeh, M. T. Kuroki and T. H. Wang, *Nat. Mater.*, 2005, **4**, 826-831.
8. C.-y. Zhang and L. W. Johnson, *Anal. Chem.*, 2009, **81**, 3051-3055.
9. X. S. Xie and J. K. Trautman, *Annu. Rev. Phys. Chem.*, 1998, **49**, 441-480.
10. S. Weiss, *Science*, 1999, **283**, 1676-1683.
11. T. Ha, I. Rasnik, W. Cheng, H. P. Babcock, G. H. Gauss, T. M. Lohman and S. Chu, *Nature*, 2002, **419**, 638-641.
12. A. Castro and J. G. K. Williams, *Analytical Chemistry*, 1997, **69**, 3915-3920.
13. A. Orte, T. D. Craggs, S. S. White, S. E. Jackson and D. Klenerman, *J. Am. Chem. Soc.*, 2008, **130**, 7898-7907.
14. C. Joo, H. Balci, Y. Ishitsuka, C. Buranachai and T. Ha, *Annu. Rev. Biochem*, 2008, **77**, 51-76.
15. W. T. Mason, ed., *Fluorescent and luminescent probes for biological activity.*, 2nd edn., Academic Press, London, 1999.
16. I. L. Medintz and H. Mattoussi, *PCCP*, 2009, **11**, 17-45.
17. B. O. Dabbousi, J. RodriguezViejo, F. V. Mikulec, J. R. Heine, H. Mattoussi, R. Ober, K. F. Jensen and M. G. Bawendi, *J. Phys. Chem. B*, 1997, **101**, 9463-9475.
18. N. C. Shaner, P. A. Steinbach and R. Y. Tsien, *Nat. Methods*, 2005, **2**, 905-909.
19. H. Weller, *Curr. Opin. Colloid Interface Sci.*, 1998, **3**, 194-199.
20. Y. P. Sun, B. Zhou, Y. Lin, W. Wang, K. A. S. Fernando, P. Pathak, M. J. Meziani, B. A. Harruff, X. Wang, H. F. Wang, P. J. G. Luo, H. Yang, M. E. Kose, B. L. Chen, L. M. Veca and S. Y. Xie, *J. Am. Chem. Soc.*, 2006, **128**, 7756-7757.

21. M. Dahan, T. Laurence, F. Pinaud, D. S. Chemla, A. P. Alivisatos, M. Sauer and S. Weiss, *Opt. Lett.*, 2001, **26**, 825-827.

22. G. S. Baird, D. A. Zacharias and R. Y. Tsien, *Proc. Natl. Acad. Sci.*, 2000, **97**, 11984-11989.

23. I. L. Medintz, H. T. Uyeda, E. R. Goldman and H. Mattoussi, *Nat. Mater.*, 2005, **4**, 435-446.

24. T. Pons, H. T. Uyeda, I. L. Medintz and H. Mattoussi, *J. Phys. Chem. B*, 2006, **110**, 20308-20316.

25. C. Murray, D. Norris and M. G. Bawendi, *J. Am. Chem. Soc.*, 1993, **115**, 8706-8715.

26. X. Peng, J. Wickham and A. P. Alivisatos, *J. Am. Chem. Soc.*, 1998, **120**, 5343-5344.

27. P. Reiss, M. Protière and L. Li, *Small*, 2009, **5**, 154-168.

28. M. A. Hines and P. Guyot-Sionnest, *The Journal of Physical Chemistry*, 1996, **100**, 468-471.

29. X. Peng, M. C. Schlamp, A. V. Kadavanich and A. Alivisatos, *J. Am. Chem. Soc.*, 1997, **119**, 7019-7029.

30. L. Spanhel, M. Haase, H. Weller and A. Henglein, *J. Am. Chem. Soc.*, 1987, **109**, 5649-5655.

31. N. Gaponik, D. V. Talapin, A. L. Rogach, K. Hoppe, E. V. Shevchenko, A. Kornowski, A. Eychmüller and H. Weller, *The Journal of Physical Chemistry B*, 2002, **106**, 7177-7185.

32. A. L. Rogach, A. Kornowski, M. Gao, A. Eychmüller and H. Weller, *The Journal of Physical Chemistry B*, 1999, **103**, 3065-3069.

33. Y. Zheng, Z. Yang and J. Y. Ying, *Adv. Mater.*, 2007, **19**, 1475-1479.

34. V. Lesnyak, N. Gaponik and A. Eychmüller, *Chem. Soc. Rev.*, 2013, **42**, 2905-2929.

35. Y. He, H.-T. Lu, L.-M. Sai, Y.-Y. Su, M. Hu, C.-H. Fan, W. Huang and L.-H. Wang, *Adv. Mater.*, 2008, **20**, 3416-3421.

36. Q. Zeng, X. Kong, Y. Sun, Y. Zhang, L. Tu, J. Zhao and H. Zhang, *J. Phys. chem. C*, 2008, **112**, 8587-8593.

37. W. C. Chan and S. Nie, *Science*, 1998, **281**, 2016-2018.

38. H. Mattoussi, J. M. Mauro, E. R. Goldman, G. P. Anderson, V. C. Sundar, F. V. Mikulec and M. G. Bawendi, *J. Am. Chem. Soc.*, 2000, **122**, 12142-12150.

39. M. Bruchez, M. Moronne, P. Gin, S. Weiss and A. P. Alivisatos, *Science*, 1998, **281**, 2013-2016.

40. D. Gerion, F. Pinaud, S. C. Williams, W. J. Parak, D. Zanchet, S. Weiss and A. P. Alivisatos, *J. Phys. Chem. B*, 2001, **105**, 8861-8871.

41. W. Guo, J. J. Li, Y. A. Wang and X. Peng, *Chem. Mater.*, 2003, **15**, 3125-3133.

42. B. Dubertret, P. Skourides, D. J. Norris, V. Noireaux, A. H. Brivanlou and A. Libchaber, *Science*, 2002, **298**, 1759-1762.

43. B. Ballou, B. C. Lagerholm, L. A. Ernst, M. P. Bruchez and A. S. Waggoner, *Bioconj. Chem.*, 2004, **15**, 79-86.

44. F. Osaki, T. Kanamori, S. Sando, T. Sera and Y. Aoyama, *J. Am. Chem. Soc.*, 2004, **126**, 6520-6521.

45. A. P. Alivisatos, W. Gu and C. Larabell, *Annu. Rev. Biomed. Eng.*, 2005, **7**, 55-76.

46. R. Mahtab, H. H. Harden and C. J. Murphy, *J. Am. Chem. Soc.*, 1999, **122**, 14-17.

47. K.-i. Hanaki, A. Momo, T. Oku, A. Komoto, S. Maenosono, Y. Yamaguchi and K. Yamamoto, *Biochem. Biophys. Res. Commun.*, 2003, **302**, 496-501.

48. G. P. Mitchell, C. A. Mirkin and R. L. Letsinger, *J. Am. Chem. Soc.*, 1999, **121**, 8122-8123.

49. H. Y. Zhang, P. G. Stockley and D. J. Zhou, *Faraday Discuss.*, 2011, **149**, 319-332.

50. A. R. Clapp, I. L. Medintz, J. M. Mauro, B. R. Fisher, M. G. Bawendi and H. Mattoussi, *J. Am. Chem. Soc.*, 2004, **126**, 301-310.

51. I. L. Medintz, J. Konnert, A. Clapp, I. Stanish, M. Twigg, H. Mattoussi, J. M. Mauro and J. Deschamps, *Proc. Natl. Acad. Sci. USA*, 2004, **101**, 9612-9617.

52. A. M. Dennis and G. Bao, *Nano Lett.*, 2008, **8**, 1439-1445.

53. K. E. Sapsford, T. Pons, I. L. Medintz, S. Higashiya, F. M. Brunel, P. E. Dawson and H. Mattoussi, *J. Phys. Chem. C*, 2007, **111**, 11528-11538.

54. S. Pathak, S.-K. Choi, N. Arnheim and M. E. Thompson, *J. Am. Chem. Soc.*, 2001, **123**, 4103.

55. H. Zhang and D. Zhou, *Chem. Commun.*, 2012, **48**, 5097-5099.

56. R. Hong, N. O. Fischer, A. Verma, C. M. Goodman, T. Emrick and V. M. Rotello, *J. Am. Chem. Soc.*, 2004, **126**, 739-743.

57. H. T. Uyeda, I. L. Medintz, J. K. Jaiswal, S. M. Simon and H. Mattoussi, *J. Am. Chem. Soc.*, 2005, **127**, 3870-3878.

58. X. Gao, Y. Cui, R. M. Levenson, L. W. Chung and S. Nie, *Nat. Biotechnol.*, 2004, **22**, 969-976.

59. J. R. Lakowicz, ed., *Principles of Fluorescence Spectroscopy*, 2nd edn., Kluwer Academic, New York, 1999.

60. R. Wargnier, A. V. Baranov, V. G. Maslov, V. Stsiapura, M. Artemyev, M. Pluot, A. Sukhanova and I. Nabiev, *Nano Lett.*, 2004, **4**, 451-457.

61. N. N. Mamedova, N. A. Kotov, A. L. Rogach and J. Studer, *Nano Lett.*, 2001, **1**, 281-286.

62. A. R. Clapp, I. L. Medintz, B. R. Fisher, G. P. Anderson and H. Mattoussi, *J. Am. Chem. Soc.*, 2005, **127**, 1242-1250.

63. L. Dyadyusha, H. Yin, S. Jaiswal, T. Brown, J. J. Baumberg, F. P. Booy and T. Melvin, *Chem. Commun.*, 2005, 3201-3203.

64. I. Potapova, R. Mruk, C. Hubner, R. Zentel, T. Basche and A. Mews, *Angew. Chem. Int. Ed*, 2005, **44**, 2437-2440.

65. W. R. Algar and U. J. Krull, *Anal. Bioanal. Chem.*, 2008, **391**, 1609-1618.

66. D. J. Zhou, J. D. Piper, C. Abell, D. Klenerman, D. J. Kang and L. M. Ying, *Chem. Commun.*, 2005, 4807-4809.

67. I. L. Medintz, A. R. Clapp, H. Mattoussi, E. R. Goldman, B. Fisher and J. M. Mauro, *Nat. Mater.*, 2003, **2**, 630-638.

68. A. R. Clapp, I. L. Medintz, H. T. Uyeda, B. R. Fisher, E. R. Goldman, M. G. Bawendi and H. Mattoussi, *J. Am. Chem. Soc.*, 2005, **127**, 18212-18221.

69. T. Pons, I. L. Medintz, X. Wang, D. S. English and H. Mattoussi, *J. Am. Chem. Soc.*, 2006, **128**, 15324-15331.

70. H. Lu, O. Schops, U. Woggon and C. M. Niemeyer, *J. Am. Chem. Soc.*, 2008, **130**, 4815-4827.

71. D. E. Prasuhn, A. Feltz, J. B. Blanco-Canosa, K. Susumu, M. H. Stewart, B. C. Mei, A. V. Yakovlev, C. Loukov, J. M. Mallet, M. Oheim, P. E. Dawson and I. L. Medintz, *Acs Nano*, 2010, **4**, 5487-5497.

72. W. R. Algar, M. G. Ancona, A. P. Malanoski, K. Susumu and I. L. Medintz, *Acs Nano*, 2012, **6**, 11044-11058.

73. W. R. Algar, A. P. Malanoski, K. Susumu, M. H. Stewart, N. Hildebrandt and I. L. Medintz, *Anal. Chem.*, 2012, **84**, 10136-10146.

74. H. T. Li, L. M. Ying, J. J. Green, S. Balasubramanian and D. Klenerman, *Anal. Chem.*, 2003, **75**, 1664-1670.

75. R. W. Clarke, A. Orte and D. Klenerman, *Anal. Chem.*, 2007, **79**, 2771-2777.

76. H. T. Li, D. J. Zhou, H. Browne, S. Balasubramanian and D. Klenerman, *Analytical Chemistry*, 2004, **76**, 4446-4451.

77. H. C. Yeh, Y. P. Ho, I. M. Shih and T. H. Wang, *Nucleic Acids Res.*, 2006, **34**, e35.

78. C. Y. Zhang and L. W. Johnson, *Analyst*, 2006, **131**, 484-488.

79. B. D. Chithrani and W. C. W. Chan, *Nano Lett.*, 2007, **7**, 1542-1550.

80. Y. Zheng, S. Gao and J. Y. Ying, *Adv. Mater.*, 2007, **19**, 376-380.

Chapter 2
FRET between small-molecule ligands capped QD donors and FP acceptors

2.1 Introduction

The development of rapid, sensitive and selective detection methods for water-soluble analytes is of critical importance in biosensing, environmental surveys and clinical diagnostics. Over the past decade, strongly fluorescent semiconductor nanocrystals (also known as QDs) that have prominent photo-stability, wide absorption cross sections and size-tunable, narrow symmetric emission, have been demonstrated as promising fluorescent probes for a wide range of imaging, biosensing and diagnostic applications.[1-7] In particular, their broad absorption and narrow symmetric emission make the QDs extremely well-suited as donors in FRET based sensors with organic fluorophores or FPs as acceptors.[8-9] This is because this FRET design can take the full advantage of the broad absorption and narrow symmetry emission of the QD; such that wide choices of the excitation wavelengths can be selected to minimise direct excitation of the acceptor and narrow band-path filters used to effectively separate the donor-acceptor fluorescence which lead to greatly reduced fluorescence background and hence higher sensitivity.[9-11] Over the past decade, QD-FRET based sensors have attracted considerable interest because of their important applications in biosensing, disease diagnostics, explosive detection, and environmental monitoring.[7, 12-14]

Since most high quality QDs (*e.g.* CdSe/ZnS core/shell) are synthesized by a high- temperature organometallic route in high-boiling point, coordinating organic solvents, they are naturally capped with hydrophobic ligands, such as trioctylphosphine oxide (TOPO), trioctylphosphine, and therefore insoluble in aqueous media.[15-18] To facilitate their biological applications, QDs have to be made water-soluble; the hydrophobic TOPO ligands are either capped with amphiphilic polymers/PEGylated lipids *via* hydrophobic van der Waals interactions[19-20] or completely substituted by hydrophilic small molecule ligands *via* ligand exchange reactions.[21-25] For biosensing applications, functional biomolecules acting as the bio-recognition elements also need to be conjugated to the QD. This can be done by using covalent or non-covalent linking approaches. In addition, most QD sensors are FRET based, where the efficiency E decreases dramatically with the increasing donor-acceptor distance (r), $E = [1 + (r/R_0)^6]^{-1}$ where R_0 is the Förster radius of the QD-dye FRET pair at 1:1 molar ratio. A key requirement is therefore to create a compact, stable QD-bioconjugate to increase sensor sensitivity and robustness. Over the past few years, metal ion-polyhistidine coordination based self-assembly has proven to be an attractive way to prepare compact, functional QD-bioconjugates.[13, 26-29] This is because polyhistidine is able to chelate the metal ions on some of the most commonly used CdSe/ZnS or CdTe QD surfaces.[26] It can produce functional, compact QD-FRET systems with relatively small donor- acceptor distances. Moreover, the number of acceptors arrayed on a single QD can also be controlled through modulation of the respective molar ratios in this highly efficient, self-assembly process.[30-31]

More recently, FRET systems based on the self-assembly of mFruit FPs (His_6-tagged) and several commercial water-soluble CdSe/ZnS core/shell QDs have been reported.[12-13, 32-33] Results show that different QD surface capping agents

have a profound impact on the FRET efficiency of the self-assembled systems.[33] For example, at a mCherry:QD ratio of 12, an *E* of ~50% was observed for a DHLA capped QD; while the QD capped by DHLA-PEG_{600}-OH exhibited an *E* of only ~ 20%, possibly due to the steric hindrance from the PEG coating that may prevent efficient FP binding.[33] However, to date, FRET systems with CdSe/ZnS core/shell QDs capped with other commonly used short thiolated ligands, which may form more compact QD-FP conjugates and hence more efficient FRET, and how such ligands may affect their FRET behaviour have not yet been reported.

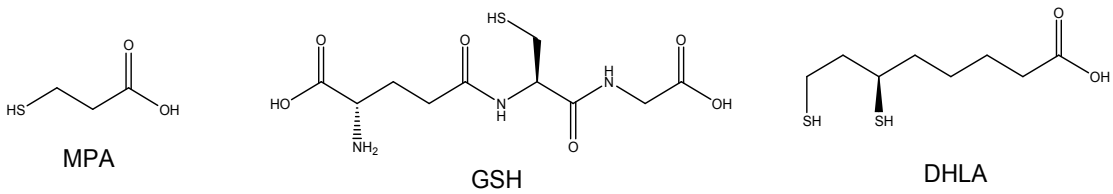

Figure 2.1 Chemical structures of the three ligands used in this study. (Reprinted by permission of the PCCP Owner Societies)[34]

In this chapter, systematic studies on the FRET between QD donors capped with different small-molecule ligand coatings (MPA; DHLA; and GSH, see Figure 2.1) and a His_6-tagged FP (mCherry) acceptor are described. The FP was self-assembled onto the QDs capped with three different short thiolated ligands to form the QD-FP FRET systems. I found that the QD-FP FRET was strongly dependent on the QD surface small-molecule coating in terms of both the resulting donor-acceptor distance and FRET efficiency. Two types of QD-FP interaction schemes were proposed to explain the significant difference in the apparent donor-acceptor distance for QDs capped with these different short

thiolated ligands. The dissociation constants K_d for specific QD-FP self-assembly interactions were also measured.

2.2 Materials and methods

2.2.1 Instruments

UV-vis absorption spectra of QDs and mCherry were recorded on Varian Cary 50 UV-Visible Spectrophotometer (range from 300-800 nm). Fluorescence measurements were performed on a Spex Fluoro Max-3 Spectrofluorometer. Transmission electron microscopy (TEM) micrographs were taken on the Philips CM200 transmission electron microscope. The specimen for TEM study was prepared by depositing a drop of the QD solution onto a carbon-coated TEM grid. pH adjustments were done using a Fisher brand Hydrus 300 pH meter at room temperature. Millipore water (resistance >18.2 MΩ·cm), purified by ELGA Purelab classic UVF system, was used for all experiments and making buffers. All other chemicals and reagents were purchased from Fisher Scientific and used as received unless otherwise stated. The QYs of QDs were measured in water against rhodamine 6G in ethanol standard (QY = 95%) as described in a previous publication.[35-36]

2.2.2 QDs and mCherry preparations

Table 2.1 shows the constituents information of phosphate-buffered saline (PBS) solution and ten-fold concentrated PBS (10 × PBS) I used. All of the salts are dissolved in the deionized water, and the pH is adjusted to 7.4 with HCl or NaOH.

Table 2.1 Information of PBS constituents

Salt	PBS Concentration (Mm)	10 × PBS Concentration (mM)
NaCl	137	1370
KCl	10	100
Na_2HPO_4	2.7	27
KH_2PO_4	1.8	18

The CdSe/ZnS core/shell QDs (EM ~540) were purchased from Evident Technologies Inc (Troy, USA). They were supplied in toluene solutions capped with TOPO ligands with an average crystal core diameter of ~3.4 nm (namely the TOPO-QD). The water soluble QDs used in this study were prepared by ligand exchange[5, 22-25, 37-39] by Haiyan Zhang, School of Chemistry, University of Leeds (See appendix for details).

The FP, mCherry and its fluorophore engineered version (P, with the fluorophore residue sequences mutated and so no longer fluorescent), were engineered, expressed and purified by Dr Michael Webb and Dr Jeff Hollins at the School of Chemistry at Leeds. Both proteins were tagged with an N-termini His_6-tag that can facilitate the QD-FP self-assembly *via* metal affinity coordination interactions. The detailed synthetic procedures are given in the Appendix.

2.2.3 FRET assays and data analysis

The method for QY determination used here is the comparative method, which involves the use of a standard sample of known QY value. In this regard, Rhodamine 6G (in ethanol under 480 nm excitation) was used as the standard whose QY is 0.95. The QY of the QD were calculated by the equation[5]:

$$Y_u = Y_s \times (F_u/F_s) \times (A_s/A_u) \quad (2.1)$$

Where *Yu, Fu* and *Au* are the QY, integrated fluorescence intensity and absorbance at 480 nm of the QD sample, and *Ys, Fs*, and *As* are the QY, integrated fluorescence intensity and absorbance at 480 nm of Rhodamine 6G.

For steady-state titration studies, the solutions were placed in a 10 mm optical path quartz fluorescence cuvette. The steady-state fluorescence spectra were recorded under an exciting wavelength of 425 nm, corresponding to the minimum absorption of mCherry to minimise the direct excitation of the FP. Both the excitation and emission band-pass were 5 nm and scan rate was 10 nm/s.

The FRET efficiency, *E*, represents the fraction of photon energy that is transferred from the donor to the acceptor non-radiatively. Here, FRET efficiency is presented by donor quenching efficieny which is defined as,[40]

$$E = 1 - \frac{I_{DA}}{I_D} \quad (2.2)$$

Where I_{DA} is the fluorescence intensity of the donor in the presence of the acceptors and I_D is the fluorescence intensity of the donor in the absence of acceptors.

Using the Förster dipole-dipole interaction formulism, the energy transfer efficiency *E* for a single donor FRET with multiple identical acceptors can be expressed as[28]

$$E = \frac{n{R_0}^6}{n{R_0}^6 + r^6} \qquad (2.3)$$

Where *n* is the average number of acceptor molecules interacting with one single donor. R_0 is the Förster radius of the FRET pair at single donor-single acceptor situation, under which *E* = 50% and *r* is the apparent donor-acceptor distance. The Förster radius R_0 is defined as[28]:

$$R_0 = \left(\frac{[9000\times(ln\,10)]{k_p}^2}{128\,\pi^5\,{n_D}^4 N_A}\,Q_Y\,I\right)^{1/6} \qquad (2.4)$$

Where Q_Y is the QY of the donor; n_D is the refractive index of the medium and its value is estimated at 1.4 here; N_A is Avogadro's number; ${k_p}^2$ is the orientation factor and its value varies between 0 (for orthogonal alignment) and 4 (for parallel dipoles), and for random orientated fluorophores ${k_p}^2$ =2/3. The integral of the spectral overlap *I*, is defined as[28]

$$I = \int_0^\infty J(\lambda) = \int_0^\infty F_{D-corr}(\lambda)\,\epsilon_A(\lambda)\,\lambda^4\,d\lambda \qquad (2.5)$$

Where *I* represents the integral of the donor-acceptor spectral overlap over all wavelengths λ; in equation (2.5), $F_{D\text{-}corr}$ and ε_A designate the normalized donor emission profile and the acceptor absorption spectrum, respectively.

For binding strength investigations of the self-assembly interaction between QD and FP, the chosen excitation wavelength was 425 nm and the emission wavelengths were 538 nm for the QD(MPA) and 546 nm for QD(GSH) which corresponded to their respective maximum emission wavelengths. Both the excitation and emission band-pass are 5 nm. The required amount of H_2O, 10 × PBS and QD solutions were first added into a cuvette, and then the time-based scan was started. After about 40 seconds, the required amount of the FP solution was added rapidly and the time-dependent QD emission intensity was monitored continuously.

The photoluminescence (PL) intensity values at different QD concentrations prior to FP addition were normalized by their corresponding highest value to give a value of 1. After the addition of FP, FRET happened immediately. The decrease of QD PL intensity caused by dilution was also corrected. The correction was done by using a concentration dilution factor (DF). According to equation (2.2), the formula used to calculate QD quenching efficiency is modified to be

$$\mathrm{E} = 1 - \mathrm{I}/\mathrm{DF} \qquad (2.6)$$

Where *I* represents the final normalized QD PL intensities at different concentrations; *DF* represents the dilution factor.

The general form of Hill equation is

$$\frac{[AB]}{[A]_{total}} = \frac{{[B]_{free}}^{h}}{{[B]_{free}}^{h} + {K_d}^{h}} \qquad (2.7)$$

And the condition under which $[B]_{free}$ ~ $[B]_{total}$ is $[B]_{free}$>>[AB], which usually requires $[B]_{total}$ >> $[A]_{total}$. And the hill equation utilized here to fit the fluorescence data is defined as[13, 41]

$$E = E_{max}\left[\frac{1}{1+(K_d/c)^h}\right] = \frac{E_{max}\times c^h}{c^h + {K_d}^h} \qquad (2.8)$$

Where E_{max} is the maximum FRET efficiency, c is the concentration of the acceptor, K_d is the dissociation constant defined as the acceptor concentration at which the quenching efficiency of the QDs is 50%.[13] Comparison of equations 2.7 and 2.8 shows that it is assumed $c = [B]_{free}$ and $E / E_{max} = [AB] / [A]_{total}$. The hill coefficient, h, in this equation could provide specific information about the cooperativity of the self-assembly interaction.

For the investigation of the relationship between concentration and acceptor emission intensity in QD-FP systems, the required amounts of H_2O, PBS and FP were first mixed in the cuvette with the scan started. Then after about 40 seconds of base line scan, the required amount of the QD solution was added rapidly and the FP fluorescence was monitored continuously. The corresponding QD solutions without FP were used for background control here. Sensitized FP emission intensity was obtained by deducting the QD contribution from the total emission intensity at 605 nm, the maximum FP emission wavelength.

2.3 FRET studies between QD and FP

2.3.1 Determination of the Förster radius for QD-FP pairs

According to the obtained fluorescence intensity of QD and Rhodmine 6G (see Figure 2.2), the QYs of the three QDs were calculated following the equation (2.1). Compared to the parent TOPO-QD, the QYs of QD(MPA) and QD(DHLA) decreased by around 60% (from 71% to ~30%), in good agreement with earlier reports.[22, 38] However, the QD(GSH) showed a much smaller QY decrease of only 8% (from 71% to 65%), suggesting that GSH is better at preserving the QY of QD than MPA or DHLA.

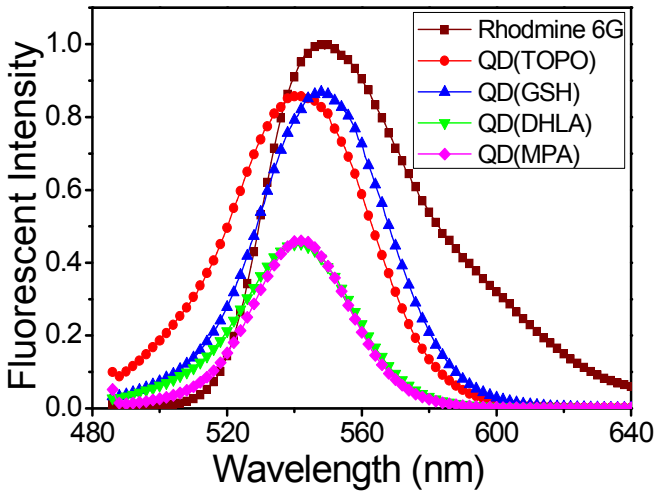

Figure 2.2 The relative fluorescence spectra of the QDs (all of the same concentration). (Reproduced by permission of the PCCP Owner Societies) [34]

The much smaller decrease of QY for QD(GSH) compared to the MPA- or DHLA- capped QD after the ligand exchange may reflect the mild reaction conditions (simply stirring at room-temperature) used to make QD(GSH), which lead to smaller levels of damage to the ZnS shell quality (*e.g.* etching away some surface Zn^{2+} ions to create surface defects) as compared to the harsher

conditions used to prepare the QD(DHLA) (heating under reflux), enabling the QD to maintain a higher QY.[42]

The normalized fluorescence spectra of the three prepared QDs are shown in Figure 2.3. They all show the characteristic narrow (with a full-width at half-maximum of *ca* 30 nm) and symmetric fluorescence emission of the parent QD (TOPO capped), where the emission peaks remain virtually unchanged for the MPA and DHLA capped QDs, which remained at ~538 nm, while that for the GSH capped QDs appeared to have red-shifted by 7 nm to 545 nm. This suggests that all the QD emissions are from exiton recombinations.

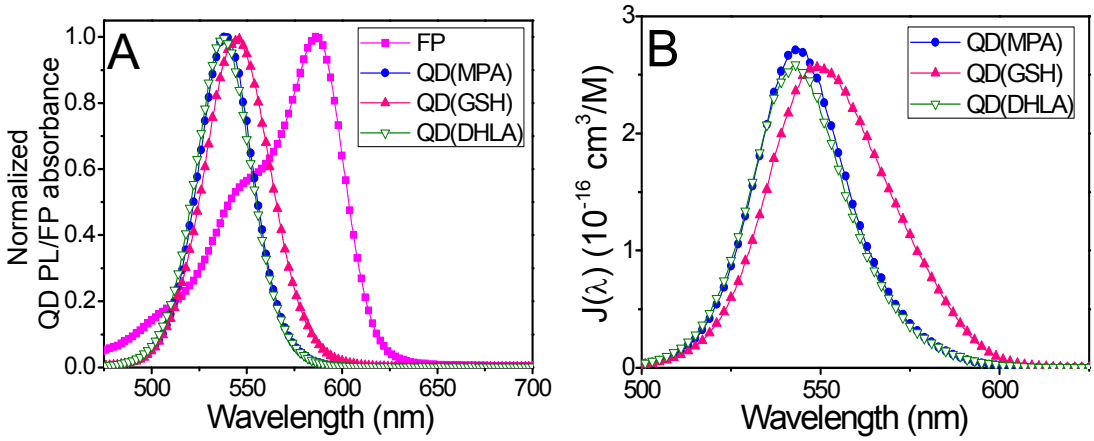

Figure 2.3 Photophysical characteristics of the QD donors and FP acceptor.

(A) Normalized emission spectra of the three QDs (QD(MPA), QD(GSH) and QD(DHLA) are shown in blue, red and green lines, respectively) and the absorption spectrum of FP (purple square). **(B)** Spectral overlap functions for each of the three QD -FP pairs. (Reproduced by permission of the PCCP Owner Societies) [34]

The Förster radius of the donor-acceptor pair (R_0) is the distance at which the energy transfer efficiency is 50% for a single-donor-single-acceptor FRET system. R_0 value depends on several parameters, especially the overlap integral of the donor emission spectrum with that of the acceptor absorption spectrum (See Figure 2.3). The corresponding R_0 values for these QD-FP FRET pairs were determined using equation (2.4): the results are summarized in Table 2.2. The values of the overlap integral (I) for each of the systems were also calculated. The R_0 value varies from one pair to another, with the QD(GSH) being the largest while the QD(MPA) being the smallest, which is largely determined by the magnitudes of the spectral overlap and the QY of the QDs.

Table 2.2 Calculated Förster radiuses (R_0) for the three QD -FP pairs. (Reproduced by permission of the PCCP Owner Societies)[34]

D-A pair	Overlap integral I /cm^3×M^{-1}	QY	Förster distance R_0 /Å
QD(MPA)-FP	9.27×10^{-14}	0.27	39.5
QD(GSH)-FP	1.10×10^{-13}	0.65	47.1
QD(DHLA)-FP	8.97×10^{-14}	0.31	40.2

2.3.2 QD-FP FRET study by static fluorescence scan

2.3.2.1 QD-FP FRET titrations

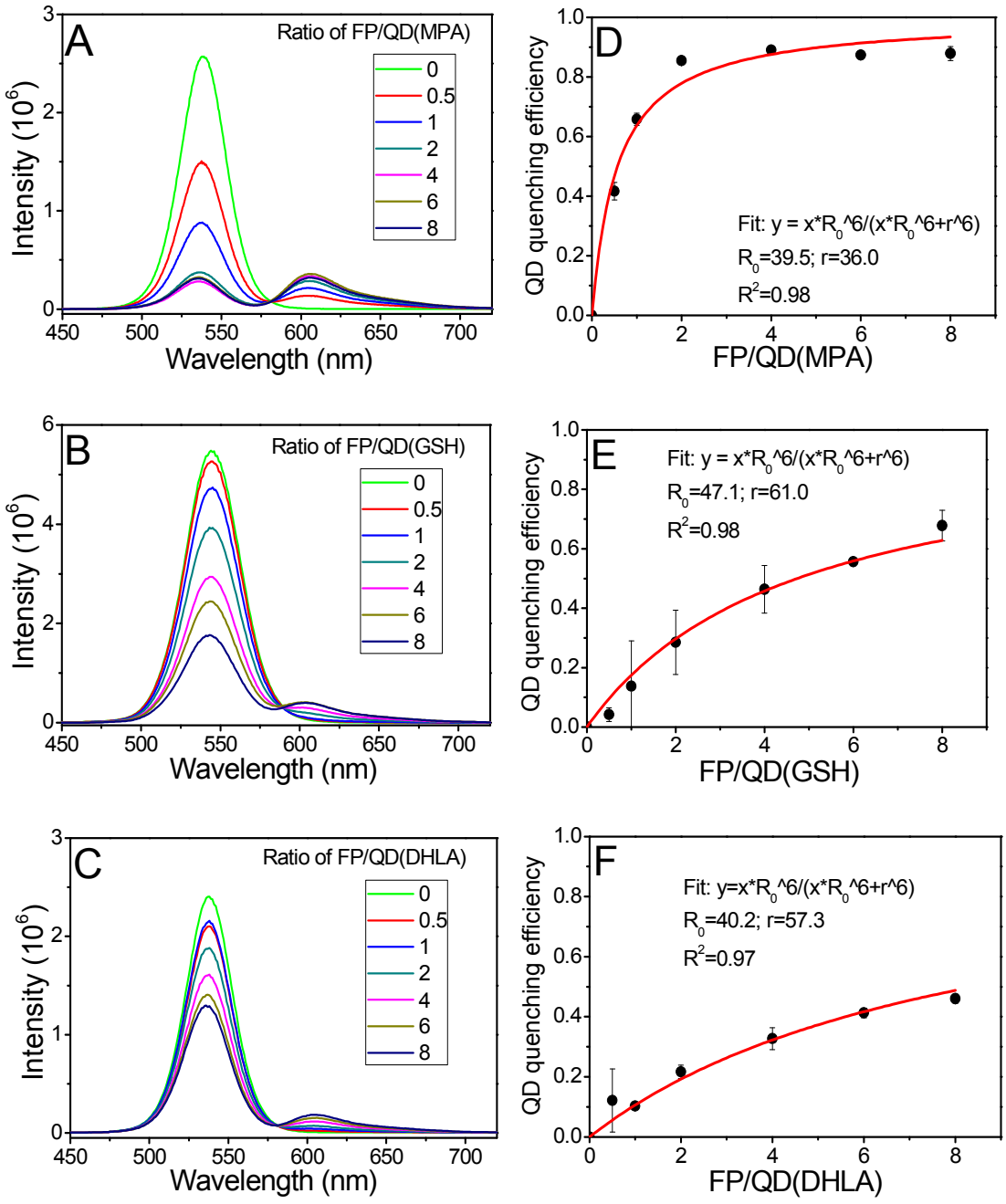

Figure 2.4 Fluorescent emission spectra and the corresponding QD quenching efficiencies for different ligand capped QD-FP FRET systems at different QD:FP ratios.

The excitation wavelength is 425 nm. **(A-C)** correspond to the fluorescence spectra of QD(MPA)-FP, QD(GSH)-FP, and QD(DHLA) -FP pairs, respectively, and **(D-F)** give the plots of the corresponding FRET efficiencies as a function of the FP-to-QD ratio with fits for the three QD-FP pairs. (Reproduced by permission of the PCCP Owner Societies)[34]

QD-FP bioconjugate complexes were prepared by adding appropriate amounts of the FP and QDs capped with different small molecule coatings into PBS. The final concentration for the QDs in the conjugates was 40 nM and the FP/QDs molar ratios were ranged from 0 to 8.

The fluorescent emission spectra after excitation at 425 nm for three QD-FP FRET systems at increasing ratio of FP to QD are shown in Figure 2.4A-C. The fluorescence backgrounds from FP direct excitation (determined from FP-only samples excited at 425 nm, the λ_{min} of the FP), although small, were also carefully subtracted from these spectra. The corresponding donor quenching (FRET) efficiency as a function of the FP:QD ratio are shown in Figure 2.4D-F, respectively. The fluorescence quenching data were fitted accordingly to the single QD donor-multiple identical acceptor FRET model,[32] and the apparent separation distances between the donor and acceptor in each of the FRET pairs were calculated from these steady-state fluorescence data using equations (2.2) and (2.3) and the results are summarized in Table 2.3. The measured donor-acceptor FRET distance (*r*) for the QD(DHLA)-FP complex is *ca* 58 Å, which is consistent with the literature.[13]

Figure 2.4A-C show that the QD fluorescence (~540 nm) is quenched significantly while the FP fluorescence (~605 nm) is simultaneously enhanced with the increasing FP:QD ratio, suggesting QD-sensitized FRET. Comparing the donor quenching efficiencies and the apparent donor-acceptor distances obtained for the three FRET systems, it is clear that different small-molecule ligand capping on the QD appears to have a significant impact on the QD-FP FRET behaviours. The FRET interactions could be roughly categorized into two groups. For Group I, (QD(MPA), the QD fluorescence quenching efficiency as

well as the FP FRET signal) increased very rapidly with the increasing FP:QD ratio, reaching a saturated value of ~85% at a low FP:QD ratio of only 2:1. As the accepter-to-donor ratio further increases to above 2, the donor quenching efficiency (as well as the FP FRET signal) did not show any apparent change. While for the GSH- and DHLA- capped QDs (Group II), there was a progressive decrease in the QD fluorescence accompanied with a simultaneous gradual increase in the FP emission as the FP:QD ratio is systematically increased from 0 to 8, similar to the observations for the DHLA-QD system reported by Bao *et al.*[33] There was no sudden change of the quenching behaviour as a function of the increasing FP:QD ratio. Furthermore, the apparent FRET distance (r ~60 Å) between the QD and FP calculated using the single-donor-multiple-acceptor FRET model (fitted based on equation 2.3 using Origin software) for the Group II is significantly greater than that for the Group I (*ca.* ~35 Å).

2.3.2.2 QD-FP (P) FRET titrations

To eliminate the possible variation of QD fluorescence QY at different QD:FP ratios (which has been reported previously), a corresponding set of samples with the mutated non-fluorescent mCherry (P, essentially the same protein but with the fluorophore core being mutated so that it became non-fluorescent) were also tested. In this system, the final QD concentrations of the conjugates were also 40 nM, while the molar ratios of FP to the QDs were systematically varied but the overall ratio of the protein (FP + P) to the QD was always maintained at 8. This configuration allowed us to maintain a fixed number of proteins per QD, removing issues associated with the possible QD QY change which would further affect the R_0 of the resulting QD-FP FRET pair and hence interfere with the QD-FP FRET study.

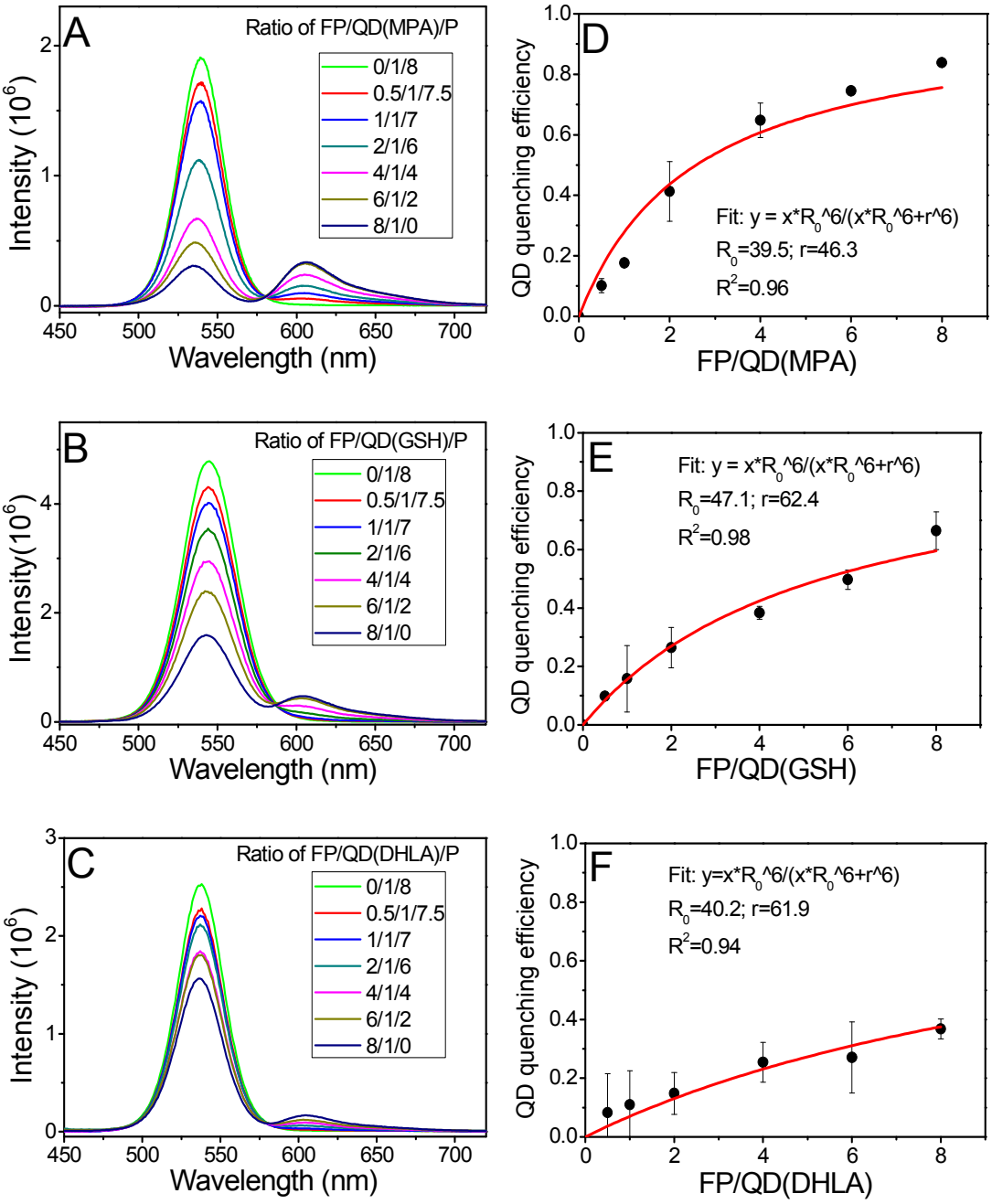

Figure 2.5 Fluorescent emission spectra and the resulting QD quenching efficiencies for the QD-FP-P systems.

The excitation wavelength is 425 nm. The ratios of (FP+P):QD were fixed at 8:1 in these systems. Fluorescent emission spectra **(A-C)** correspond to the QD(MPA)-FP-P, QD(GSH)-FP-P, and QD(DHLA)-FP-P respectively. **(D-F)** show the plots of the corresponding FRET efficiencies as a function of the FP-to-QD ratio for QD(MPA)-FP-P, QD(GSH)-FP-P and QD(DHLA)-FP-P conjugates. (Reproduced by permission of the PCCP Owner Societies)[34]

Table 2.3 The calculated Förster radius (R_0) and measured donor-acceptor FRET distances (r) for the three QD-FP pairs.

FP and (FP + P = 8) show the FRET studies done in the absence and presence of the engineered non-fluorescent mCherry (P) respectively. (Reproduced by permission of the PCCP Owner Societies)[34]

D-A pair	Förster distance R_0 (Å)	*r* (Å) (FP)	*r* (Å) (FP+P=8)
QD(MPA)-FP	39.5	36.0 ± 0.7	46.3 ± 1.0
QD(GSH)-FP	47.1	61.0 ± 0.7	62.4 ± 0.8
QD(DHLA)-FP	40.2	57.5 ± 0.7	61.9 ± 0.9

The fluorescent spectra of the QD-FP-P systems were shown in Figure 2.5A-C. The corresponding FRET (donor quenching) efficiencies as a function of FP to QD ratio were shown in Figure 2.5D-F respectively. Similarly, according to the equation (2.2) and (2.3), the apparent separation distances between donor and acceptor pairs were calculated from these steady-state fluorescence data and the results were shown in Table 2.3. The fluorescent spectra clearly showed that for all the MPA-, GSH-, and DHLA- QD-FP (P) FRET systems, there was a progressive decrease of the QD PL intensity with a simultaneous increase of the FP FRET signal as the number of FPs per QD was increased from 0 to 8, suggesting that all of the FPs were able to bound to the QD and produce FRET.

This conclusion was further supported by a gel-filtration experiment where almost all of the FPs were found to be bound to the QD and co-migrated

together on the gel-filtration column with little free FPs as monitored at 580 nm, the λ_{max} for the FP (the QD does not absorb at this wavelength, see Figure 2.6 for details).

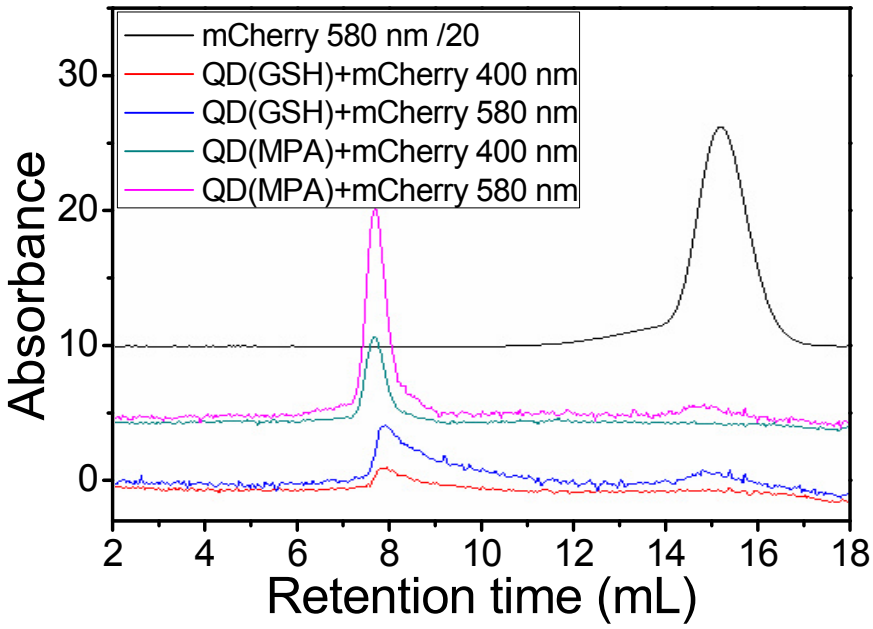

Figure 2.6 Gel-filtration chromatography for QD(MPA), QD(GSH) and FP. Absorption at 580 nm comes from the FP only (corresponding to its maximum absorption, λ_{max}), while that at 400 nm mainly comes from the QD. (Reproduced by permission of the PCCP Owner Societies)[34]

Interestingly, the two QD-FP FRET groups also showed different behaviours in the apparent donor-acceptor distance (*r*) in the presence of the non-fluorescent protein (P), for group I, there was a considerable increase of *r* by about 10 Å (from ~35 to ~46 Å), while for Group II, the *r* values appeared to be effectively unchanged, suggesting that there were some degrees of FP re-arrangement in the self-assembled Group I system but not the group II system.

2.3.3 QD-FP FRET Interaction by time-based scan

2.3.3.1 QD-FP FRET titrations

As representatives of the two groups, titrations of the two QD-FP systems (QD(MPA)-FP and QD(GSH)-FP) were investigated here using the time based scan program (Figure 2.7). The concentration of the QDs was maintained at 40 nM while the ratio of FP/P to QD was changed. The required amount of H_2O, 10 × PBS and FP were first added into a cuvette placed in the fluorimeter, and then the time based scan program was triggered immediately once the required amount of QD solution was added in.

The excitation wavelength (425 nm) was the same as that used in the emission scan method, while the emission wavelengths, where the data were collected, were carefully selected to be 538 nm for QD(MPA) and 545 nm for QD(GSH) which correspond to the maximum emission peaks of the two QDs. Both the excitation and emission band-pass are 5 nm.

The studies on QD-FP titrations using the time based scan method show that the calculated distances between QD and FP are 34.7 ± 0.7 Å for QD(MPA)-FP and 56.8 ± 0.7 Å for QD(GSH)-FP, which are consistent with the QD-FP titrations results (36.0 ± 0.7 Å for QD(MPA)-FP and 61.0 ± 0.7 Å for QD(GSH)-FP) obtained by the static emission scan method. For the QD-P (1:1) system, the engineered non-fluorescent protein P with His_6-tag could also quench the QD PL intensity. The quenching effect is stronger for the QD(MPA)-P compared

to the QD(GSH)-P system with quenching efficiencies of 0.30 and 0.14 respectively.

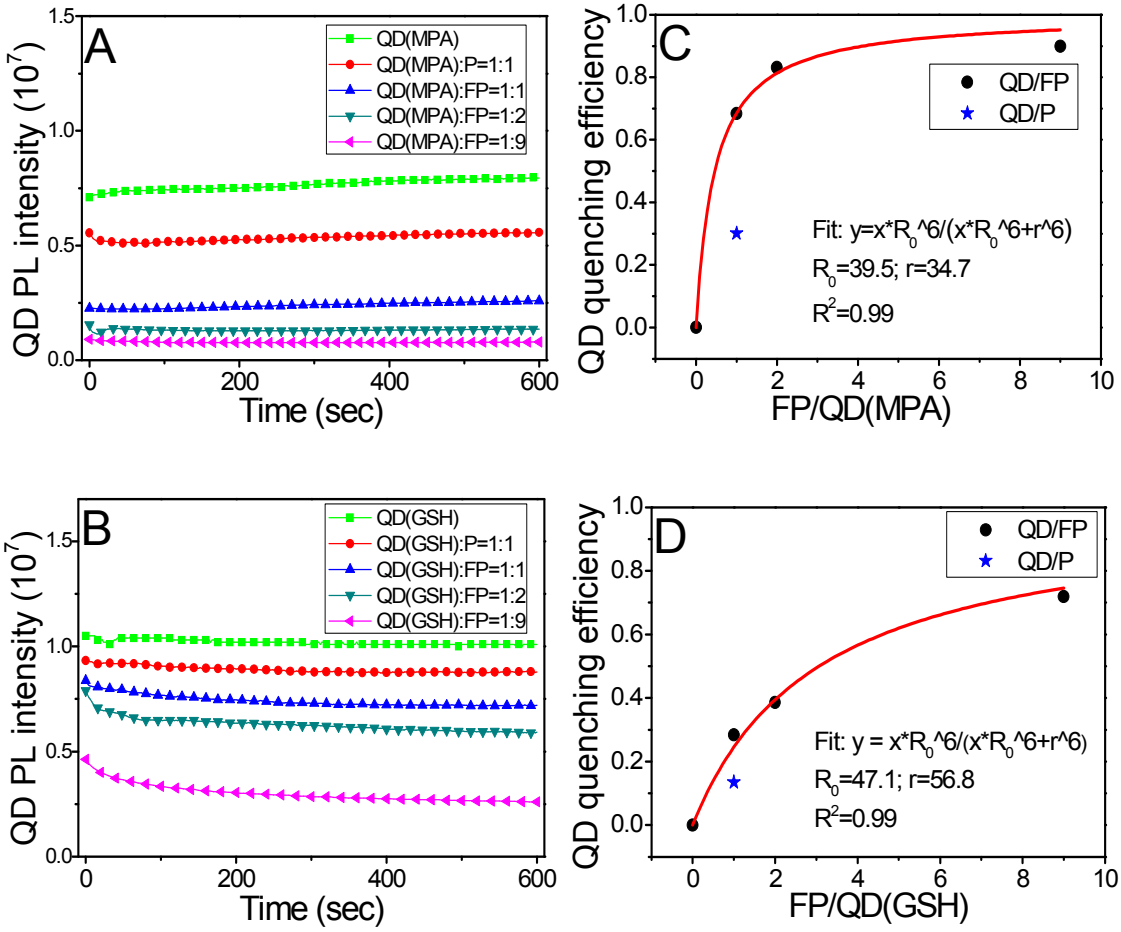

Figure 2.7 Time based fluorescent intensity scans and the corresponding QD quenching efficiencies.

Time based QD PL intensity of QD(MPA)-FP (**A**) and QD(GSH)-FP (**B**) conjugates. Plots of the QD quenching as a function of the FP-to-QD ratio for QD(MPA)-FP **(C)** and QD(GSH)-FP conjugates **(D)**. (Reproduced by permission of the PCCP Owner Societies)[34]

2.3.3.2 Equilibrium dissociation constant for QD-FP FRET interaction

Two representative QD-FP systems (using QD(MPA) and QD(GSH)) were used to estimate the strength of binding between the QD and His_6-tagged proteins by

using the time-based scan method. In this case, the ratio of FP to QD was maintained at 1:1 following the literature[26] while the concentration of QD (FP) was systematically changed from 1 to 16 nM.

To derive the equilibrium dissociation constant K_d of the QD-FP self-assembly, the time based scan method was implemented by following the fluorescence intensity of the QD and the resulting plots of corrected QD intensity as a function of time are shown in Figure 2.8A and 2.8B, respectively. The data were corrected by the sample dilution factor. The corresponding donor quenching efficiencies were fitted by the Hill function in Equation (2.8). Because the basic assumption of Hill equation is $[B]_{total} >> [A]_{total}$ (see equation 2.7), the use of Hill equation for this system may be inappropriate. Hence the K_d and h values are unreliable. Nevertheless, the data do suggest that the binding between QD and FP is srong, and stronger for QD(GSH)-FP than for QD(MPA)-FP.

The time-dependent QD fluorescence traces show a rapid decrease of the QD fluorescence upon the FP addition, and quickly reaching completion in minutes, suggesting the QD-FP self-assembly happens very rapidly and reaches equilibrium in minutes even at low nM concentrations. Fitting of the binding curves using the Hill equation yields apparent K_d values of 1.4 nM for QD(MPA)-FP and 0.63 nM for QD(GSH)-FP systems, respectively (see Table 2.4).

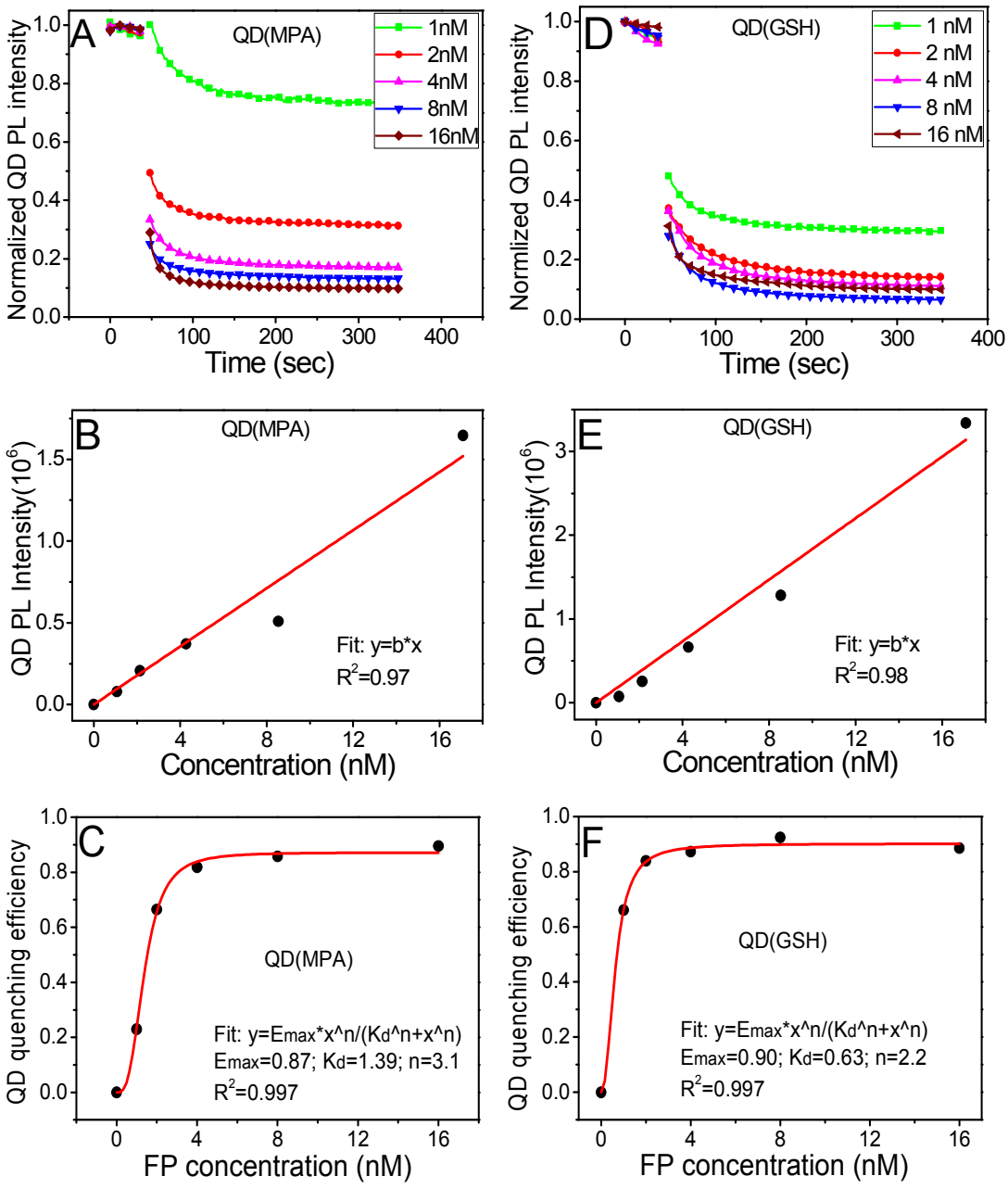

Figure 2.8 K_d measurement for the QD-FP self-assembly interaction using time based scan.

Normalized and corrected time-based QD fluorescence intensity scans (at 540 nm) of the QD(MPA)-FP **(A)** and QD(GSH)-FP **(D)** systems upon the addition of FP at different concentrations. Plots of PL intensity (absolute value of initial QD emission before addition of FP and without normalization) as a function of concentration for QD(MPA) **(B)** and QD(GSH) **(E)**. The QD quenching efficiency (the differences of the PL intensities at 40 s and 300 s) as a function of concentration for the QD(MPA)-FP **(C)** and QD(GSH)-FP **(F)** systems. (Reproduced by permission of the PCCP Owner Societies)[34]

Table 2.4 The calculated FRET and thermodynamic parameters for the QD-FP self-assembly interactions by time-based scan method. (Reproduced by permission of the PCCP Owner Societies)[34]

D-A pair	E_{max}	K_d /nM	*h*
QD(MPA)-FP	0.87±0.01	1.39±0.04	3. 1±0.3
QD(GSH)-FP	0.90±0.02	0.63±0.10	2.2±0.7

These K_d values are at least an order of magnitude lower than those reported for the T2 EviTag-QD-FP systems (~40-90 nM),[13] but are consistent with those of DHLA-QD-Histag-peptide systems (*e.g.* 1.7 nM for His_6-peptide).[26] This observation suggests that QD-Histag based self-assembly is stronger for QD capped by small-molecule ligands than by the T2-Evitag, possibly due to the fact that the Histag has to overcome steric hindrance of the hydrophobic inner-ligands of the T2-Evitag to reach the QD core for binding (the T2-Evitag QD is based on the TOPO-QD capped with PEGylated phospholipids), but this is not required for small-molecule capped QDs.

The Hill coefficients *h* were found to be 3.1 for the QD(MPA)- FP and 2.2 for QD(GSH)-FP interactions, which are both greater than 1, suggesting that the QD-FP self-assembly interaction is positively cooperative, *i.e.* once one FP molecule is bound to a QD, the affinity of the QD for a second FP molecule is increased.[13] This is possibly due to increased tendency to form multimeric structures (*e.g.* DsRed appeared as a tetramer in its crystal structure) of the modified red-fluorescent proteins.[43]

2.3.3.3 Relationship between concentration and acceptor emission intensity

As a representative, the QD(GSH)-FP system was used to study the relationship between concentration and acceptor emission intensity. The QD sensitized FP FRET emission intensity traces (at 605 nm) as a function of time at different concentrations (FP:QD ratio was fixed at 1:1) were studied and the results were shown in Figure 2.9 (all traces were corrected for the residue QD fluorescence and direct excitation of the FP at this wavelength). Following the addition of the QDs at 50 s, a rapid increase of the FP FRET signal was observed (Figure 2.9A).

A good positive linear relationship between the saturated FP FRET signal and FP concentration was found (Figure 2.9B), confirming that the QD-FP self-assembly is very efficient even at low nM concentrations. This is because FRET only happens over short distances (< 10 nm), any free FPs not attached to the QD do not produce any FRET signal. The FP FRET signal enhancement also happened very rapidly, and reached saturation within 100 s of QD addition even at low nanomolar (*e.g.* 4 nM) concentrations.

This behaviour is very similar to that observed in the QD fluorescence quenching shown in Figure 2.8. The fact that the quenching of the QD fluorescence and the enhancement of FP FRET signal happened simultaneously, strongly suggests the observed fluorescence changes are indeed due to QD-FP FRET interactions.

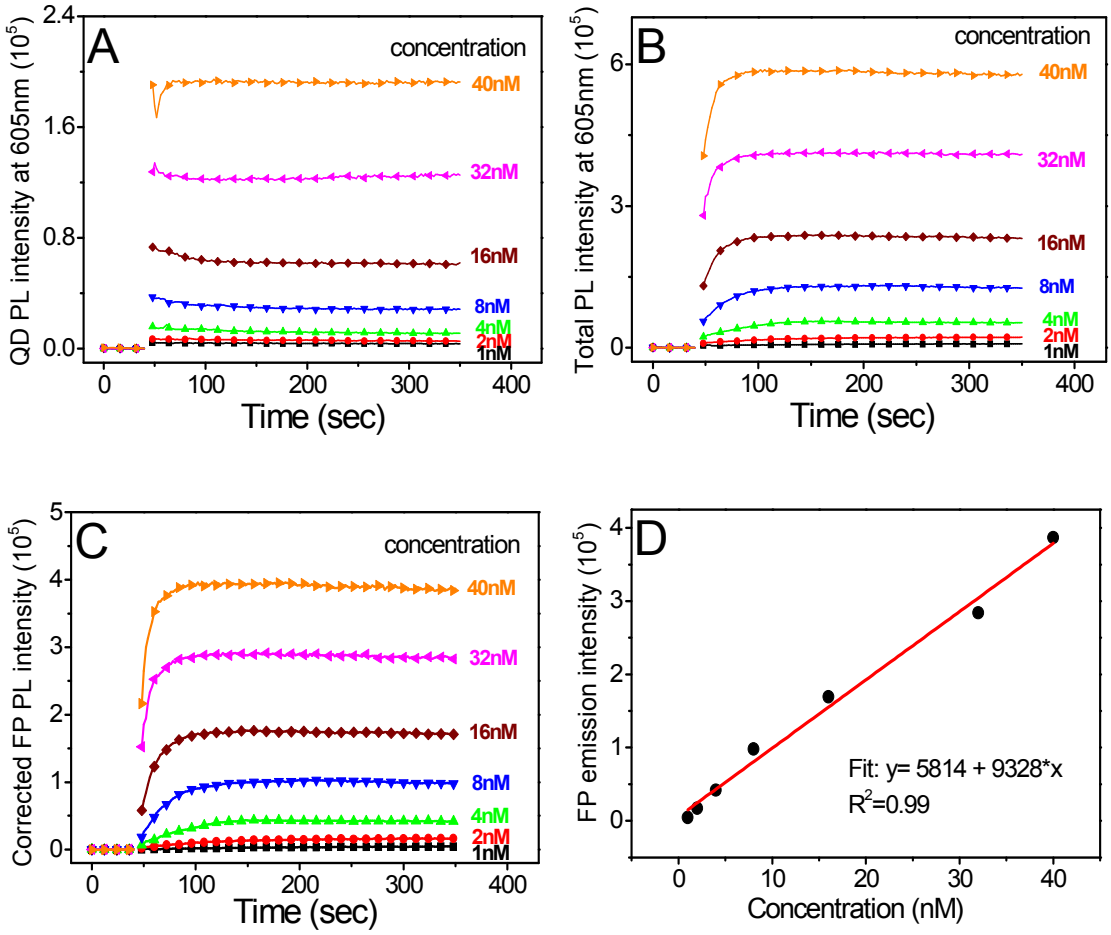

Figure 2.9 Study on relationship between QD(FP) concentration and FP emission intensity using time based scan.

(A) Time based PL intensity scan at 605 nm for QD(GSH) only samples. **(B)** Time based total emission intensity scan at 605 nm (QD + FP) samples. **(C)** QD sensitized FP FRET emission (at 605 nm) intensity traces at different concentrations using time-based scan method. All traces were corrected for the residue QD fluorescence background at this wavelength and FP direct excitation. The required amounts of QDs were added to the FPs at the time point of 50 s to reach a fixed FP:QD ratio of 1:1. **(D)** The corresponding plot of the FP FRET emission intensity as a function of concentration. (Reproduced by permission of the PCCP Owner Societies)[34]

2.3.4 Proposed interaction models for the QD-FP assemblies

To examine whether the size of the core/shell QDs has changed after the ligand exchange, *i.e.* the original TOPO ligands were substituted by water-soluble ligands, TEM images have been taken (see Figure 2.10) on MPA and GSH capped core/shell QDs. It is possible to see QD particle crystal lattice, suggesting these QDs are highly crystalline, but the particle borders could not be identified clearly. A few white circles drawn on each QD crystals were used to indicate the rough diameters of the QD particles, and these gave a rough QD diameter of about 3.4 nm, consistent with the product description from the manufacture (*e.g.* crystal diameter ~ 3.4 nm).

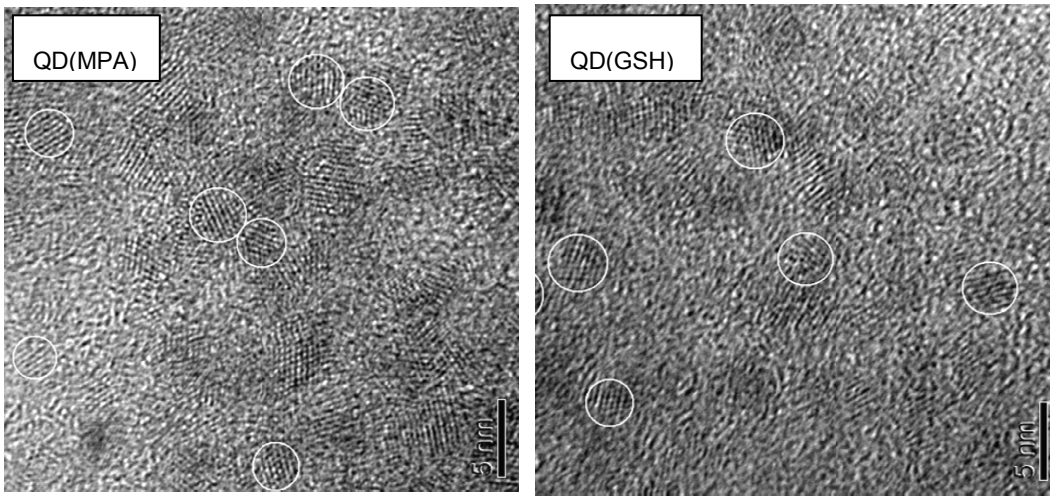

Figure 2.10 Representative TEM images for QD(MPA) and QD(GSH).
(Reproduced by permission of the PCCP Owner Societies)[34]

In thisHis_6-tagged FP design, there is a linker of 4 amino acid residues before the His_6-Tag and the linker between the His_6-tag and the N-terminal of mCherry is 21 residues long. The FP β-barrel structure has dimensions of approximately 50 Å × 25 Å (length × barrel diameter), obtained from the crystal structure of mCherry from the Swiss PDB Viewer.[12] The fluorophore of the mcherry was assumed to be in the middle of the protein barrel.

From the experimental data, the small molecule ligands capping the QD have a significant impact on the FRET between the QD and FP. It is widely accepted that the QD-FP self-assembly interaction is mainly through coordination of the His_6-tag inserted at the N-terminus of the mCherry to the Zn^{2+} ions on the QD ZnS shell surface, which brings the two into close proximity for FRET interaction.[26, 33, 44-45] The small-molecule capping ligands also bind to the QD surface primarily through coordination of their thiolate (with minor contribution from the amine and carboxylic acid) groups to the QD surface Zn^{2+}. Therefore the introduced FPs will compete with the small molecule capping ligands for the QD surface Zn^{2+} ion binding and effectively displace some of the small-molecule ligands. The multi-dentate nature of the QD-DHLA (or GSH) interaction, means the binding strength should be significantly stronger than that for the QD-MPA interaction, which is effectively mono-dentate. As a result, few GSH or DHLA ligands may be displaced by the incoming His_6-tag (FP), leading to high surface ligand densities that repel the FP from QD surface to greater distances, and hence a relatively long QD-FP (donor-acceptor) distance for the GSH or DHLA coated QDs.

Similarly, the weak binding between the MPA and QD means that not only could the His_6-tag substitute more MPA ligands and bind more strongly to the QD but also the FP protein could itself interact with the QD by some weak electrostatic and/or coordination (*via* surface carboxylate and amine groups) interactions that could also displace some coating ligands. This may lead to stronger QD-FP interaction and hence a much shorter apparent QD-FP separation distance.

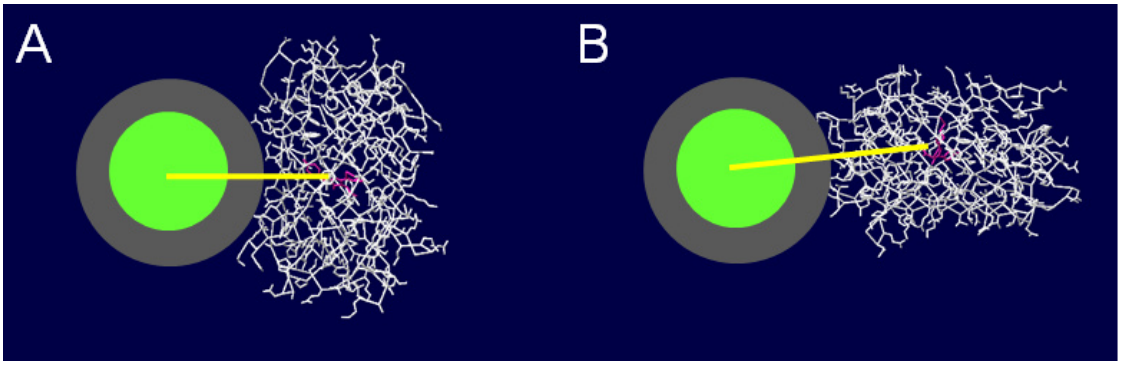

Figure 2.11 Possible model structures for the QD(MPA)-FP **(A)** and QD(GSH)-FP and QD(DHLA)-FP **(B)** conjugates.

The QD with a radius of ~17 Å (**green**) is coated by organic ligands (**grey**). The thickness of all three organic shells is assumed to be 10 Å. The FP is attached to QD surface via His6-tag and the fluorophore is assumed in the middle of the FP (**magenta**). The yellow line corresponds to the theoretical separation distance (39.5 Å for **(A)** and 52 Å for **(B)**). The separation (His6-tag and the 21 amino acid linker between the terminal His6-tag and FP) have been omitted. And only one FP per QD is shown here for simplification.

Effects of the small molecule ligands on the QD-FP self-assembled structure may be qualitatively explained from a simple molecular model shown in Figure 2.11, which illustrates two model conformations for the QD-FP assembly.

According to the measured donor-acceptor distance, Group I (MPA-) QD-FP conjugate that has a smaller separation distance of ~37 Å may correspond to the configuration shown in Figure 2.11A; while the Group II conjugates with bigger separation distances of 60 Å may adapt the configuration shown in Figure 2.11B. Assuming that the QD core/shell crystal is perfectly spherical with a radius of 17 Å (**green**, the same as the manufacture' product description and also the TEM image) and is surrounded by a uniform organic ligand coating shell of ~10 Å (**grey**), and the FP is attached to the QD *via* its His_6 sequence, and the flexible 21 amino acid linker does not contribute to any donor-acceptor

distance, and the chromophore is located at the centre of the FP structure (shown in **magenta**), then these simplified models would yield a donor-acceptor distance of ~40 (17 + 10 + 12.5) and 52 (17 + 10 + 25) Å for structure models **A** and **B,** respectively. These values are in reasonable good agreement with the experimental values of ~37 Å (for Group I, *i.e.* model **A**) and ~60 Å (for Group II, model B). The small deviations from the predicted values may due to the fact that the thickness of the organic ligands in the Group I QD is shorter than 10 Å (the thickness is more likely to be ~ 5 rather than 10 Å), while in model **B**, the distance contribution from the 21 amino acid residue linker cannot be neglected. Despite small differences between the model and experimental values, these simple models can nevertheless provide a qualitative explanation about the different spatial arrangements of the QD-FP assemblies in the two QD-FP FRET groups.

2.4 Conclusions

In summary, I have shown that the FP appended with a His_6-tag can rapidly and effectively self-assemble onto the QDs capped with different short thiolated ligands to form efficient FRET systems. The QD-FP interaction schemes can be roughly categorized into two groups from their corresponding apparent donor-acceptor distance, *r*, values. Highly efficient FRET (*E* ~ 85%) has been achieved at the low FP:QD copy number of 2 for QD capped by weak mono-thiolate ligands (MPA) which has short *r* values of ~35 Å. In contrast, QDs capped by strong chelative ligands (*e.g.* DHLA and GSH) have significantly greater *r* values of ~60 Å. Therefore different short thiolate ligands surrounding the QD can significantly affect the *r* value of the resulting QD-FP FRET systems by as much as 25 Å, despite using the same attachment chemistry (metal

coordination between the His_6-tag and the QD surface Zn^{2+} ions). This implies that the original short thiolate ligands on the QD surface have a profound impact on the orientation of subsequently attached FPs. The possible different conformations for the QD-FP conjugates have been illustrated from two simplified models that can qualitatively explain the observed significant *r* value differences.

The QD-FP self-assembly interactions appeared to happen very rapidly (complete in minutes at low nM concentration), to be very strong (with apparent K_d ~ 1 nM) and positively cooperative. These results suggest that the QD-His_6-tagged biomolecule self-assembly can be used as a general, efficient way for preparing compact, functional QD-bioconjugates. Extension of this self-assembly strategy to other proteins and/or DNA/RNA aptamers[39, 46] may lead to the development of a range of compact, functional QD-bioconjugates that may have broad ranges of sensing and biomedical applications. In general, QDs capped with weak ligands can offer higher FRET efficiency and hence sensitivity, however, they often cannot prevent non-specific adsorption and can compromise sensor robustness and specificity; while strong ligand capped QDs are generally more stable and resistant to non-specific adsorption, they are however generally bulkier, with lower FRET efficiency and potentially less sensitive. Therefore a balance between the requirements for sensitivity, stability and specificity should be carefully considered in designing QD-FRET based sensors, as these requirements are often non-compatible.

2.5 Appendix (Preparations of QD and mCherry)

2.5.1 QD synthesis

As mentioned before, the QDs used in this study are provided by Haiyan Zhang, School of Chemistry, and University of Leeds. The following synthetic protocol is provided by her.

2.5.1.1 Modification of QDs with DHLA

DHLA was used to replace the native TOP/TOPO ligands via ligands exchange.[23, 47-48] QD-TOPO was repeatedly dispersed in toluene and precipitated by adding ethanol, followed by centrifugation and discarding clear supernatant. This process removes the free TOP/TOPO ligands that are not bound to the QDs. The precipitated QD was dissolved in chloroform and mixed with a large excess of DHLA (approx 1:1000 molar ratio). The mixture was purged N_2 for 5-10 minutes, and heated to 60-80 °C for 3~4 hours. The DHLA capped QDs were separated from the dissociated TOP/TOPO by precipitation with heptane and chloroform. EtOH was used to remove the excess DHLA. The DHLA capped QDs (QD-DHLA) were soluble in water, but not in organic solvents. The transformed solubility was the most direct evidence that the ligand exchange had taken place.

2.5.1.2 Preparation of GSH-capped QDs

Glutathione is a small tri-peptide (Glu-Cys-Gly) which has a free thiol amine and two carboxylic acid groups. The thiol group can bind on to the QD surface, while the amine and carboxylic acid groups can promote water-solubility. The preparation of GSH capped QDs has been reported [24].

2.5.1.3 Preparation of MPA-capped QDs

TOPO capped QDs (83.9 nmol/ml 0.25 mL) were precipitated by EtOH as above. The precipitate was dissolved in chloroform (1 mL) to form 20 μM QDs solution. 2000 mg TMAH (Tetramethyl ammonium hydroxide) was mixed with 1000 μL MPA in 20 ml chloroform. The solution was mixed well by vigorous shaking and allowed to stand for 1 h to equilibrate. The bottom organic phase was transferred to a polypropylene tube for ligand exchange with QD. 500 μL 20 μM QD was added to the MPA chloroform solution and mixed well. The solution was allowed to stand at room temperature for 40 h and then 40 h. At the beginning of the reaction, the TOPO-capped QDs were homogenously dispersed in chloroform with MPA. After standing at room temperature for 40 h, the QDs was separated out and gathered as a highly fluorescent droplet suspended on the top of the chloroform. After a further 40 h, the fluorescent droplet precipitated down to the bottom. The precipitate was collected and was washed with ethanol for three times, and then dissolved in water.

2.5.2 Preparation of mCherry and mCherry mutant

As mentioned before, the mCherry (FP) and mCherry mutant (non-fluorescent) used in this study are provided by Jeff Hollins, School of Chemistry, and University of Leeds. The following protocol is provided by him.

Site directed mutagenesis to generate the expression construct pRSETB-mCherryY22F was performed via the QuikChange Site-Directed Mutagenesis protocol (Stratagene). The sequences of the oligonucleotides were 5´-

CCTCAGTTCATG*TT*CGGCTCC-3´ (forward) and 5´-GGCCTTGGAGCC*GA*ACATGAA-3´. Mutation was confirmed by DNA sequencing (GATC Biotech). mCherry and mCherry-Y22F were overexpressed in *Escherichia coli* C41 (DE3)[49] by growth for 24 hours in auto-induction media following the protocol of Studier.[50] Cells were harvested by centrifugation at 10,000*g* for 15 mins at 4 °C before storage at -80 °C. The cell pellet was resuspended in buffer A (50 mM Potassium Phosphate pH 7.4, 100 mM NaCl) with 10 mM imidazole and lysed by sonication using a Bandelm Sonopuls HD2070 sonicator. The lysate was cleared by centrifugation (31,000*g* for 45 min at 4 °C) and the supernatant applied to a pre-equilibrated nickel-NTA agarose column (5ml, Qiagen), and the column washed sequentially using buffer A with 20 mM imidazole and buffer A with 50 mM imidazole. Protein was eluted using buffer A with 500 mM imidazole and collected in 5 ml fractions. Fractions containing protein were pooled, concentrated and further purified by gel filtration (Superdex 200, 26/60 isocratic elution with buffer A).

2.6 References

1. J. M. Klostranec and W. C. W. Chan, *Adv. Mater.*, 2006, **18**, 1953-1964.
2. X. Michalet, F. F. Pinaud, L. A. Bentolila, J. M. Tsay, S. Doose, J. J. Li, G. Sundaresan, A. M. Wu, S. S. Gambhir and S. Weiss, *Science*, 2005, **307**, 538-544.
3. I. L. Medintz and H. Mattoussi, *PCCP*, 2009, **11**, 17-45.
4. R. C. Somers, M. G. Bawendi and D. G. Nocera, *Chem. Soc. Rev.*, 2007, **36**, 579-591.
5. D. J. Zhou, L. M. Ying, X. Hong, E. A. Hall, C. Abell and D. Klenerman, *Langmuir*, 2008, **24**, 1659-1664.

6. C. Y. Zhang, H. C. Yeh, M. T. Kuroki and T. H. Wang, *Nat. Mater.*, 2005, **4**, 826-831.

7. D. E. Prasuhn, J. B. Blanco-Canosa, G. J. Vora, J. B. Delehanty, K. Susumu, B. C. Mei, P. E. Dawson and I. L. Medintz, *Acs Nano*, 2010, **4**, 267-278.

8. U. Resch-Genger, M. Grabolle, S. Cavaliere-Jaricot, R. Nitschke and T. Nann, *Nat. Methods*, 2008, **5**, 763-775.

9. W. R. Algar and U. J. Krull, *Anal. Bioanal. Chem.*, 2008, **391**, 1609-1618.

10. H. Weller, *Curr. Opin. Colloid Interface Sci.*, 1998, **3**, 194-199.

11. Y. P. Sun, B. Zhou, Y. Lin, W. Wang, K. A. S. Fernando, P. Pathak, M. J. Meziani, B. A. Harruff, X. Wang, H. F. Wang, P. J. G. Luo, H. Yang, M. E. Kose, B. L. Chen, L. M. Veca and S. Y. Xie, *J. Am. Chem. Soc.*, 2006, **128**, 7756-7757.

12. I. L. Medintz, T. Pons, K. Susumu, K. Boeneman, A. M. Dennis, D. Farrell, J. R. Deschamps, J. S. Melinger, G. Bao and H. Mattoussi, *J. Phys. Chem. C*, 2009, **113**, 18552-18561.

13. A. M. Dennis and G. Bao, *Nano Lett.*, 2008, **8**, 1439-1445.

14. D. E. Prasuhn, A. Feltz, J. B. Blanco-Canosa, K. Susumu, M. H. Stewart, B. C. Mei, A. V. Yakovlev, C. Loukov, J. M. Mallet, M. Oheim, P. E. Dawson and I. L. Medintz, *Acs Nano*, 2010, **4**, 5487-5497.

15. D. V. Talapin, A. L. Rogach, A. Kornowski, M. Haase and H. Weller, *Nano Lett.*, 2001, **1**, 207-211.

16. R. Xie, D. Battaglia and X. Peng, *J. Am. Chem. Soc.*, 2007, **129**, 15432-+.

17. N. Pradhan and X. G. Peng, *J. Am. Chem. Soc.*, 2007, **129**, 3339-3347.

18. L. Li and P. Reiss, *J. Am. Chem. Soc.*, 2008, **130**, 11588-+.

19. W. W. Yu, E. Chang, J. C. Falkner, J. Y. Zhang, A. M. Al-Somali, C. M. Sayes, J. Johns, R. Drezek and V. L. Colvin, *J. Am. Chem. Soc.*, 2007, **129**, 2871-2879.

20. B. Dubertret, P. Skourides, D. J. Norris, V. Noireaux, A. H. Brivanlou and A. Libchaber, *Science*, 2002, **298**, 1759-1762.

21. K. Susumu, B. C. Mei and H. Mattoussi, *Nature Protocols*, 2009, **4**, 424-436.

22. B. C. Mei, K. Susumu, I. L. Medintz and H. Mattoussi, *Nature Protocols*, 2009, **4**, 412-423.

23. H. T. Uyeda, I. L. Medintz, J. K. Jaiswal, S. M. Simon and H. Mattoussi, *J. Am. Chem. Soc.*, 2005, **127**, 3870-3878.

24. R. Freeman, T. Finder and I. Willner, *Angew. Chem. Int. Ed*, 2009, **48**, 7818-7821.

25. H. Wu, H. Zhu, J. Zhuang, S. Yang, C. Liu and Y. C. Cao, *Angew. Chem. Int. Ed*, 2008, **47**, 3730-3734.

26. K. E. Sapsford, T. Pons, I. L. Medintz, S. Higashiya, F. M. Brunel, P. E. Dawson and H. Mattoussi, *J. Phys. Chem. C*, 2007, **111**, 11528-11538.

27. H. Lu, O. Schops, U. Woggon and C. M. Niemeyer, *J. Am. Chem. Soc.*, 2008, **130**, 4815-4827.

28. I. L. Medintz, A. R. Clapp, H. Mattoussi, E. R. Goldman, B. Fisher and J. M. Mauro, *Nat. Mater.*, 2003, **2**, 630-638.

29. I. L. Medintz, L. Berti, T. Pons, A. F. Grimes, D. S. English, A. Alessandrini, P. Facci and H. Mattoussi, *Nano Lett.*, 2007, **7**, 1741-1748.

30. I. L. Medintz, A. R. Clapp, F. M. Brunel, T. Tiefenbrunn, H. T. Uyeda, E. L. Chang, J. R. Deschamps, P. E. Dawson and H. Mattoussi, *Nat. Mater.*, 2006, **5**, 581-589.

31. T. Pons, I. L. Medintz, X. Wang, D. S. English and H. Mattoussi, *J. Am. Chem. Soc.*, 2006, **128**, 15324-15331.

32. A. R. Clapp, I. L. Medintz, J. M. Mauro, B. R. Fisher, M. G. Bawendi and H. Mattoussi, *J. Am. Chem. Soc.*, 2004, **126**, 301-310.

33. A. M. Dennis, D. C. Sotto, B. C. Mei, I. L. Medintz, H. Mattoussi and G. Bao, *Bioconj. Chem.*, 2010, **21**, 1160-1170.

34. Y. Zhang, H. Zhang, J. Hollins, M. E. Webb and D. Zhou, *PCCP*, 2011, **13**, 19427-19436.

35. M. Grabolle, M. Spieles, V. Lesnyak, N. Gaponik, A. Eychmuller and U. Resch-Genger, *Anal. Chem.*, 2009, **81**, 6285-6294.

36. D. J. Zhou, J. D. Piper, C. Abell, D. Klenerman, D. J. Kang and L. M. Ying, *Chem. Commun.*, 2005, 4807-4809.

37. K. Susumu, B. C. Mei and H. Mattoussi, *Nat. Protoc.*, 2009, **4**, 424 **-** 436.

38. B. K. Pong, B. L. Trout and J. Y. Lee, *Langmuir*, 2008, **24**, 5270-5276.

39. H. Y. Zhang, P. G. Stockley and D. J. Zhou, *Faraday Discuss.*, 2011, **149**, 319-332.

40. J. R. Lakowicz, ed., *Principles of Fluorescence Spectroscopy*, 2nd edn., Kluwer Academic, New York, 1999.

41. E. G. Guignet, R. Hovius and H. Vogel, *Nat. Biotechnol.*, 2004, **22**, 440-444.

42. D. J. Zhou, Y. Li, E. A. H. Hall, C. Abell and D. Klenerman, *Nanoscale*, 2011, **3**, 201-211.

43. M. A. Wall, M. Socolich and R. Ranganathan, *Nat. Struct. Biol.*, 2000, **7**, 1133-1138.

44. C. M. Niemeyer, *Angew. Chem. Int. Ed*, 2001, **40**, 4128-4158.

45. J. F. Hainfeld, W. Q. Liu, C. M. R. Halsey, P. Freimuth and R. D. Powell, *J. Struct. Biol.*, 1999, **127**, 185-198.

46. D. H. J. Bunka and P. G. Stockley, *Nat. Rev. Microbiol.*, 2006, **4**, 588-596.

47. S. K. Mei B. C., Medintz Igor L, Mattoussi Hedi, *Nat. Protoc.*, 2009, **4**, 421-422.

48. M. B. C. Susumu Kimihiro, Mattoussi Hedi, *Nat. Protoc.*, 2009, **4**, 424436.

49. B. Miroux and J. E. Walker, *J. Mol. Biol.*, 1996, **260**, 289-298.

50. F. W. Studier, *Protein Expression Purif.*, 2005, **41**, 207-234.

Part Ⅱ

Development of Magnetic nanoparticle (MNP) -based biosensor

Chapter 3
Magnetic particle (MP) based ultrasensitive biosensors and bioassays

Magnetic particles (MPs) have recently received significant research interests due to their unique magnetic properties and low toxicity.[1] They can be easily prepared in different sizes and functionalized with stable, nontoxic protective coatings with well-controlled surface functional groups for efficient bioconjugation.[2-4] Moreover, their tiny particle sizes combined with strong superparamagnetic properties allow them to form stable dispersions in reaction media for rapid homogenous reaction in the absence of an external magnetic field, while they are still easily collectable upon application of an external magnetic field. These unique properties make them well suited for target capture, separation, enrichment and biosensing. Indeed, MP-bioconjugates have been widely used in bioimaging[5], targeted delivery of therapeutic agents[6], biosensing and diagnostics[7], bio-separation[3, 8], and catalysis[9].

3.1 MP properties

The magnetic properties of MPs are dominated by two key features: (1) The single domain limit and (2) the superparamagnetic limit.

3.1.1. Single-domain-limit

Magnetic domains here indicate groups of molecules whose spins are all pointing in the same direction, *i.e.* all magnetic moments of the constituent

atoms are all parallel to each other. In conventional magnetic materials, domains are usually separated by domain walls and each domain possesses a unique size and spin direction. In ferromagnetic bulk materials, large domains tend to be split up into several smaller domains to decrease the magnetostatic energy (ΔE_{MS}) of the materials.[10] Nevertheless, domain walls require some energy (E_D) associated with their creation. Therefore, the domain size must have a limit, below which the energy required for the generation of one more domain wall exceeds the amount of reduced magnetostatic energy (ΔE_{MS}). Thus, when the diameter of MP decreases to a critical size, the domain wall formation is not favourable at all such that the MP would rather contain one single domain.[10-11] Critical single-domain sizes for some common MPs have been estimated by Kittle[11-12] (See Table 3.1).

Table 3.1 Estimated critical single–domain sizes for spherical MPs with no shape anisotropy. (Reprinted by permission of the American Chemical Society)[11]

Material	Diameter (nm)	Material	Diameter (nm)
Co	70	Fe_3O_4	128
Fe	14	γ–Fe_2O_3	166
Ni	55		

3.1.2. Superparamagnetic limit

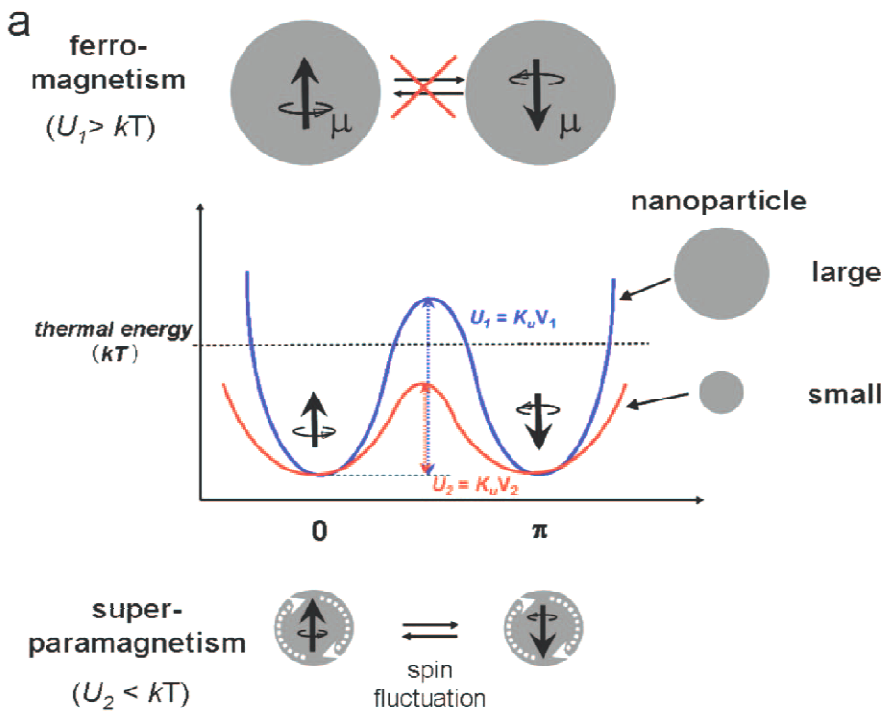

Figure 3.1 Illustrations of MNPs of ferromagnetism and superparamagnetism.

In the middle is the energy diagram of MNPs. For large MPs (blue line), the magnetic anisotropy energy (U1) is higher than the thermal energy. Thus the spins are not able to flip freely and the material behaviour is ferromagnetic; whereas for small MPs (red line), the magnetic anisotropy energy (U2) is lower than the thermal energy. Thus the spin can fluctuate freely and the material behaviour is superparamagnetic. (Reprinted by permission of the American Chemical Society)[14]

As illustrated in Figure 3.1, the magnetic anisotropy energy (U) barrier which hinders the spin fluctuations in a single domain particle, is proportional to K_uV (Ku is the magnetic anisotropic constant and V is the particle volume).[13] Usually, the magnetic anisotropic energy of MPs is higher than the thermal energy kT (k is the thermal constant and T represents temperature). Thus the magnetic moments are not allowed to flip from one direction to the opposite. As the size of MNPs decreases, the magnetic anisotropic energy is also reduced correspondingly. If the MNPs are small enough, such that their magnetic anisotropic energy can be lower than the thermal energy kT, the magnetic moments are able to overcome the energy barrier and reverse the spin direction.

In this case, the MNP is deemed to be superparamagnetic, because it behaves like a paramagnet and all the individual atomic moments add up to one (super) moment. Sometimes, MNPs with a certain diameter can show different magnetisms (ferro- or super-) according to different temperatures, *i.e.* thermal energy. The transition temperature (TB) where $K_uV = kTB$, is called the blocking temperature.

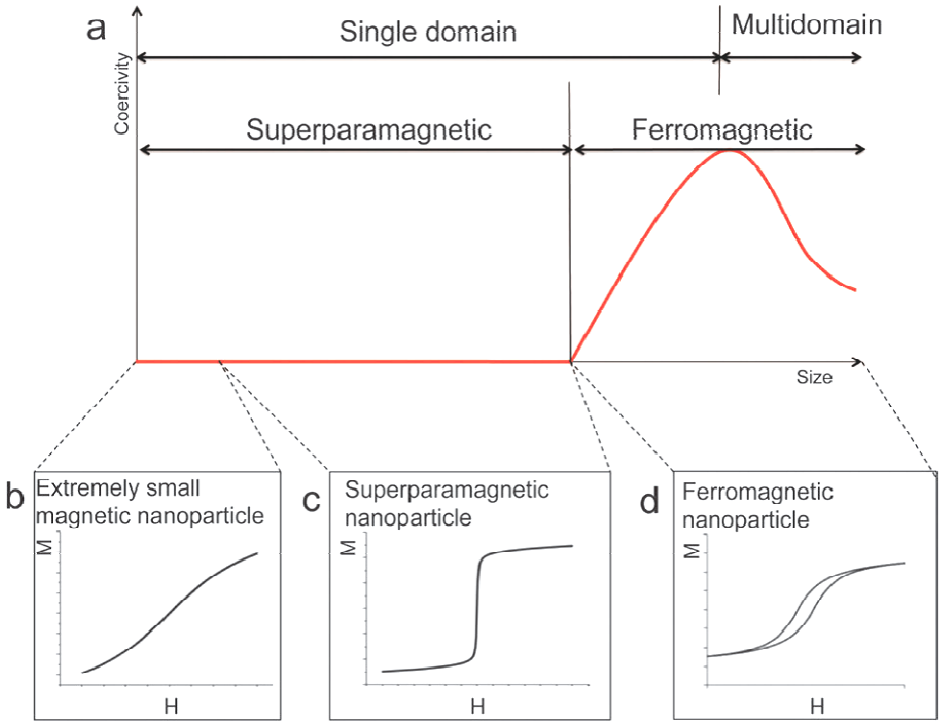

Figure 3.2 (a) Relationship between coercivity and nanoparticle size. **(b-d)** Magnetization curves of MPs.

Single-domain ferromagnetic nanoparticles exhibit remanence and coercivity. (Reprinted by permission of the Royal Society Chemistry)[15]

Figure 3.2 shows three typical hysteresis curves for MPs with different sizes. For the extremely small MP, the magnetization and magnetic field exhibits linear relationship, and the magnetization is not saturated until very high magnetic field is applied (Figure 3.2b). As the MNP size increases (still in the single domain range), it exhibits superparamagnetism, where the magnetization curve

shows rapid magnetic saturation with no remanence and coercivity (Figure 3.2c). As the particle size increases further, it exhibits ferromagnetism showing significant remanence and coercivity in its magnetization curve (Figure 3.2d). Maximum coercivity is observed at the transition from the multidomain to single domains. In a multidomain regime, the coercivity increases as the overall particle size decreases. While In a single domain regime, the coercivity decreases to zero as the particle size decreases (Figure 3.2a).[15]

3.2 MP synthesis and modifications

Magnetite (Fe_3O_4) and maghemite (γ–Fe_2O_3) are the main representatives of the MPs, which have attracted massive attention so far in the medical and biosensing fields, due to their good biocompatibility and non-toxicity. As mentioned above, MPs exhibit unique, sized-dependent magnetic properties that are quite different and unavailable from the bulk counterparts, and their magnetic properties are strongly dependent on their dimensions, size distribution and surface functionality. In order to obtain uniform size MPs, several different synthetic approaches have been reported which are critical for realizing their specific bio-related applications.

The co-precipitation approach is one of the most often used methods to produce magnetite (Fe_3O_4) and maghemite (γ–Fe_2O_3) nanoparticles due to its facile and convenient procedure. In this approach, the synthesis of iron oxide is usually carried out by co-precipitation of iron (II)-, and iron (III) salts (*e.g.* chlorides, sulfates, nitrates) in aqueous solution assisted by addition of alkaline reagent.[16-18] Besides its simplicity, this method has other advantages such as high product yield, low cost and good reproducibility.[19] In addition, this method can also control the nanoparticle size effectively by adjusting the reaction pH,

time and temperature, *etc*. Nevertheless, this approach does suffer a few disadvantages, such as the prepared iron oxide nanoparticles can be poorly crystalline if carried out at or near room temperature, or easily aggregated if performed at higher temperature (80~100°C).[20]

High-temperature decomposition of organometallic precursors in high-boiling solvents in the presence of surfactant molecules is another often used method for MP preparation. Inspired by the successful preparation of high quality semiconductor nanocrystals in organic phase,[21-22] this approach has been developed to prepare monodisperse MPs. For example, uniform size Fe_3O_4 MPs have been synthesized by thermally decomposing iron acetylacetonate [$Fe(C_2H_3O_2)_2$)] in an inert gas protected atmosphere.[23] In addition, using the synthesized small MPs as seeds, larger MPs could be prepared by this means. Thus controlled synthesis of different sized MPs could be realized by carefully optimizing the experimental conditions.[23] Compared with the co-precipitation method, the thermal decomposition strategy is more complicated but could narrow the size distribution and improve the morphology of the MPs. Nevertheless, MPs prepared by this method are often coated by organic ligand and have to be transferred to the aqueous phase for further bio-applications.

Hydrothermal synthesis is another favourite approach for nanomaterial preparation because it is facile and convenient.[24-26] This method is often carried out in a sealed autoclave at high pressure and temperature which is well above the boiling point of the solvent used. Thus the iron salts (nitrates, sulfates, chlorides, acetates, *etc*) are forced to hydrolyse and then dehydrated, resulting in the nucleation for nanoparticle formation. With this strategy, many nanomaterials could be prepared at temperatures well below those required by the thermal decomposition approach. Similarly to the chemical co-precipitation method, this approach is able to control the geometry of the resulting

nanomaterials by choosing suitable reactants and solvent and tuning the reaction time, temperature and the reactant concentrations.[27] Nevertheless, MPs prepared by this method are usually composed of fine crystals compared with those prepared by the chemical co-precipitation method.[25]

Besides these frequently used methods discussed above, there are some other means for MP preparations such as microemulsions[28-29], gas phase deposition[30], sol-gel method.[31-32] Researchers could choose the most suitable strategy to synthesis MPs according to their desire and research requirements.

Generally, due to their high surface/volume ratio, the prepared MPs have high surface energy which makes them readily aggregated or easily oxidized, which can significantly reduce their intrinsic magnetic properties. In this regard, the prepared MPs are usually modified with a protective coating to improve their stability. A number of different surface coating have been explored, which include siloxane[33-35], amphiphilic micelles (such as PEG-phospholipids[36], PEG-Phosphine Oxide Polymer[37]), or polymeric ligands (such as polypyrrole[38], polyaniline[39], polyethyleneimine[40]).[10, 32, 41] Not only can these coatings increase their stability, but they are also able to introduce functional groups such as amine or carboxyl moieties to facilitate their further conjugation with biomolecules. Besides, Au coating is another favourite means[42-43], which not only enables surface plasmon resonance (SPR), but also gives the particles strong and specific affinity for thiolate compounds through the facile gold-thiol self-assembly.

For any bio-related applications, the ability of controlled and efficient attachment of biomolecules to the outer shell of the MPs is of critical importance.[44] Table 3.2 summarises some of the main immobilization approaches that have been used to conjugate biomolecules with MPs.

Table 3.2 A list of immobilisation protocols of biomolecules used to my knowledge on MPs

Surface functional group	Immobilisation protocol-linker	Functional group on biomolecules	Reference
Amine	Sulfo-SMCC SM(PEG)n	Thiol	45
Amine	glutaradehyde	amine	46
gold	--	Thiol	47
gold	2-iminothiolane	amine	48-49
carboxyl	EDC, NHS	amine	9
avidin	--	biotin	50

These strategies listed above facilitated the applications of MPs especially in the bioanalytical and disease diagnostic areas. Indeed, MP-bioconjugates have been widely used in bioimaging [5], targeted delivery of therapeutic agents [6], biosensing and diagnostics [7], bio-separation [3, 8], and catalysis [9]. In the following section, the recent developments of MP-based ultrasensitive biosensors for diagnostics will be discussed.

3.3 Biosensors and bioassays based on MPs

Currently, the most often used assay in clinical disease diagnosis is enzyme linked immunosorbent assay (ELISA), an antibody (Ab) based technique using a surface immobilized Ab1 and an enzyme-linked Ab2 to sandwich the target, converting each target into an Ab1/target/Ab2 sandwich for sensitive enzymatic detection. Although widely used, its sensitivity is often limited by factors such as the low activity of surface- bound Abs, inefficient target capture and slow binding kinetics.[51] As a result, ELISA often cannot provide the speed and, particularly sensitivity, required for early diagnosis because of the extremely low levels of biomarkers. Therefore there is great clinical need to develop faster, more sensitive assays for early diagnosis.

In this regard, MPs have recently received significant research interest due to their unique magnetic properties and low toxicity [1]. These sensors employing MPs include three major types, DNA-, antibody- and aptamer- based assays, from their target-recognition elements used.

Ab is the most often used target-binding element in current clinical assays. The use of MP-Ab conjugates in immunoassays can offer several advantages over surface-immobilized Abs, 1) improve target capture efficiency *via* the use of excess MP-Ab conjugates that can push the equilibrium toward the captured protein state [51] as well as increased target-binding affinity from the multi-valency of the MP-Ab capture probes; [51-52] 2) increase target binding kinetics (the binding interaction now takes place in homogeneous solution rather than solid/solution interface); [51] and 3) enable more efficient signal amplification (*via* multi-tags on each MP).[53] Over the past decade, several ultrasensitive assays with limit of detection (LOD) down to low fM to aM level (several orders of magnitudes lower than ELISA) have been reported. These are mostly based on sandwich assays similar to ELISA. A few significant developments are highlighted below.

Aptamers are short, single-stranded DNA or RNA molecules selected from large random pool of sequence libraries by SELEX (systematic evolution of ligands by exponential enrichment) process [54-56]. Compared to Abs, aptamers have several advantageous properties, such as broader target choice (e.g. proteins, small molecules, metal ions and even whole cells) with comparable affinity, higher thermal and long-term stability, cheaper and easier production and modification, and no batch-to-batch variations [57-58]. Therefore it is unsurprising that aptamers have been widely used in MP-based biosensing and diagnostic applications [59]. Herein the sensors are highlighted accordingly to their readout strategies.

The unique magnetic properties of the MPs allow for efficient target capture, and enrichment by convenient magnetic separation and removal of unwanted species, making them ideally suited for developing ultrasensitive assays. Furthermore MPs can be combined with sensitive readout and signal amplification strategies to achieve femtomolar - attomolar sensitivities. Some typical biosensing approaches based on MPs will be highlighted in the following section defined by their signal-amplifying means.

3.3.1 The giant magnetoresistive (GMR) sensor

Instead of using MP purely for target capture and enrichment, this sensor, developed by the Wang group, detects the magnetic field of the MPs by the underlying giant magnetoresistive (GMR) sensor by applying a small external modulated magnetic field.[60] As illustrated in Figure 3.3, capture DNAs (grey) immobilized on the sensor surface (**a**) are used to capture the biotinylated target DNAs *via* specific DNA hybridization (blue, **b**); (**c**) after washing away any free unbound species, streptavidin modified MPs are bound to the duplexes *via*

streptavidin-biotin interactions. The magnetic fields from the MPs are then detected by the underlying GMR sensor in real-time in the presence of a small external modulated magnetic field. Nevertheless, this sensing platform needs to be further improved for label-free detection, which is more valuable for real applications rather than biotinylated DNA strands detection.

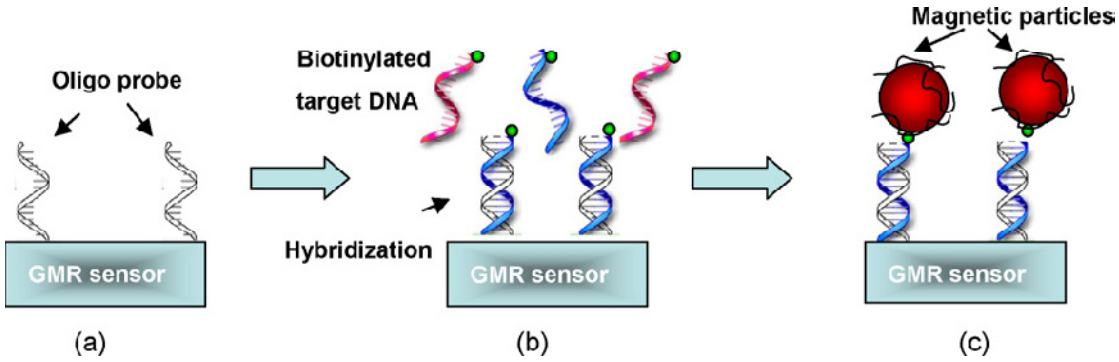

Figure 3.3 Schematic principle of the GMR sensor. (Reprinted by permission of the Elsevier)[60]

Subsequently, this sensor has been used to detect protein targets via a sandwich assay format.[61] Here, Capture Abs were first immobilized on the sensor surface to capture the target antigens. After washing away free unbound antigens, biotinylated probe Abs were added into the system, where only the Abs specific for the target antigens will bind and any unbound free Abs are washed away. Streptavidin-modified MPs were then added in to bind with the sandwiches via streptavidin–biotin interactions. Thus label-free protein target detection has been realized by applying the GMR sensor.

Furthermore, it is claimed that the sensor can simultaneously quantitate multiple proteins in various clinical fluids with LODs down to approximately 50 aM, and can monitor multiple protein markers in real time.[61] More importantly, this sensor is matrix-insensitive: its sensing performance is not affected by

environmental changes, such as pH, temperature, ionic strength, and serum proteins, making it a very promising ultrasensitive sensing platform for early clinical diagnosis.

3.3.2 Magnetic relaxation switch (MRS) assay

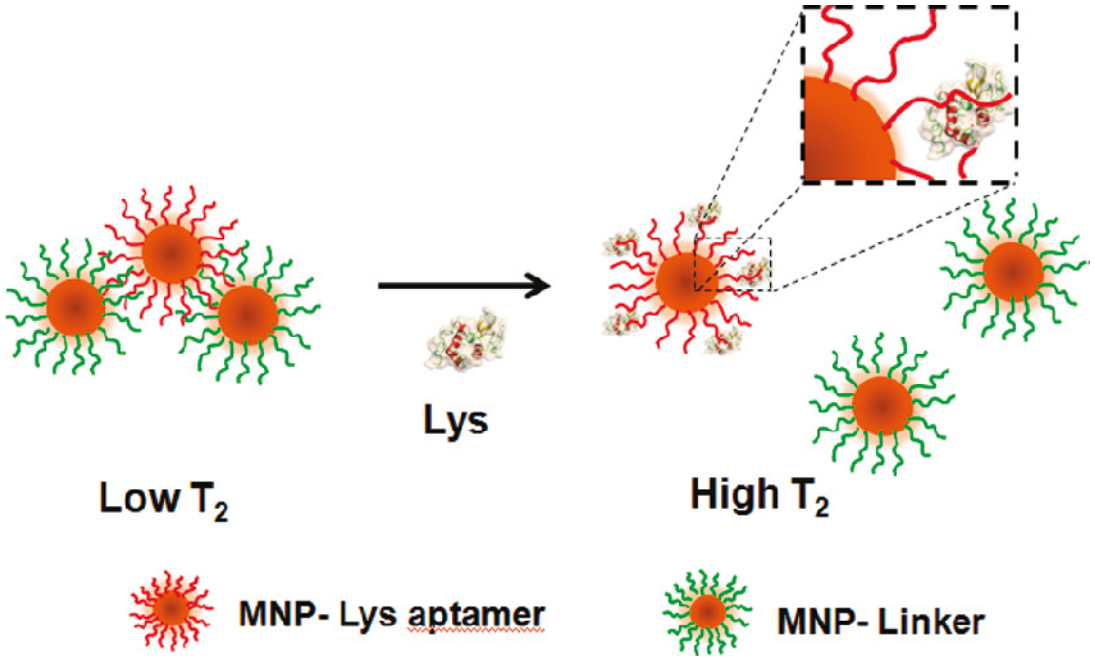

Figure 3.4 Schematic representation of the MRS assay principle for lysozyme detection.

Self-assembled MPs aggregates (via hybridization of complementary DNAs tagged on two kinds of MPs) disassemble on introduction of the lysozyme, leading to T2 increase. (Reprinted by permission of the American Chemical Society)[64]

MP based biosensors that do not use other signal transducers usually use magnetic relaxation switch (MRS) as the readout signal, by measuring the change in the spin-spin relaxation time (T2) between dispersed MPs and their aggregated forms. The MRS assay was first developed by the Weissleder group for specific DNA detection.[62] Subsequently, this strategy was extended to detect

thrombin using corresponding aptamers by the same group.[63] This assay uses two well-dispersed gold-coated Fe_3O_4 MPs, each tagged with a different aptamer targeting each of the two binding sites on thrombin. When thrombin is present, both aptamers bind to thrombin, leading to the MP aggregation and T2 decrease. Using this approach, a detectable T2 change is observed in the presence of 1 nM human -thrombin.

This method has recently been used for lysozyme detection using a single aptamer-MP conjugate (with LOD ~ 0.5 nM).[64] As illustrated in Figure 3.4, two kinds of MPs are modified with anti-lysozyme DNA aptamer and linker DNA respectively. Since the lysozyme aptamer and linker DNA are complimentary, the MPs self-assemble into aggregates *via* DNA hybridization initially. After introduction of lysozyme, the aggregates disassemble leading to T2 increase. The MRS assays are simple with good selectivity, although their sensitivities (typically low nanomolar) have yet to match current clinical assays.

3.3.3 Surface plasmon resonance (SPR)-based assay

SPR is a label-free surface based bioassay widely used to detect target binding induced changes of reflection intensities or angles. It can follow the bindings in real time without target labelling.

Figure 3.5 shows the principle for detection of a small-molecule target (ATP).[65] Firstly, the ssDNA which is partial complementary to the ATP aptamer was immobilized on an SPR gold film as a sensing surface. In the absence of ATP, ATP-aptamer functionalized MPs (MPs-apt) would bind to the SPR sensor by DNA hybridization reaction resulting in a significant change of SPR signal due to the huge mass of MPs. Whereas in the presence of ATP, the aptamer would

conjugate with ATP. Thus more ATP target existence leads to less MP-apt binding to the SPR surface. The concentration of ATP has a proportional relationship with the SPR signal decrease (with nanomolar sensitivity).

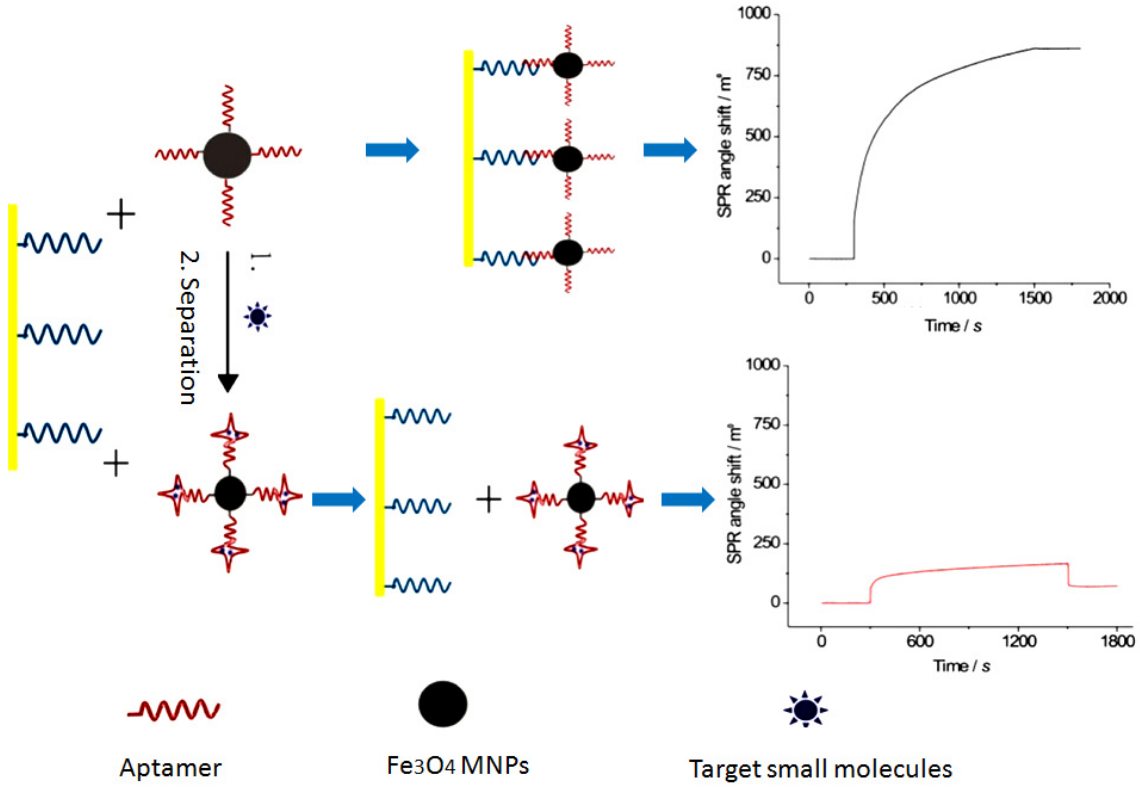

Figure 3.5 Schematic principle of the SPR biosensor for the detection of small molecule (ATP). (Reprinted by permission of the American Chemical Society)[65]

This developed SPR biosensor has also been used for detection of protein (*e.g.* thrombin) with picomolar sensitivity[66]. The MPs here are used as signal amplification tags for each target binding event *via* their significant mass.

3.3.4. The bio-bar-code-based assay

The Bio-Bar-Code-Based assay was developed by the Mirkin group, where two types of probes were applied: a probe DNA1-conjugated magnetic microparticle (MMP; P1-MMP) and a probe DNA2-attached gold nanoparticle (GNP) each tagged with hundreds of barcode DNAs (P2-GNP), which were used to sandwich the target associated with the anthrax lethal factor (T), forming a MMP-P1/T/P2-GNP sandwich. It was then separated magnetically, followed by washing to remove any unbound species. Then the barcode DNAs were released from the sandwich, converting each target DNA into hundreds of barcode DNAs, which were detected sensitively by scanometric assay coupled with silver amplification. This assay combines efficient target capture, enrichment, target conversion and amplification (each target is amplified to hundreds of barcode DNAs, which greatly reduces the background). As a result, it can achieve label-free detection of target DNA down to 500 zeptomolar (zM = 10^{-21} M) sensitivity (see Figure 3.6).[67]

This assay has also been used to detect prostate specific antigen (PSA, a protein biomarker for prostate cancer) achieving a sensitivity of ~ 30 aM level, approximately five orders of magnitudes lower than ELISA allows.[51] Subsequently, multiplexed detection of protein cancer markers based on bio-bar-coded nanoparticle probes has been performed using two different DNA barcodes for respective protein targets for signal amplifications.[68] Moreover, this assay has been recently adapted to monitor the PSA level of patients after surgical treatments far below what was possible by ELISA,[51, 69-70] thus highlighting its great potential in early clinical diagnosis.

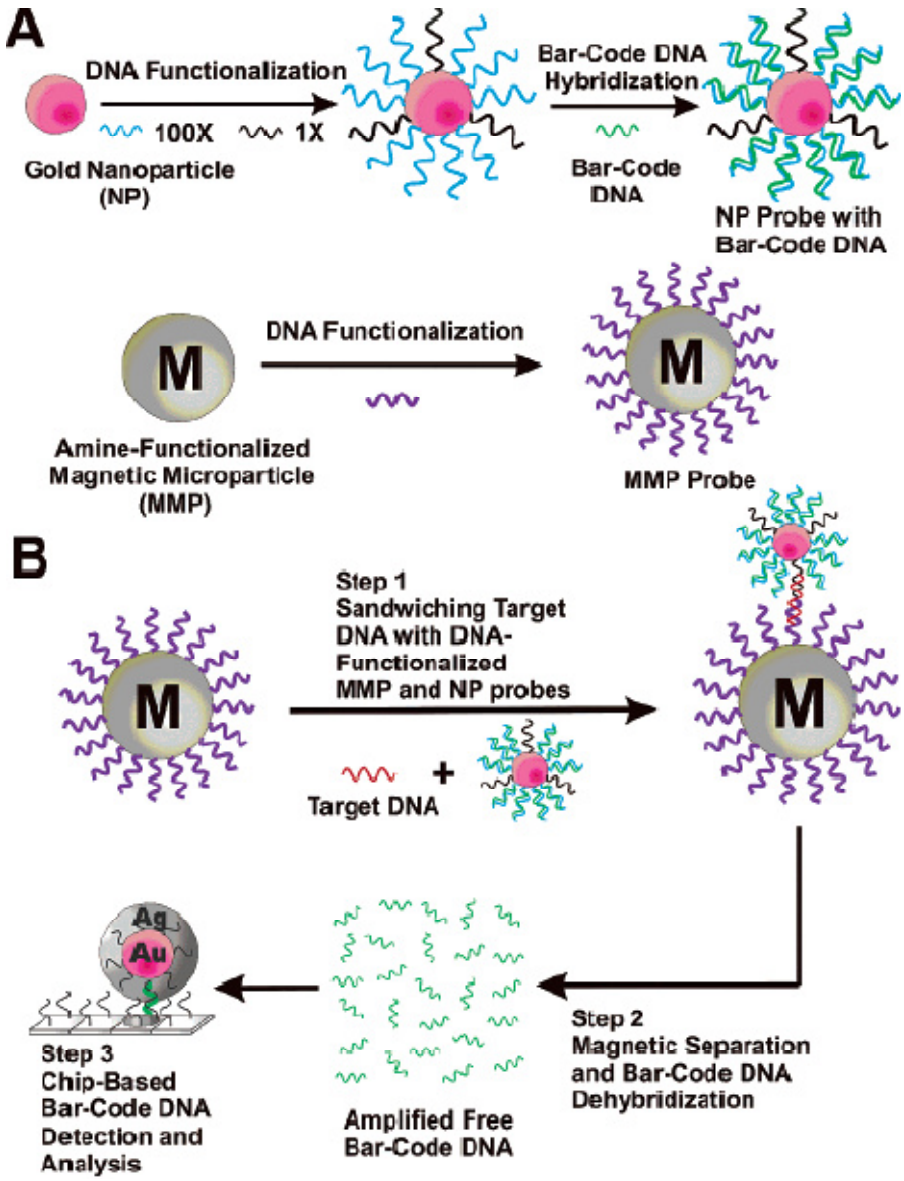

Figure 3.6 The DNA detection based on bio-bar-coded assay.

(A) Preparations of the two types of probes conjugated particle. **(B)** Illustration of the DNA amplification and analysis procedures. (Reprinted by permission of the American Chemical Society)[67]

3.3.5 Enzymatic assay

Enzymes are efficient biocatalysts that can offer great amplification power through efficient catalytic turnover of specific substrates under mild reaction

conditions mostly in aqueous environment, and thus are often regarded as “green” and environmental friendly. They are therefore often combined with the MPs to develop ultrasensitive sensors. Several readout strategies, such as electrochemical,[71] colorimetric,[72] fluorimetric,[73] chemiluminescence,[71, 74] and more recently *via* a personal glucose meter,[50] have been used in these assays.

3.3.5.1 Electrochemical redox detection

Electrochemical redox detection is one of the most widely used readout strategies in MP-aptamer sensors. For example, ochratoxin A (OTA), an important mycotoxin contaminant in food, has been detected sensitively in an electrochemical competitive assay. This is based on the fact that OTA can effectively compete with the binding of OTA tagged HRP on anti-OTA aptamer-MP conjugates. Therefore, when OTA is added, it reduces the amount of OTA-HRP that can bind to the MPs, reducing the electrochemical response (originating from OTA-HRPs remaining attached to the MPs) for OTA readout. This ‘signal-off’ sensor gives a detection limit of 0.07 ng/mL OTA and works in food extracts [71].

More recently, multi-HRP-tagged GNP has been used for greater signal amplification in a thrombin sensor. This assay took the unique feature of the thrombin target, having two independent binding sites recognized by two different aptamers; therefore, an aptamer-MP conjugate (MP-Apt1) and a second aptamer-GNP conjugate tagged with multi-HRPs (Apt2-GNP-HRP_m) can sandwich thrombin, forming an MP-Apt1/thrombin/Apt2-GNP-HRP_m sandwich, which was separated magnetically, and effectively converting each thrombin into multiple HRPs. The HRPs within the sandwich were detected electrochemically. This ‘signal-on’ sensor offered an impressive sensitivity for thrombin (LOD: ~30 fM)[75]. Despite displaying high sensitivity, this assay only

works for targets with two or more binding sites, limiting the scope of its application. The combined use of HRP_m-GNP and MP-Apt conjugates has recently been extended to the detection of cocaine [76].

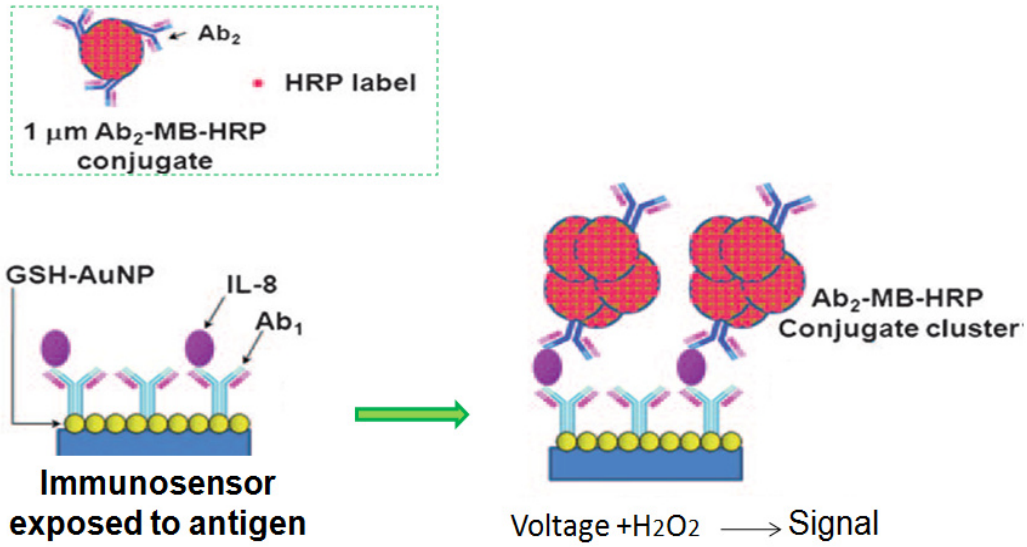

Figure 3.7 Detection principles of the immunosensor based on MB-HRP conjugated cluster and Au NPs.

In the left corner is the Ab2 functionalized MB-HRP conjugate (HRP is denoted as ●). The immunosensor immobilized with Ab1 was exposed to target antigen. And after protein capture, Ab2-MB-HRP conjugate clusters were added for specific binding to obtain amplification. (Reprinted by permission of the Wiley-vch Verlag GmbH)[53]

In addition, an electrochemical-based sandwich nanostructured assay has recently been reported by Munge et al.[53] As depicted in Figure 3.7, this immunosensor involved a glutathione-modified GNP surface tagged with Ab1, and a second Ab functionalized MMP tagged with approximately 500,000 enzymes (HRPs), which were employed to sandwich the target cancer marker, Interleukin-8, for sensitive electrochemical redox detection. The massive number of HRP tags on the MMP greatly increased the signal amplification,

allowing detection of Interleukin-8 down to 100 aM level in serum, over four orders of magnitudes lower than ELISA allows.

3.3.5.2 Chemiluminescence (CL) detection

This simple and sensitive readout strategy is widely used in MP based sensors.[77-79] For instance, HRP mimicking DNAzymes, mostly using a hemin/G-quadruplex complex for catalysis of luminol-H_2O_2 based Chemiluminescence (CL), have been used for amplified DNA detection by the Zhang group.[78] A nicking endonuclease assisted strand-scission cycle has been delicately developed in this study.

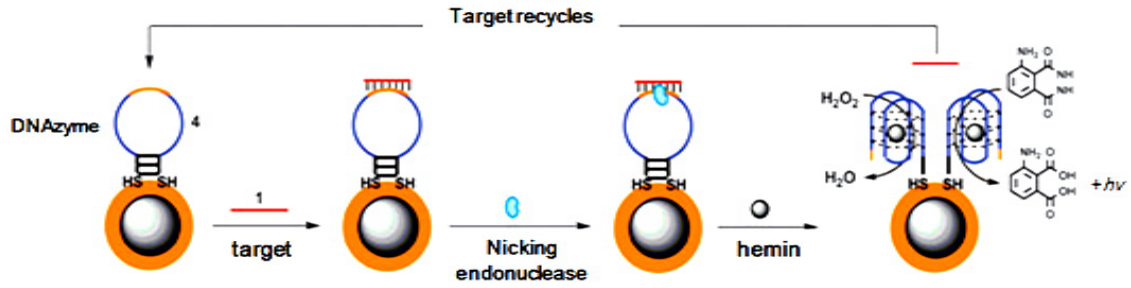

Figure 3.8 Schematic presentation of the amplified DNA detection base on strand-scission cycle. (Reprinted by permission of the Royal Society Chemistry)[78]

As presented in Figure 3.8, the thiolated hairpin DNA, which includes a specific sequence (**orange**) for nicking endonuclease and two domains of the DNAzyme sequences (**blue**), were immobilized on the gold coated MP surface. Since the orange region of the hairpin DNA is complimentary to target DNA (**red**), thus in the existence of target DNA, they hybridize with target DNA forming duplex. Subsequently, nicking endonuclease was added, which recognizes only the

specific sequences (orange) in dsDNA and cleaves them to generate two separated DNAzyme domains and release the target DNA spontaneously at an elevated temperature. Consequently, the target strands were recycled for further strand-scission cycles and the signal enhancement was realized with an estimated LOD down to 76 aM. More importantly, this developed sensing platform could be extended to analyze the concentration of cancer cells (Ramos cells) assisted by respective aptamers.[78]

Similar sensitivity has also been achieved by combining the DNAzyme with rolling circle amplification (RCA) by the same group.[79] Instead of converting each target into one DNAzyme as above, a novel sensing strategy combining DNA-ligation and efficient RCA amplification was designed, where each target was converted into many DNAzymes, and hence greatly improved the signal amplification power. Impressive sensitivities have been realized for both protein (thrombin, LOD: 6.6 pM) and DNA (LOD: 71 aM) targets. Moreover, this sensor had extremely high single-nucleotide polymorphism (SNP) discrimination factors > 10,000:1, and worked in human serum without polymerase chain reaction (PCR) pre-amplification[79]. Since SNP is widely associated with diseases, this sensor is likely to have broad applications in diagnosing many genetic-related diseases.

Furthermore, the Lu group has used two different enzymes, alkaline phosphatase (ALP) and HRP, and substrate-resolved chemiluminescence (CL) technology to simultaneously detect adenosine and cocaine (see Figure 3.9).[80] In this system, a set of a capture DNA-MP conjugate, biotin- (or digoxigenin-) modified probe DNA, and a specific aptamer (the capture and probe DNAs are complementary to each half of the aptamer sequence) were used for each target. They were assembled into two individual MP-capture DNA/aptamer/probe DNA sandwiches. Introduction of a specific target

displaced its specific probe DNA from the sandwich, reducing the amount of streptavidin-HRP (or anti-digoxigenin-tagged ALP) that could bind to the MPs, leading to reduced CL as readout signal. This signal-off sensor could simultaneously quantitate adenosine and cocaine down to an approximately 10 nM level.

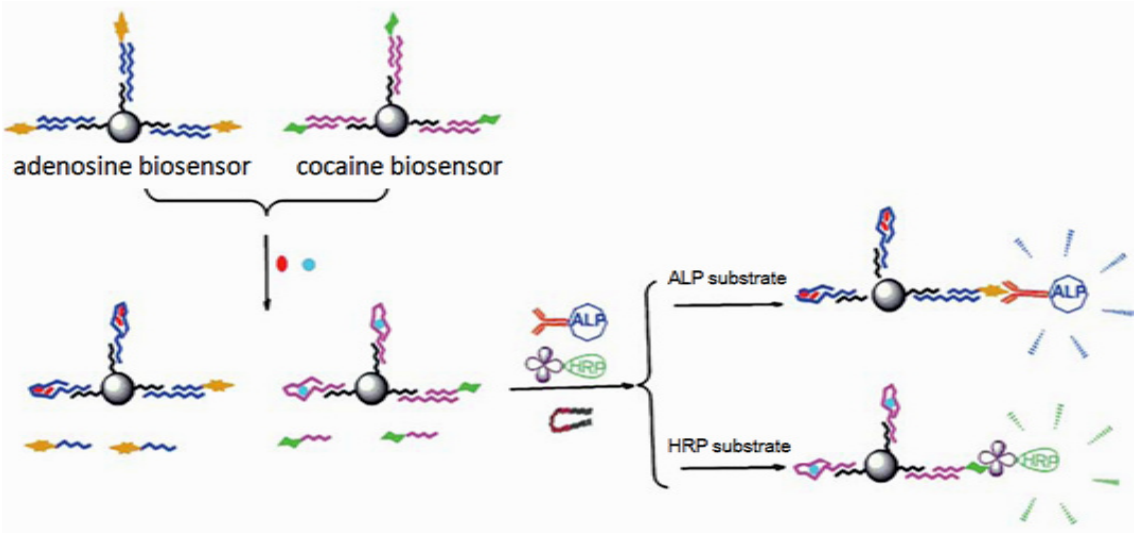

Figure 3.9 Schematic illustration of the CL detection of two small molecules (adenosine ● and cocaine ●).

Two aptamers for adenosine and cocaine are sandwiched by MP-capture DNA and probe DNA-HRP (or ALP). Upon target-aptamer recognition events, the probe DNA-HRP (or ALP) would detach from the MP. Thus after magnetic separation, the reduced enzymatic signals of the system represent the target concentration (Reprinted by permission of the Royal Society Chemistry)[80]

3.3.5.3 Detection *via* personal glucose meters

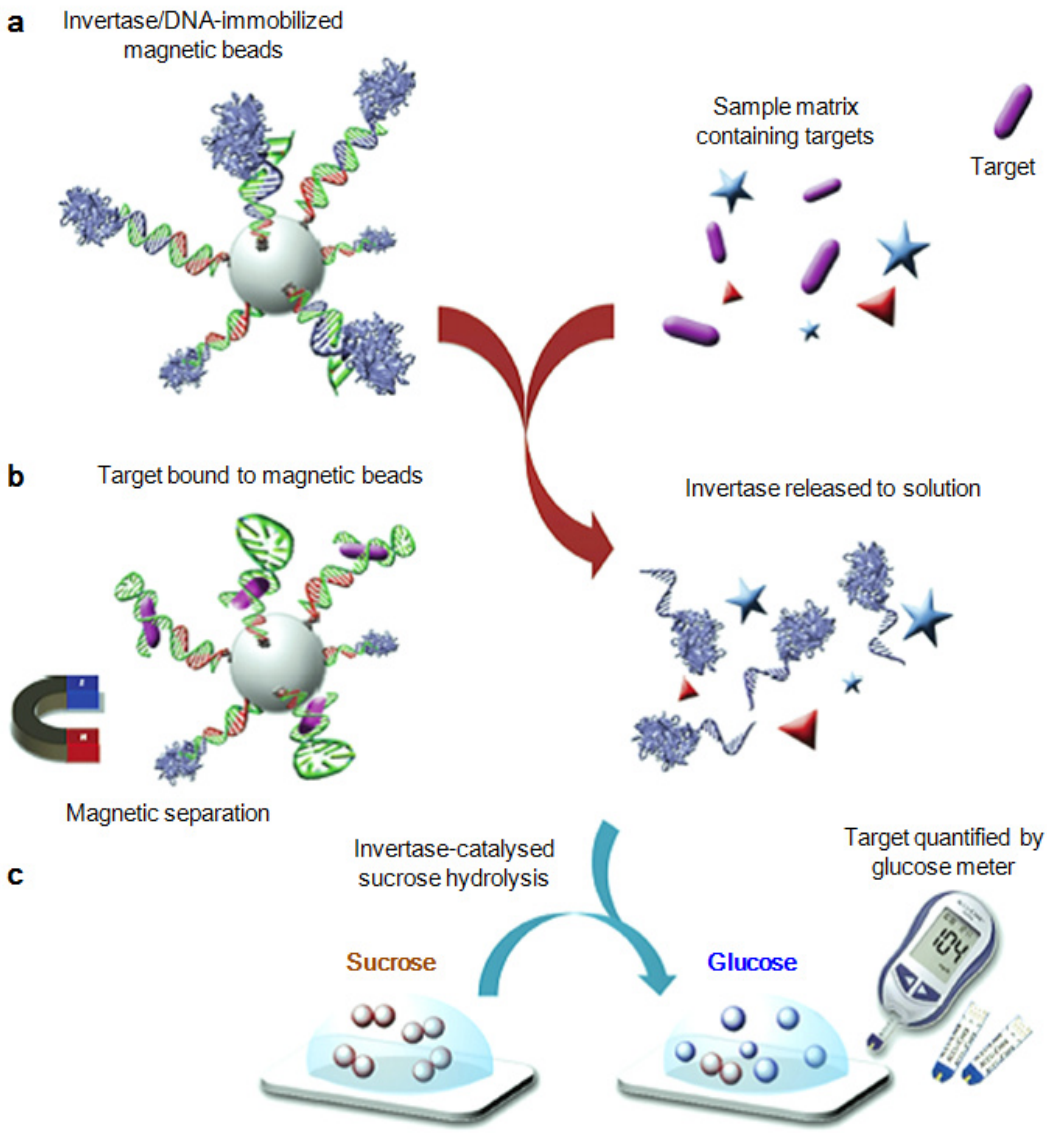

Figure 3.10 Detection of small molecules using MP-aptamer and glucose meter. First, DNA-invertases are immobilized on the MP-aptamer conjugate surface through hybridization. Then target molecules are captured by the MP surface aptamers, releasing invertases from the MP. After magnetic separation, sucrose is added to initiate the invertase- catalysed glucose production. Target quantitation is realized by measuring the glucose concentration using a glucose meter. (Reprinted by permission of the Nature Publishing Group)[50]

This simple, general 'sweet-sensing' aptasensor developed by the Lu group can quantitate multiple targets: cocaine, adenosine, interferon-gamma (IFN-γ) of

tuberculosis and uranium.[50] This assay used a MP-conjugated with multiple different aptamers, each hybridized to a specific, short DNA-tagged invertase. The specific recognition of a target by its aptamer triggers the release of a DNA-invertase from the MP surface. After magnetic separation to remove the MPs, sucrose was added to the supernatant, and glucose production catalyzed by the released invertase in the supernatant was monitored by a personal glucose meter for target quantitation (see Figure 3.10).

This assay is general (applicable to any targets with known aptamers) and simple (detection *via* existing personal glucose sensors), so is well-suited for home diagnosis. However, its sensitivity (approximately micromolar for small molecules and nanomolar for proteins) has yet to match those of current clinical assays. Therefore it is most suitable for detection of relatively highly abundant targets only, limiting its potential for early diagnosis.

Lately, this sensing platform has also been applied for DNA detection based on the sandwich assay format by the same research group with a detection limit of ~40 pM with SNP discrimination ability.[81]

3.3.6 Fluorescence detection

Adenosine detection using a DNA aptamer as the recognizing element and MPs as carriers has also been performed using fluorescence detection.[82] This fluorescence-based detection approach uses a fluorophore-labelled aptamer (F*-aptamer)-MP conjugate hybridized with a quencher-tagged anti-aptamer strand. Upon target binding to the aptamer, the quencher-tagged anti-aptamer is displaced from the MP conjugate, resulting in a significant increase of the

fluorescence intensity of the MP–F*-aptamer conjugate that can be used for target quantitation.

An advantage here is that it can be combined with flow cytometry to measure each individual MP–F*-aptamer conjugate under a capillary flow that significantly reduces the background and improves assay throughput (see Figure 3.11). However, the sensitivity achieved here (LOD: ~170 μM) is considerably lower than other ultrasensitive approaches described above.

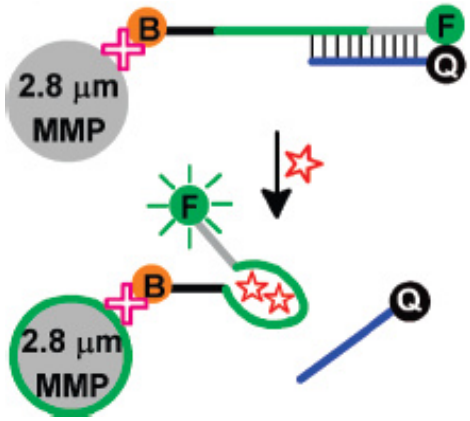

Figure 3.11 MMP assisted fluorescent aptamer sensor for adenosine.

In the presence of adenosine (denoted as a red star), a quencher labelled DNA is displaced making the fluorescence signal enhanced. F represents FAM fluorophore and Q represents quencher. (Reprinted by permission of the American Chemical Society)[82]

In addition, two sets of F*-aptamer and MP–aptamer conjugate probes have been used to simultaneously detect two protein targets, thrombin and lysozyme, using the sandwich-binding format with LODs of 60 and 200 pM, respectively.[83] A limitation of the sandwich assay is that it only works for a target that has two accessible binding sites, limiting its application scope. More recently, an F*-aptamer has been combined with molecular beacon and RCA for greater signal

enhancement. The resulting sensor achieved an impressive LOD of 0.48 nM for cocaine, a small-molecule target.[84]

Lately, a RCA immunoassay for protein detection based on DNA enriching MPs and assembled fluorescent DNA nanotags has been designed.[85] In this versatile assay illustrated in Figure 3.12, one target protein detection event was first converted into the detection of massive p-DNA in one binding event. Then through the RCA process, p-DNA probes were extended to much longer DNA strands with repeated units.

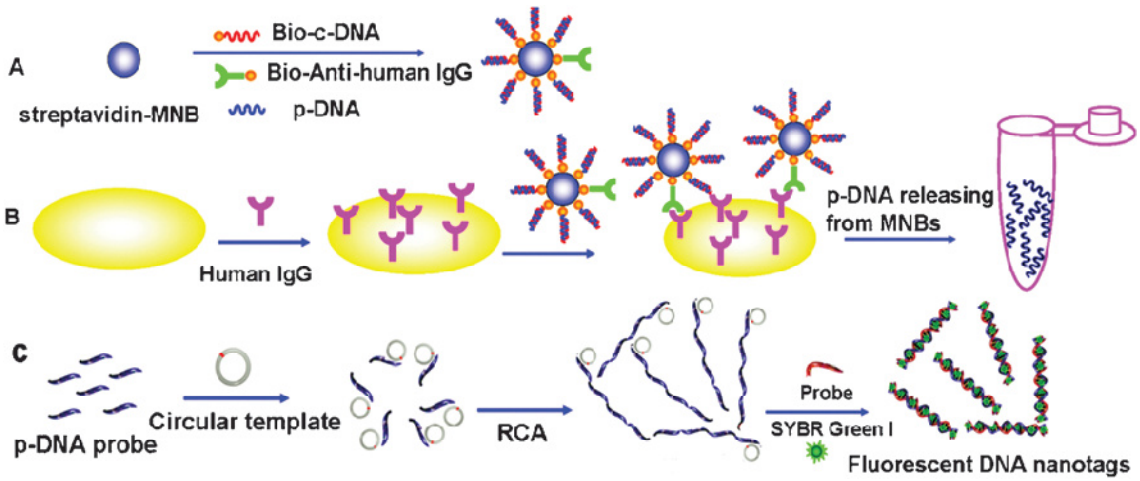

Figure 3.12 Principle of the ultrasensitive MPs-RCA immunoassay facilitated by fluorescent DNA nanotags.

(A) Design and preparation of dsDNA (p-DNA–c-DNA) and Anti-human IgG modified MPs; **(B)** Process of the immunoreaction for specific protein (Human IgG) detection followed by the release of p-DNA for further signal amplification; **(C)** Process of the RCA initiated by p-DNA probes and formation of the fluorescent DNA nanotags (dsDNA- SYBR Green 1). (Reprinted by permission of the Royal Society Chemistry)[85]

Subsequently, probe DNA was added in to hybridize with the RCA product forming duplex DNA. SYBR Green 1 is an intercalating dye whose fluorescence will significantly increase after intercalation in dsDNA. Thus the fluorescent DNA

nanotags (SYBR Green 1 in dsDNA) were self-assembled. Thus the protein quantification could be realized by monitoring the fluorescence of the assembled DNA nanotags, whose fluorescence is significantly stronger than that of the non-intercalating SYBR Green 1 molecules. This developed sensing platform achieves a competitive estimated LOD of 8.3 aM.

3.3.7 Electrochemiluminescence (ECL) detection

Electrochemiluminescence (ECL) is another sensitive readout strategy recently exploited by the Zhang group in detecting whole cancer cells using structure-switching MP-aptamer sensors [47, 74, 86]. A MP-Au-CdS complex[74] or a CuS/DNA/Au/DNA/MP nanoprobe[86] was used for efficient amplification of the CL or ECL signal used in these sensitive MP-based sensors. These sensors showed impressive sensitivities for specific target DNA sequences (LOD: 6.8 aM) and Ramos cells (LOD: 56 cells/mL)[86].

More recently, a multiple CdSe/ZnS QDs -modified dendrimer and a nicking enzyme catalyzed target cycling strategy have been combined for the sensitive detection of cancer cells.[47] As depicted by Figure 3.13, multiple dendrimer/QDs-DNA probes were attached to gold-coated MPs through a thiolated linker DNA sequence. Meanwhile, a signal anti-aptamer DNA was hybridized to an aptamer-MP conjugate, which upon binding to target cell, was displaced. The displaced anti-aptamer DNA could then hybridize to the linker DNA in-between the gold-coated MPs and dendrimer/QDs-DNA probe, promoting specific cleavage on the linker DNA by a nicking enzyme, and was subsequently recycled for further cleavage, releasing multiple dendrimer/ QDs-DNA probes. The released dendrimer/QDs-DNA probes were then hybridized to a capture DNAs-coated GNP surface for sensitive ECL detection. This sensors showed high sensitivity for cancer cells (LOD: 68 cells/mL), so may have potential in

early cancer diagnosis by directly detecting the low level of circulating cancer cells.

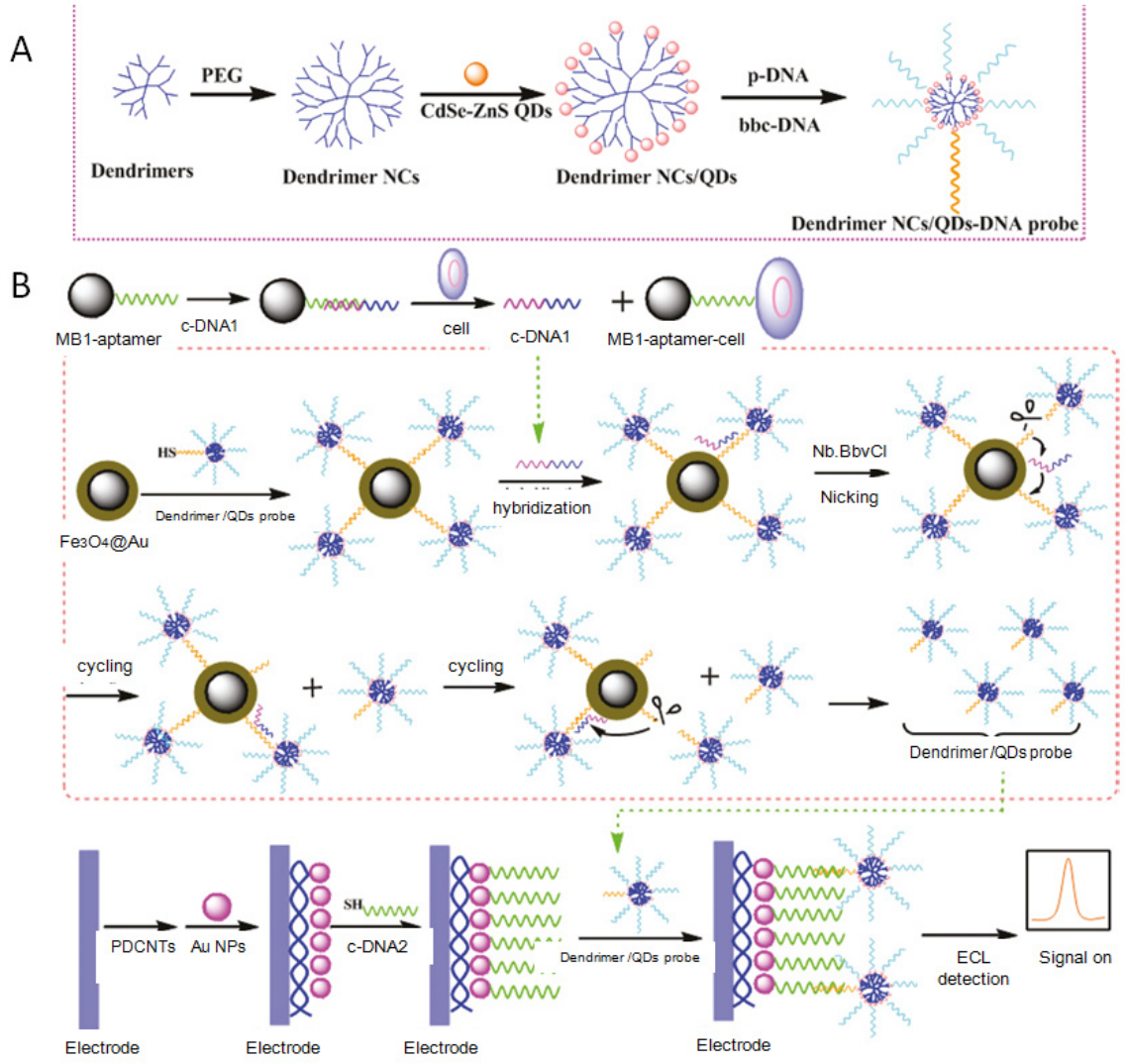

Figure 3.13 Illustration of the process for cancer cell detection.

(A) Preparation of the dendrimer /QD probes and **(B)** ECL assays for cancer cells based on dendrimer/QD Nanoclusters assisted with nicking cycles. (Reprinted by permission of the American Chemical Society)[47]

3.4 Overview of the project (part Ⅱ)

The unique magnetic properties of the MPs have been most exploited in ultrasensitive MP-based assays, where MPs are combined with sensitive readout and signal amplification strategies to achieve femtomolar - attomolar sensitivities, several orders of magnitudes higher than ELISA. These assays appear well suited for early disease diagnosis by detecting the very low levels of disease biomarkers that are impossible to detect with current clinical assays. A few significant examples here include the nanoparticle barcode assay[69], the nanostructured immunosensor[53], and enzyme based amplification coupled with sensitive fluorescence or CL (ECL) detections[47, 86].

Nevertheless, most of these sensors have demonstrated high sensitivity for just a single target, and biosensors based on MPs for sensitive multiplexed analysis of biomolecule targets (DNA[87], protein[61], small molecule[80]) have rarely been reported.

Multiplexed DNA detections based on a MP-dye sandwich assay have been reported by the He group.[87] In this assay, two dyes (Cy3 and Cy5) were employed as signal reporters for respective DNA targets. Although this strategy is simple and easy to handle, its sensitivity (~100 pM) has yet to be able to match the more established clinical assays. A “signal-off” biosensor for simultaneous analysis of adenosine and cocaine has been designed by adapting two enzymes (ALP and HRP) for signal amplification.[80] Nevertheless, the LOD of this assay is ~10 nM, which may be further improved by switching the “signal-off” to the “signal-on” principle. The giant magnetoresistive sensor, which combines ultra-high sensitivity, multiplexed- and matrix-insensitive detection, appears to be extremely well-suited for early clinical diagnosis.[61]

However, this assay requires specific instrumentation and well-trained researchers, which limits its generalization.

Consequently, the second part of my project is to develop a facile sensitive DNA sensor with multiplexing ability based on a MP-based enzymatic sandwich assay. Firstly, uniform and stable MPs are to be prepared, modified and functionalized with capture DNA strands. In this regards, a careful management of the MP surface and DNA conjugation chemistry is key to ensure a low background (by reducing non-specific absorption). Then efficient enzymes (HRP and ALP) will be used to enhance the signal significantly, which is very important for pushing down the detection limit. Another issue to be addressed is to realize ultrasensitive SNP discriminations in cancer specific genes, which is key to develop sensitive, reliable early clinical diagnostic assays (most protein biomarker based diagnostics are often of poor diagnostic accuracy).[88]

3.5 References

1. A. H. Lu, E. L. Salabas and F. Schüth, *Angew. Chem. Int. Ed.*, 2007, **46**, 1222-1244.
2. I. J. Bruce and T. Sen, *Langmuir*, 2005, **21**, 7029-7035.
3. Y.-F. Huang, Y.-F. Wang and X.-P. Yan, *Environ. Sci. Technol.*, 2010, **44**, 7908-7913.
4. Y. Deng, D. Qi, C. Deng, X. Zhang and D. Zhao, *J. Am. Chem. Soc.*, 2007, **130**, 28-29.
5. J. H. Lee, Y. M. Huh, Y. Jun, J. Seo, J. Jang, H. T. Song, S. Kim, E. J. Cho, H. G. Yoon and J. S. Suh, *Nat. Med.*, 2006, **13**, 95-99.
6. N.-H. Cho, T.-C. Cheong, J. H. Min, J. H. Wu, S. J. Lee, D. Kim, J.-S. Yang, S. Kim, Y. K. Kim and S.-Y. Seong, *Nat. Nanotechnol.*, 2011, **6**, 675-682.

7. H. Nagaoka, Y. Sato, X. Xie, H. Hata, M. Eguchi, N. Sakurai, T. Watanabe, H. Saitoh, A. Kondo, S. Sugita and N. Ohnishi, *Anal. Chem.*, 2011, **83**, 9197-9200.

8. K. E. Scarberry, E. B. Dickerson, J. F. McDonald and Z. J. Zhang, *J. Am. Chem. Soc.*, 2008, **130**, 10258-10262.

9. J. Garcia, Y. Zhang, H. Taylor, O. Cespedes, M. E. Webb and D. Zhou, *Nanoscale*, 2011, **3**, 3721-3730.

10. T. D. Schladt, K. Schneider, H. Schild and W. Tremel, *Dalton Transactions*, 2011, **40**, 6315-6343.

11. D. L. Leslie-Pelecky and R. D. Rieke, *Chem. Mater.*, 1996, **8**, 1770-1783.

12. C. Kittel, *Physical Review*, 1946, **70**, 965.

13. D. Jiles, *Introduction to magnetism and magnetic materials*, CRC Press, 1998.

14. Y.-w. Jun, J.-w. Seo and J. Cheon, *Acc. Chem. Res.*, 2008, **41**, 179-189.

15. N. Lee and T. Hyeon, *Chem. Soc. Rev.*, 2012, **41**, 2575-2589.

16. Y. S. Kang, S. Risbud, J. F. Rabolt and P. Stroeve, *Chem. Mater.*, 1996, **8**, 2209-2211.

17. J. Cheon, N.-J. Kang, S.-M. Lee, J.-H. Lee, J.-H. Yoon and S. J. Oh, *J. Am. Chem. Soc.*, 2004, **126**, 1950-1951.

18. J. Viota, J. Duran, F. Gonzalez-Caballero and A. Delgado, *J. Magn. Magn. Mater.*, 2007, **314**, 80-86.

19. A. S. Teja and P.-Y. Koh, *Prog. Cryst. Growth Charact. Mater.*, 2009, **55**, 22-45.

20. Z. J. Zhang, Z. L. Wang, B. C. Chakoumakos and J. S. Yin, *J. Am. Chem. Soc.*, 1998, **120**, 1800-1804.

21. C. Murray, D. Norris and M. G. Bawendi, *J. Am. Chem. Soc.*, 1993, **115**, 8706-8715.

22. X. Peng, J. Wickham and A. P. Alivisatos, *J. Am. Chem. Soc.*, 1998, **120**, 5343-5344.

23. S. Sun and H. Zeng, *J. Am. Chem. Soc.*, 2002, **124**, 8204-8205.

24. C. Rath, K. Sahu, S. Anand, S. Date, N. Mishra and R. Das, *J. Magn. Magn. Mater.*, 1999, **202**, 77-84.

25. T. Daou, G. Pourroy, S. Begin-Colin, J. Greneche, C. Ulhaq-Bouillet, P. Legaré, P. Bernhardt, C. Leuvrey and G. Rogez, *Chem. Mater.*, 2006, **18**, 4399-4404.

26. C.-J. Jia, L.-D. Sun, F. Luo, X.-D. Han, L. J. Heyderman, Z.-G. Yan, C.-H. Yan, K. Zheng, Z. Zhang and M. Takano, *J. Am. Chem. Soc.*, 2008, **130**, 16968.

27. F. Chen, Q. Gao, G. Hong and J. Ni, *J. Magn. Magn. Mater.*, 2008, **320**, 1775-1780.

28. A. K. Gupta and S. Wells, *NanoBioscience, IEEE Transactions on*, 2004, **3**, 66-73.

29. P. Tartaj, M. Morales, T. Gonzalez-Carreno, S. Veintemillas-Verdaguer and C. Serna, *J. Magn. Magn. Mater.*, 2005, **290**, 28-34.

30. G. Ketteler, W. Weiss, W. Ranke and R. Schlögl, *PCCP*, 2001, **3**, 1114-1122.

31. H. Itoh and T. Sugimoto, *J. Colloid Interface Sci.*, 2003, **265**, 283-295.

32. L. H. Reddy, J. L. Arias, J. Nicolas and P. Couvreur, *Chem. Rev.*, 2012, **112**, 5818-5878.

33. Y. Lu, Y. Yin, B. T. Mayers and Y. Xia, *Nano Lett.*, 2002, **2**, 183-186.

34. N. R. Jana, C. Earhart and J. Y. Ying, *Chem. Mater.*, 2007, **19**, 5074-5082.

35. D. B. Tada, L. L. R. Vono, E. L. Duarte, R. Itri, P. K. Kiyohara, M. S. Baptista and L. M. Rossi, *Langmuir*, 2007, **23**, 8194-8199.

36. B. Dubertret, P. Skourides, D. J. Norris, V. Noireaux, A. H. Brivanlou and A. Libchaber, *Science*, 2002, **298**, 1759-1762.

37. S.-W. Kim, S. Kim, J. B. Tracy, A. Jasanoff and M. G. Bawendi, *J. Am. Chem. Soc.*, 2005, **127**, 4556-4557.

38. M. Butterworth, S. Bell, S. Armes and A. Simpson, *J. Colloid Interface Sci.*, 1996, **183**, 91-99.

39. M. Wan and J. Li, *J. Polym. Sci., Part A: Polym. Chem.*, 1998, **36**, 2799-2805.

40. S. McBain, H. Yiu, A. El Haj and J. Dobson, *J. Mater. Chem.*, 2007, **17**, 2561-2565.

41. L. Zhou, J. Yuan and Y. Wei, *J. Mater. Chem.*, 2011, **21**, 2823-2840.

42. S. I. Stoeva, F. Huo, J.-S. Lee and C. A. Mirkin, *J. Am. Chem. Soc.*, 2005, **127**, 15362-15363.

43. I. Y. Goon, L. M. Lai, M. Lim, P. Munroe, J. J. Gooding and R. Amal, *Chem. Mater.*, 2009, **21**, 673-681.

44. N. Jaffrezic-Renault, C. Martelet, Y. Chevolot and J.-P. Cloarec, *Sensors*, 2007, **7**, 589-614.

45. F. Patolsky, Y. Weizmann, E. Katz and I. Willner, *Angew. Chem. Int. Ed.*, 2003, **42**, 2372-2376.

46. Z. Liu, Y. Liu, H. Yang, Y. Yang, G. Shen and R. Yu, *Anal. Chim. Acta*, 2005, **533**, 3-9.

47. G. Jie, L. Wang, J. Yuan and S. Zhang, *Anal. Chem.*, 2011, **83**, 3873-3880.

48. S. S. Ghosh, P. M. Kao, A. W. McCue and H. L. Chappelle, *Bioconj. Chem.*, 1990, **1**, 71-76.

49. E. Katz and I. Willner, *Angew. Chem. Int. Ed.*, 2004, **43**, 6042-6108.

50. Y. Xiang and Y. Lu, *Nat Chem*, 2011, **3**, 697-703.

51. J. M. Nam, C. S. Thaxton and C. A. Mirkin, *Science*, 2003, **301**, 1884-1886.

52. C. Tassa, J. L. Duffner, T. A. Lewis, R. Weissleder, S. L. Schreiber, A. N. Koehler and S. Y. Shaw, *Bioconj. Chem.*, 2009, **21**, 14-19.

53. B. S. Munge, A. L. Coffey, J. M. Doucette, B. K. Somba, R. Malhotra, V. Patel, J. S. Gutkind and J. F. Rusling, *Angew. Chem. Int. Ed.*, 2011, **50**, 7915-7918.

54. A. D. Ellington and J. W. Szostak, *Nature*, 1990, **346**, 818-822.

55. C. Tuerk and L. Gold, *Science*, 1990, **249**, 505-510.

56. A. B. Iliuk, L. Hu and W. A. Tao, *Anal. Chem.*, 2011, **83**, 4440-4452.

57. L. Gold, B. Polisky, O. Uhlenbeck and M. Yarus, *Annu. Rev. Biochem*, 1995, **64**, 763-797.

58. N. K. Navani and Y. Li, *Curr. Opin. Chem. Biol.*, 2006, **10**, 272-281.

59. J. Liu, Z. Cao and Y. Lu, *Chem. Rev.*, 2009, **109**, 1948-1998.

60. L. Xu, H. Yu, M. S. Akhras, S.-J. Han, S. Osterfeld, R. L. White, N. Pourmand and S. X. Wang, *Biosens. Bioelectron.*, 2008, **24**, 99-103.

61. R. S. Gaster, D. A. Hall, C. H. Nielsen, S. J. Osterfeld, H. Yu, K. E. Mach, R. J. Wilson, B. Murmann, J. C. Liao, S. S. Gambhir and S. X. Wang, *Nat Med*, 2009, **15**, 1327-1332.

62. L. Josephson, J. M. Perez and R. Weissleder, *Angew. Chem.*, 2001, **113**, 3304-3306.

63. G. H. Liang, S. Y. Cai, P. Zhang, Y. Y. Peng, H. Chen, S. Zhang and J. L. Kong, *Anal. Chim. Acta*, 2011, **689**, 243-249.

64. S. Bamrungsap, M. I. Shukoor, T. Chen, K. Sefah and W. Tan, *Anal. Chem.*, 2011, **83**, 7795-7799.

65. J. Wang, A. Munir, Z. Zhu and H. S. Zhou, *Anal. Chem.*, 2010, **82**, 6782-6789.

66. J. Wang, Z. Zhu, A. Munir and H. S. Zhou, *Talanta*, 2011, **84**, 783-788.

67. J.-M. Nam, S. I. Stoeva and C. A. Mirkin, *J. Am. Chem. Soc.*, 2004, **126**, 5932-5933.

68. S. I. Stoeva, J.-S. Lee, J. E. Smith, S. T. Rosen and C. A. Mirkin, *J. Am. Chem. Soc.*, 2006, **128**, 8378-8379.

69. N. L. Rosi and C. A. Mirkin, *Chem. Rev.*, 2005, **105**, 1547-1562.

70. C. S. Thaxton, R. Elghanian, A. D. Thomas, S. I. Stoeva, J. S. Lee, N. D. Smith, A. J. Schaeffer, H. Klocker, W. Horninger and G. Bartsch, *Proc. Natl. Acad. Sci.*, 2009, **106**, 18437-18442.

71. L. Bonel, J. C. Vidal, P. Duato and J. R. Castillo, *Biosens. Bioelectron.*, 2011, **26**, 3254-3259.

72. Y. Du, B. Li, S. Guo, Z. Zhou, M. Zhou, E. Wang and S. Dong, *Analyst*, 2011, **136**, 493-497.

73. Q. Zhao, X.-F. Li and X. C. Le, *Anal. Chem.*, 2011, **83**, 9234-9236.

74. C. Ding, Y. Ge and S. Zhang, *Chemistry-A European Journal*, 2010, **16**, 10707-10714.

75. J. Zhao, Y. Zhang, H. Li, Y. Wen, X. Fan, F. Lin, L. Tan and S. Yao, *Biosens. Bioelectron.*, 2011, **26**, 2297-2303.

76. Y. Li, X. T. Ji and B. W. Liu, *Anal. Bioanal. Chem.*, 2011, **401**, 213-219.

77. X. Chen, X.-E. Zhang, Y.-Q. Chai, W.-P. Hu, Z.-P. Zhang, X.-M. Zhang and A. E. G. Cass, *Biosens. Bioelectron.*, 1998, **13**, 451-458.

78. S. Bi, J. Zhang and S. Zhang, *Chem. Commun.*, 2010, **46**, 5509-5511.

79. S. Bi, L. Li and S. Zhang, *Anal. Chem.*, 2010, **82**, 9447-9454.

80. X. Yan, Z. Cao, C. Lau and J. Lu, *Analyst*, 2010, **135**, 2400-2407.

81. Y. Xiang and Y. Lu, *Anal. Chem.*, 2012, **84**, 1975-1980.

82. P. J. J. Huang and J. Liu, *Anal. Chem.*, 2010, **82**, 4020-4026.

83. L. Q. Wang, L. Y. Li, Y. Xu, G. F. Cheng, P. A. He and Y. Z. Fang, *Talanta*, 2009, **79**, 557-561.

84. C. Ma, W. Wang, Q. Yang, C. Shi and L. Cao, *Biosens. Bioelectron.*, 2011, **26**, 3309-3312.

85. Q. Xue, L. Wang and W. Jiang, *Chem. Commun.*, 2012, **48**, 3930-3932.

86. S. Bi, H. Zhou and S. Zhang, *Chemical Science*, 2010, **1**, 681-687.

87. H. Liu, S. Li, L. Liu, L. Tian and N. He, *Biosens. Bioelectron.*, 2010, **26**, 1442-1448.

88. M. Ferrari, *Nat. Rev. Cancer*, 2005, **5**, 161-171.

Chapter 4
Simultaneous quantification of multiple DNA targets using enzyme-MNPs probes

4.1 Introduction

Many important human diseases are often associated with the presence of specific biomarkers (*e.g.* DNA sequences, proteins and small molecules) in abnormal concentrations. Therefore massive attention is being paid towards the development of facile and sensitive biosensors capable of screening a wide variety of disease biomarkers in clinical samples, allowing for diagnosis of diseases, and the prediction of patients' responses to treatment, risk of relapse of disease and outcomes for clinical diagnostics.[1] Among which, DNA based diagnostics is the most important which alone has accounted for a $17.3 billion market in 2012. PCR is the most widely used technique currently for DNA detection due to its exponential amplification capability.[2-3] However, as a result of its massive amplification power, even a tiny amount of contaminant in samples could produce non- negligible false positive results which can hamper the fidelity and accuracy of this technique. Whereas enzymes, such as HRP and ALP, are highly efficient biocatalysts, offering robust and large signal amplification power even within complex media such as whole blood. As a result, they are widely used in the development of sensitive biosensors using a wide range of different readout strategies, such as electrochemical,[4] colorimetric,[5] fluorimetric,[6] chemiluminescence, [4, 7-9]

Among these methods, electrochemical detections using enzymes as sensing elements have been generally reported.[10-12] For example, enzyme based

specific DNA sensors have been demonstrated by employing a hairpin DNA probe as recognizing element and HRP as signal transducer.[13-14] ALP has also been employed to amplify signals by catalyzing soluble product into insoluble products.[15-16]

At present, the gold standard technique employed in clinical disease diagnosis of low abundant protein biomarkers is ELISA, which uses a surface immobilized antibody (Ab1) and an enzyme-conjugated antibody (Ab2-enzyme) to sandwich the target, effectively converting each captured protein target into an Ab1-target-Ab2-enzyme sandwich for sensitive target readout. This approach generally possesses good sensitivity and specificity, but constraints such as reduced reactivity and accessibility of surface immobilized Ab1, inefficient target capture (limited by the fundamental target-Ab binding affinity) and slow binding kinetics between surface immobilized Ab1 and target in solution, often result in relatively long assay time, preventing it achieving ultra-high sensitivity (fM-aM) that is highly valuable for earlier diagnosis.[17]

A major improvement on the sensing performance of ELISA has been the introduction of nanomaterials which can offer sufficient surface spaces to immobilize multiple capture molecules, and allow for fast and efficient target capture in a homogenous environment.[17] Besides these advantages, dedicated and cost-effective synthesis and modification methods of nanomaterials have also promoted their general usage. Among these nanomaterials, MNPs have recently attracted significant attention due to their unique superparamagnetic properties and low toxicity, making them especially advantageous for biosensing.[18]

MNPs can be synthesized by well established methods and modified with stable and nontoxic functional coatings [19-22] for bioconjugation. Moreover, the tiny

particle size coupled with superparamagnetic property allows them to form uniform, homogenous dispersions in solution (hence rapid, target binding) in the absence of an external magnetic field, yet they are readily retrieved upon application of an external magnetic field. These characteristics make them well-suited for target capture, separation and enrichment from real-world samples to achieve sensitive biosensing.[23]

In real-world clinical sample analysis, the detection of one single disease marker may not be able to provide an unambiguous diagnosis of disease (*to date, ″no tumor marker identified to date is sufficiently sensitive or specific to be used on its own to screen for cancer″*),[24] and therefore multiple markers should be used to improve the diagnostic robustness and accuracy. Thus development of a sensitive assay that can simultaneously detect multiple cancer markers is a necessary and urgent need for enhancing the fidelity and accuracy of early clinical diagnosis. In this regard, several nanosensors capable of simultaneously detecting multiple different targets have been reported over the past few years. For example, a GMR sensor developed in the Wang group recently has been shown to be capable of multiplexed cancer marker monitoring by using the GMR property of MNPs as signal reporter. The GMR sensor is highly sensitive and robust, and more importantly it is effectively insensitive to environmental sensing conditions (pH, temperature, ionic strength), and thus has great potential for sensing and diagnostic techniques for real-world samples.[25] In addition, gold nanoparticles are reported to have extraordinary universal quenching ability for different fluorescent dyes in close proximity.[26] Taking advantage of this, a multicolor GNP based nanobeacon has been designed for selective analysis of three DNA targets.[1] Similarly, planar graphene has been employed to detect multiple DNAs by using its universal efficient quenching property for organic dyes.[27-28] Nevertheless, the LOD of these approaches (~nM level) has to be improved to make them competitive against current clinical assays.

Herein, I developed a simple, rapid, sensitive and highly specific DNA sensor using a MNP based DNA-sandwich assay combined with efficient enzymatic amplification. Thiolated capture DNA (cDNA) strands are covalently immobilized onto the amine- functionalized MNPs using a PEGylated heterofunctional crosslinker (NHS-PEG_{12}-Maleimide) to form a MNP-cDNA probe. In the presence of DNA target, the MNP-cDNA and an enzyme conjugated signal DNA (sDNA-En) could sandwich bind the target DNA, forming a MNP-dsDNA-En sandwich, which effectively converts each captured target DNA into an enzyme and is readily separated from the reaction media. Therefore, the detection and quantification of the DNA targets could be readily realized by simply monitoring the catalyzing property of the converted enzymes.

4.2 Material and methods

4.2.1 Materials and instruments

All DNA probes and target strands were purchased commercially from IBA GmbH (Germany). They were all HPLC purified by the supplier and their sequences are summarized in Table 4.1. Both HRP-NAV and ALP-NAV were purchased from Thermo Fisher Scientific (UK). Amplex red and fluorescein diphosphate (FDP) were purchased from Invitrogen Life Technologies (UK). All other chemicals and reagents were purchased from Sigma-Aldrich (UK) and used without further purification unless otherwise stated. PBS buffer (137 mM NaCl, 10 mM Na_2HPO_4, 2.7 mM KCl and 1.8 mM KH_2PO_4, pH is 7.4 unless otherwise noted) and Tris buffer (100 mM Tris-base, 100 mM NaCl, pH 8.5) was made with ultra-pure MilliQ water (resistance > 18 $M\Omega.cm^{-1}$). The MNPs were synthesized and modified in house. All UV absorption spectra were recorded on

a Cary 50 Bio UV-Vis spectro- photometer in a quartz cuvette with an optical path length of 1.0 cm.

Table 4.1 DNA sequences used (5'-3') in this study.

Name	Sequence (5'-3')
cDNA1	HS-TTT TTT- TCCGACCTGGGG
sDNA1	GAGTATTGCGGAGGA-TTTTTT-Biotin
DNA1	TCCTCCGCAATACTCCCCCAGGTCGGA
cDNA2	HS-TTTTTT-GGGAGTCCGTGGTAG
sDNA2	GGCAGGTTGGGGTGA-TTTTTT-Biotin
DNA2	TCACCCCAACCTGCCCTACCACGGACTGCC
cDNA3	TGGCGTAGGCAAGAGTTT TTT TTT TT-HS
sDNA3	Biotin-TTT TTT-GTGGTAGTTGGAGCTG**G**
DNA3	ACTCTTGCCTACGCCA**C**CAGCTCCAACTACCAC

4.2.2 Experimental methods for MNP synthesis

The MNPs were prepared by a co-precipitation method.[21, 29-31] The synthetic and functionalizing procedure of the MNP is shown schematically in Figure 4.1.

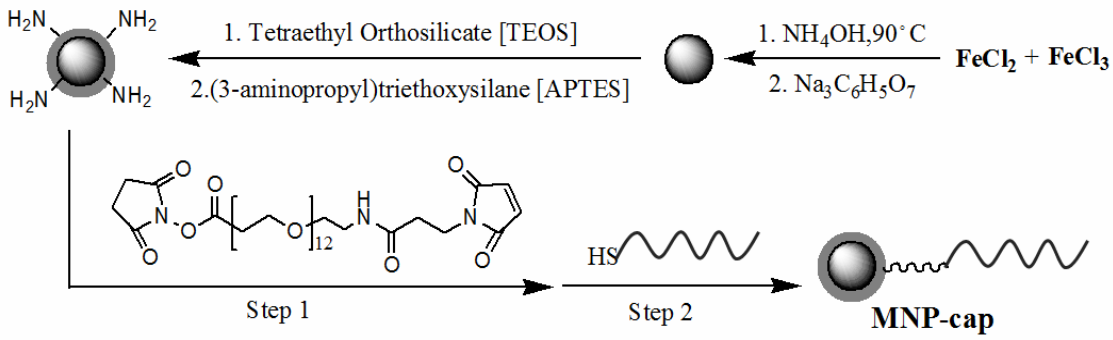

Figure 4.1 Illustration of the procedures for MNPs Preparation and modification. It should be noted that several hundred strands of the cDNAs are attached to each MNP, and only one is shown here for simplicity. (Reprinted by permission of the Royal Society Chemistry)[32]

5 mmol $FeCl_2 \cdot 4H_2O$ and 10 mmol $FeCl_3 \cdot 6H_2O$ were dissolved in 50 mL deoxygenated H_2O under magnetic stirring. Then 4.3 ml $NH_3 \cdot H_2O$ (35%) solution mixed with 50 mL deoxygenated H_2O was added into the above solution dropwise with N_2 gas bubbling, forming black precipitates. The mixture was heated at 80 ^oC for 30 min in an oil bath under vigorous stirring and then for another 2 h at 90 ^oC following the addition of 50 mL of 0.2 M trisodium citrate (see Figure 4.1). The obtained Fe_3O_4 MNPs appeared as a black precipitate which was separated by centrifugation (4000 g for 3 min) and then washed once with acetone. Finally, the MNPs were dispersed in deionized water (with the volume being adjusted to 30 mL).[21, 29-31]

Fe_3O_4/SiO_2 core/shell MNPs were prepared by using a modified Stöber method.[33] In typical preparation, 1 mL of the hydrophilic Fe_3O_4 seeds prepared above was firstly diluted with the mixture of 4 mL deionized water and 20 mL absolute ethanol. Under continuous stirring and N_2 bubbling, 0.43 mL $NH_3 \cdot H_2O$ (35%) solution and 0.5 mL tetraethyl orthosilicate (TEOS) were consecutively added to the above suspension. The hydrolysis/condensation reaction was allowed to proceed for 3 h under N_2 gas bubbling at room temperature (see

Figure 4.1). Subsequently the obtained Fe_3O_4/SiO_2 core/shell MNPs were separated by centrifuging at 4000 rpm for 5 min and then washed by water twice. Finally, the obtained MNPs were re-dispersed in deionized water (total volume: 1 mL).

Amine functionalised Fe_3O_4/SiO_2 core/shell MNPs were prepared as follows: [20-21, 30, 33-35] 1 mL of the silica-coated Fe_3O_4/SiO_2 core/shell MNPs prepared above was dispersed in 4 mL deionized water and 20 mL absolute ethanol. Then 0.43 mL $NH_3 \cdot H_2O$ (35%) solution and 0.5 mL of (3-aminopropyl)triethoxysilane (APTES) were consecutively added to the solution under continuous stirring and N_2 gas bubbling. The reaction was carried out for 3 h at room temperature, leaving to APTES to hydrolyse and subsequently condense on the MNP surface to introduce amine groups (see Figure 4.1). Afterwards, the amine functionalized MNPs (NH_2-MNPs) were separated, washed and then re-dispersed in deionized water. Concentration of the MNP suspension was estimated by comparing the suspension's weight with pure water of the same volume.

5 mg NH_2-MNP and 2.5 mg $SM(PEG)_{12}$ were mixed and incubated in PBS buffer (containing 1mM EDTA, pH = 7.2) at room temperature for 1 h, leading to the MNP surface being functionalised with maleimide groups. Thereafter, the MNPs were washed by PBS buffer (containing 1mM EDTA, pH = 7.2) twice, and then 5 nmol of thiolated cDNA in 1 mL PBS buffer (containing 1mM EDTA, pH = 7.2) was added into the above MNPs and incubated for 1 h at room temperature. The cDNA is covalently conjugated to the MNP surface *via* Michael addition of the thiolate to the MNP surface maleimide groups (see Figure 4.1). The MNPs were subsequently washed twice by PBS buffer (containing 1mM EDTA, pH = 7.2). It should be noted that all of the original and washing supernatants were collected and combined for UV measurement at 260 nm to determine the

amount of free-unbound cDNA, allowing the estimation of the cDNA conjugation efficiency on the MNP (assuming the reduced amount of cDNA has conjugated to the MNP). The cDNA loaded MNPs were then treated with 5 µL of 2-mercaptoethanol in 1 mL PBS buffer containing 1 mg/mL BSA to cap any unreacted maleimide groups and to block the MNP surface to reduce non-specific absorption of HRP-NAV.

4.2.3 Experimental methods for MNP characterization

XRD (X-ray diffraction) tests were performed on X'pert MPD instrument by PANalytic. The scan range (2θ) was from 10 to 90 ° at increments of 0.0332 ° with a scan speed of 0.5 second/step.

The infra-red (IR) spectra were obtained from a Perkin elmer FT-IR spectrometer at room temperature. The dried sample was pressed into the disk and the transmission properties in the range between 4000 and 500 cm^{-1} were recorded.

The hydrodynamic sizes of as synthesized citrated MNPs were characterized in PBS buffer on a Brookhaven Instruments Corp BI-200SM Laser Light Scattering Goniometer with a BI-APD detector using a He-Ne laser at 633 nm (scattering angle: 90°, temperature: 25 °C).

The magnetic properties of the MNPs were tested with a MagLab vibration sample magnetometer (Oxford Instruments) operating at 55 Hz with amplitude of 1.5 mm. The sensitivity of the instrument is about 2 µemu, with a field range of up to 9 T. The samples were measured at room temperature (290 K) at a magnetic field scan rate of 9.17 mT/s.

4.2.4 Experimental methods for DNA detection

At first, HRP-NAV was incubated with biotinylated sDNA for 1 h at 1:1 molar ratio in PBS buffer containing 1 mg/mL bovine serum albumin (BSA) to make the HRP and sDNA conjugate (HRP-sDNA). Then cDNA-MNPs were mixed with HRP-sDNA and target DNA of various concentrations. The final volume of each sample is 500 µL in PBS buffer containing 1 mg/mL BSA. After incubation for 1 h at room temperature (unless otherwise noted), the resulting MNPs were retrieved magnetically and were subsequently washed several times to remove any unbound target DNA and HRP-sDNA. The washing procedures were as follows: 500 µL PBS buffer once, 500 µL PBS buffer (containing 0.1% Tween-20) twice, and 500 µL PBS buffer once again. Following that the MNPs sandwiches were dispersed in 380 µL PBS buffer, and the enzymatic amplification was initiated by the addition of 50 µL amplex red (0.2 mM) and 50 µL H_2O_2 (0.2 mM). After a certain period, the enzymatic assays were stopped by adding 20 µL NaN_3 (1 M) solution. The samples were centrifuged to remove MNPs and reduce its scattering effect, and the UV-vis absorption spectra of all the resulting supernatants were recorded.

Likewise, ALP-sDNA conjugates were prepared by mixing ALP-NAV with biotinylated sDNA for 1 h at 1: 1 molar ratio in Tris buffer (containing 1 mg/mL BSA). Then cDNA-MNPs were mixed with ALP-sDNA and target DNA at various concentrations in 500 µL Tris buffer (containing 1 mg/mL BSA). After incubation for 1 h at room temperature, all the samples were washed to remove any unbound species from the MNP-dsDNA-ALP sandwiches. The washing procedures were similar to thouse described above, simply replacing the PBS buffer with Tris buffer (*e.g.* 500 µL Tris buffer once, 500 µL Tris buffer containing 0.1% Tween-20 twice, and 500 µL Tris buffer once again). Then the MNP sandwiches were dispersed in 430 µL Tris buffer, and then each was mixed with 50 µL fluorescent diphosphate (FDP) (0.2 mM) initiating the enzymatic amplification assay. After a certain amplification time, 20 µL PBS

buffer was added to the resulting solution to stop the enzymatic reaction, and the UV spectra of the resulting supernatants were recorded.

For simultaneous two DNA target detection, MNPs-cDNA1 and MNP-cDNA2 (15 µg each) were first mixed with 15 µL ALP-sDNA1 (0.25 µM) and 15 µL HRP-sDNA2 (0.25 µM) followed by addition of two different target DNA strands (DNA1 and DNA2 with the ratio 1 to 1) with different concentrations (0 -1 nM). Due to the inhibition effect of PBS buffer on ALP activity, Tris buffer was used in preparing samples and washing procedures (*e.g.* 500 µL Tris buffer once, 500 µL Tris buffer containing 0.1% Tween-20 twice, and 500 µL Tris buffer once again).. After that the MNP sandwiches were dispersed in 330 µL Tris buffer, and 50 µL FDP (0.2 mM), 50 µL amplex red (0.2 mM) and 50 µL H_2O_2 (0.2 mM) were pipetted into each sample to initiate the enzymatic amplification assays for 1 h. After which the enzymatic amplification were stopped by the addition of 20 µL PBS buffer and 20 µL NaN_3 (1 M) respectively. Finally, the UV spectra of the resulting supernatants of all samples were recorded.

4.3 Characterization of MNPs

A series of characterization experiments for MNP and MNP-NH_2 have been carried out before they are used in the DNA sensing assays. Firstly, the magnetic retrieving property of the prepared MNP-NH_2 has been demonstrated by placing their suspension on a magnetic track.

Figure 4.2 shows that MNPs are well-dispersed in water, forming a uniform suspension before applying an external magnetic field. Upon placing onto a standard biomag separation device for 1 min, almost all of the MNPs have been

attracted to the side wall of the tube, confirming that the MNPs are easily retrieved upon applying a magnetic field for easy magnetic separation.

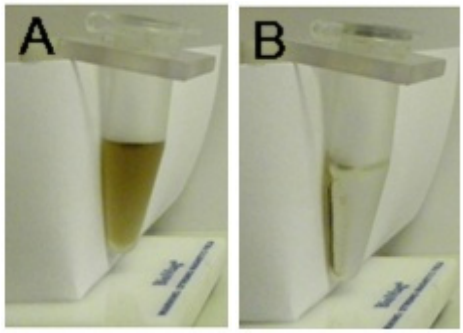

Figure 4.2 Representative photographs of the MNP-NH_2 dispersed in water. The dispersion when placed onto a biomag separation device (**A**) and after waiting for 1 min (**B**). . (Reprinted by permission of the Royal Society Chemistry)[32]

The powder XRD result is consistent with magnetite (Fe_3O_4) showing all of the major characteristic peaks expected for magnetite, which have been indicated in Figure 4.3A.

The synthesized amine functionalized MNPs were dried and characterized using IR spectroscopy. A strong IR absorption band at ~569 cm^{-1} corresponding to the v_{Fe-O} vibrations of the magnetite core is seen in Figure 4.3B. The bands at ~1085 cm^{-1} correspond to the Si–OH vibrations of the silica shell. A broad band at around 3440 cm^{-1} is related to –NH– and/or OH– stretching modes.[36-37]

Uniform suspensions of the MNP and MNP-NH_2 were tested by the dynamic light scattering (DLS) instrument and their statistical size distributions were shown in Figure 4.3C. The average hydrodynamic sizes of the MNP and MNP-NH_2 are determined as 28.9 ± 5.3 and 178 ± 26 nm, respectively.

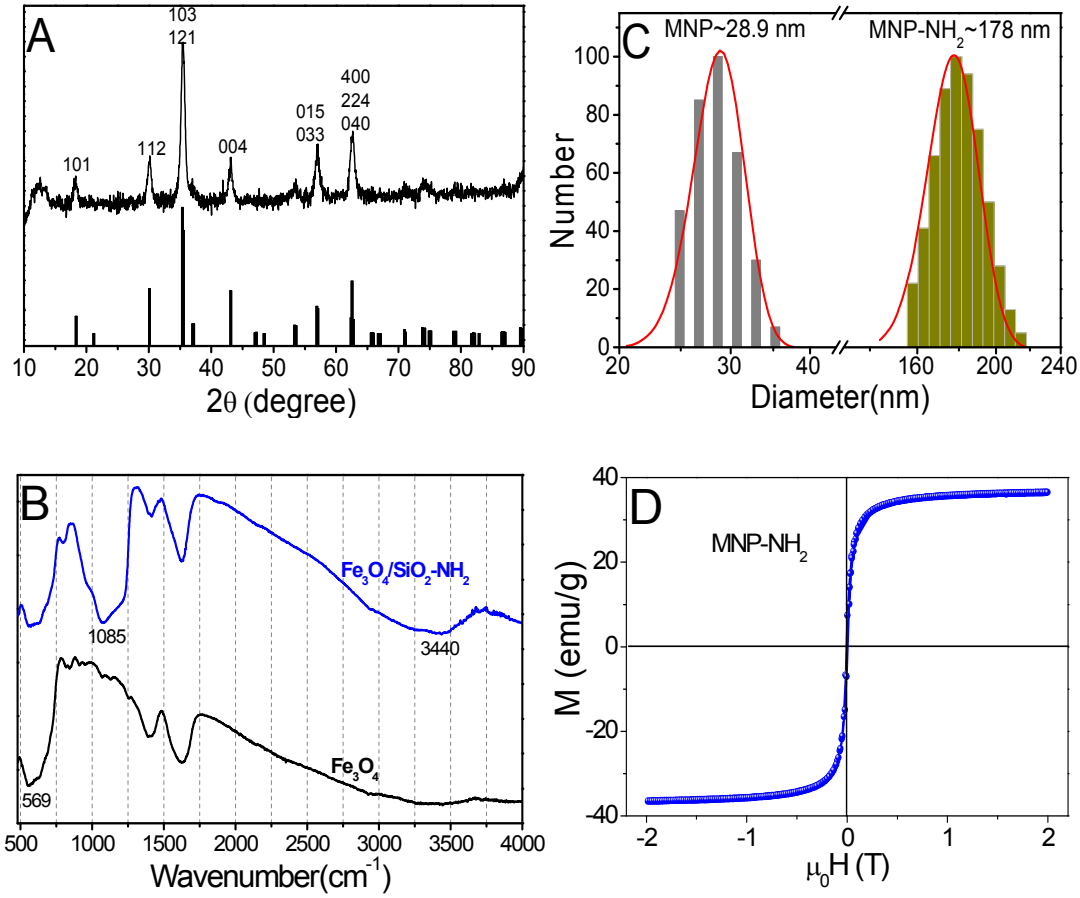

Figure 4.3 Characterizations of the prepared MNP (MNP-NH_2).

(A) Powder X-ray diffraction (XRD) spectra of core only MNP, with the expected diffraction peaks for the Fe_3O_4. **(B)** Typical IR spectra of the MNP and MNP-NH_2. **(C)** The hydrodynamic diameters for core only MNP and MNP-NH_2 were determined as ~29 and ~178 nm, respectively. **(D)** Magnetization of MNP-NH_2 as a function of magnetic field obtained by VSM.

A vibrating Sample Magnetometer (VSM) was used to characterize the magnetic properties of MNP-NH_2. Figure 4.3D displays the hysteresis loops of the MNP-NH_2. The hysteresis loops exhibit a magnetic saturation value of 40 emu/g at 290 K. The synthesized MNPs-NH_2 form a stable, homogenous dispersion without aggregation in the absence of applied external magnetic field,

and yet they can be readily retrieved from the assay media in 1 min with an applied magnetic field, making them well-suited for biosensing because they can offer rapid target capture and effective magnetic separation (see Figure 4.2B).

4.4 Enzyme activities and inhibitors

ELISA has been used to detect a wide range of targets such as proteins, nucleic acids and pathogens as standard in biochemical analysis and clinical diagnostics. ELISA assays usually employ enzymes to catalyze colorless or non-fluorescent substrates into colored and/or fluorescent products to report and amplify signals. Inspired by ELISA, here two frequently used enzymes in ELISA - HRP and ALP - are introduced in this system for signal amplification.

HRP is isolated from horseradish roots and is a single chain polypeptide containing four disulfide bridges. It is a 40,000 Dalton glycoprotein containing 18% carbohydrate whose composition depends upon the specific isozyme.[38] Apart from its small molecular weight, its glycosylation results in low non-specific binding, which makes HRP the most widely used signal amplification label in immunochemistry applications.[39]

In the presence of hydrogen peroxide (H_2O_2), HRP could convert a wide variety of substrates (*e.g.*, luminol, TMB, DAB, ABTS and amplex red). Here amplex red is used as enzyme substrate (*e.g.* hydrogen donor) to be converted to resorufin by reducing H_2O_2 to H_2O under the catalysis of HRP (see Figure 4.4A).[40-41] Resorufin has absorption (extinction coefficient: 54,000 $cm^{-1}M^{-1}$) and

fluorescence emission maxima of 563 nm and 587 nm, respectively, allowing for both absorption and fluorescence based readout.

HRP is stable and maintains catalyzing ability in the pH range of 5.0 to 9.0. HRP has been shown to possess optimum activity in the pH range of 6.0 to 6.5, and retain ~84% of the maximum activity at pH 7.5.[42] In this study, a near-physiological pH (7.4) was adapted for single DNA detection using HRP as the efficient signal amplification element. In addition, a few compounds are found having inhibitory effects on HRP activity such as sodium azide, cyanide, L–cystine, dichromate, hydroxylamine, sulfide, vanadate[42], which can be used to terminate the enzymatic reaction after a certain period to tune the signal amplification power and assay time.

ALP is a hydrolase enzyme which catalyzes the hydrolysis of phosphate monoesters by removing the phosphate substituent. As its name suggests, ALP is most effective at an alkaline pH.[43] Moreover, it requires zinc, and magnesium or calcium divalent ions for its activity.[44] Since ALP has specificity for phosphate esters of alcohols, amines, and phenols, it is often used to dephosphorylate proteins and nucleic acids.[45-46] More importantly, ALP is also a widely used enzyme which conjugates to antibodies and other proteins as a label for ELISA, Western blotting, and histochemical detection. In this system, ALP is used to hydrolyze FDP, which is a colorless and nonfluorescent molecule. Sequential hydrolysis of the two phosphate moieties yields firstly a weakly fluorescent fluorescein monophosphate followed by strongly fluorescent fluorescein (see Figure 4.4B). The produced fluorescein as the signal reporter possesses excitation and emission maximum at ~490 and 514 nm respectively. Quite a few compounds could act as inhibitors for ALP activity, such as arsenate, cystine, iodine, inorganic phosphate.[47]

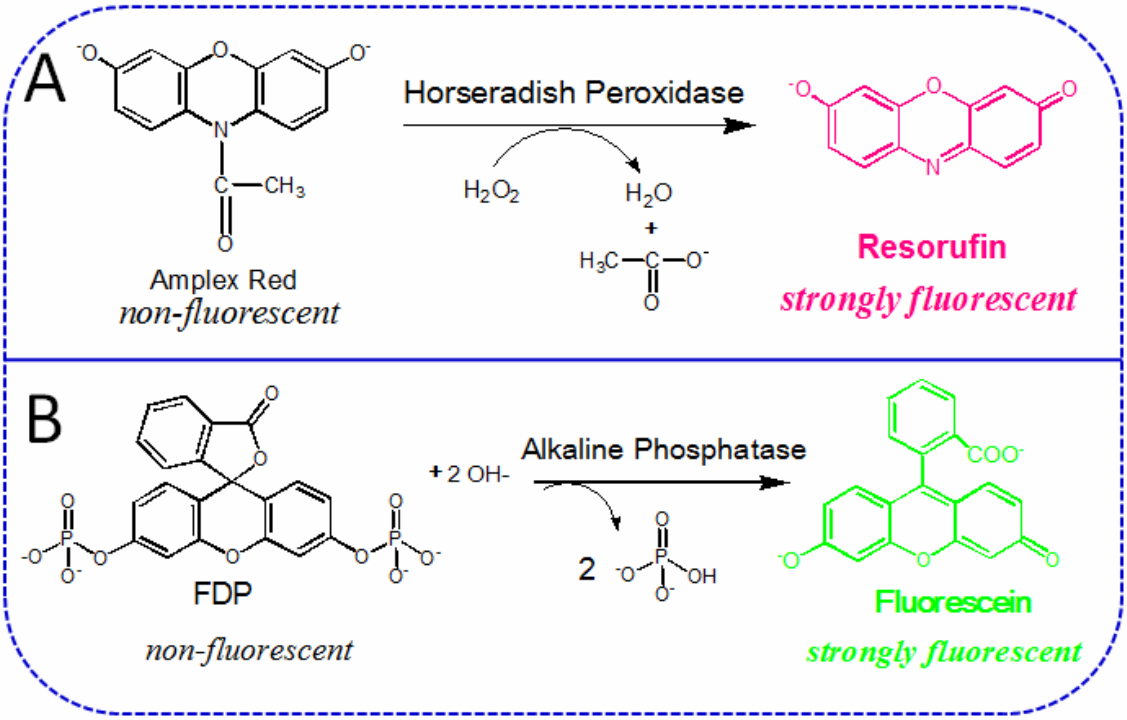

Figure 4.4 Illustrations for the HRP and ALP catalyzed enzymatic assays

In this research, NaN_3 was chosen as the stopping reagent for the enzymatic reaction of the HRP-NAV. To test its inhibition effect on the enzymatic assay, the enzymatic catalyzed absorbance change at 571 nm was monitored before and after addition of this inhibitor by UV spectroscopy. In the beginning, the enzymatic reaction of 100 fmol (200 pM in PBS buffer, final concentration) HRP-NAV was triggered by addition of substrates (amplex red and H_2O_2, 20 µM each, final concentration). After about 15 min, 20 µL NaN_3 (1M) was pipetted into the reaction cuvette, and the enzymatic assay was continuously recorded (see Figure 4.5).

As inorganic phosphate is known as an inhibitor for the ALP-NAV catalyzed reaction, herein the inhibition ability of PBS buffer was studied. The absorbance change at 485 nm was monitored before and after addition of PBS buffer. The enzymatic reactions of 100 fmol (200 pM in Tris buffer, final concentration) ALP-

NAV was initially triggered by addition of its substrates (FDP, 20 µM, final concentration). After about 10 min, 20 µL PBS buffer was pipetted into the reaction cuvette, and the enzymatic assay was continuously recorded (Figure 4.5, red line).

As shown in Figure 4.5, initially, the absorbance for both assays (at 485 nm for ALP-NAV and 571 nm for HRP-NAV) increased steadily with the increasing assay time, which indicated the formation of coloured products (resorufin and fluorescein) catalyzed by HRP-NAV and ALP-NAV, respectively. Upon addition of their respective inhibitors (NaN_3 and PBS buffer for HRP-NAV and ALP-NAV systems respectively), the absorbance decreased at first, due to the dilution effect and then kept constant because the colored products were no longer being produced due to inhibition of the respective enzymes. The results clearly demonstrate that these two enzymatic reactions can be stopped immediately upon addition of their corresponding inhibitors. Because the enzymatic amplification time is critical for signal readings, the discovery of appropriate inhibitors allows us to control the enzymatic amplification time accurately and reduce the signal variations before measurement. This is especially important for carrying out high-throughput detections, where the use of appropriate enzyme inhibitors is indispensible.

Moreover, the assay curves also allow us to determine the substrate turnover rates of HRP-NAV in PBS buffer and Tris buffer and ALP-NAV in Tris buffer. The extinction coefficients (ε) of the enzymatic products resorufin and fluorescein are 54 $(mM*cm)^{-1}$ and 50.4 $(mM*cm)^{-1}$. Slopes for each kinetic curve could be obtained by linear fitting the data for the first 5 mins. According to the equation below,

$$Rate=Slope/([enzyme]*\varepsilon) \quad (4.1)$$

From the slope of the assay curve, the substrate turnover rates for each enzymatic assay could be calculated. HRP-NAV could turnover 65 and 56

amplex red molecules into resorufin per second in PBS buffer and Tris buffer, respectively. While ALP-NAV could turnover 65 FDP molecules into fluorescein per second in Tris buffer at pH 8.5.

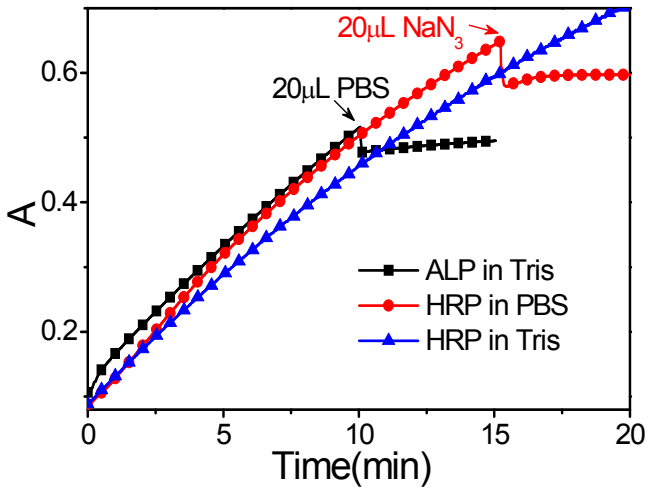

Figure 4.5 Activities and inhibitions of the enzymes used in this study.

Typical UV-vis assay curves show the catalytic activities of the HRP and ALP in different buffers and their inhibition by NaN_3 and phosphate.

4.5 DNA sensing using HRP as sensing element

Figure 4.6 shows this approach schematically. Two short ssDNA probes, each complementary to one half of the DNA target, are designed. The two probes are modified with a biotin (blue, to be conjugated with enzymes for signal amplification) and -thiol (green, to be conjugated onto MNP surface for target capture and separation), respectively. In the presence of a target DNA strand, the two probes are hybridised with it forming a sandwich structure with an exposed terminal biotin, through which HRP is bound to the MNP surface. Thus detection of target DNA is now converted into detection of enzymes. After a series of washing procedures and magnetic separation, excess sDNA-HRP is

washed off from the mixture to reduce background. Subsequently, the enzymatic assay is carried out for signal amplification and the spectra are recorded. Since HRP could catalyze hundreds of thousands of amplex red molecules (colourless) into strongly colored resorufin over a 1 h assay period. The method allows sensitive DNA detection *via* the resulting absorption signals.

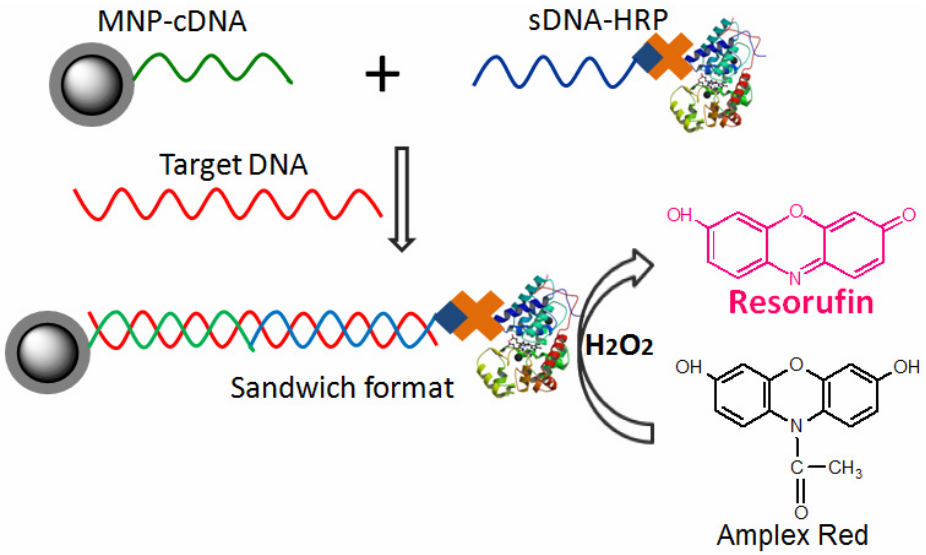

Figure 4.6 Schematic illustration of this strategy to DNA detection.

A biotin-probe DNA (blue) is conjugated with HRP and a thiol-probe DNA (green) is bound with MNP, which are then hybridized to each half of a complementary DNA target. The formed sandwiches are then separated and subjected to enzymatic assay.

4.5.1 Optimization of the MNP-enzyme sandwich sensing platform

4.5.1.1 Effect of cDNA-MNP surface blocking

As shown in the Figure 4.1 the MNP-NH_2 was first reacted with $SM(PEG)_{12}$ to introduce maleimide function groups upon which the thiolated cDNA was covalently conjugated. A PEG_{12} linker is used here because it is well-known to

be one of the most effective coatings in resisting non-specific adsorption of biomolecules, reducing background and improving sensitivity.[48] In addition, the amount of the MNP surface maleimide functional groups was in large excess over the amount of cDNA to ensure high conjugation efficiency. Therefore there should still be considerable unreacted free maleimide groups left on the nanoparticle surface, which can lead to non-specific adsorption of the HRP-NAV and hence significantly increased background. Thus, 2-mercaptoethanol was used to react with any free maleimide groups remaining after cDNA conjugation. Next the MNPs were further treated with a cheap protein, BSA, to block any un-occupied sites and hence reduce non-specific adsorption of the HRP-NAV. The effect of cDNA-MNP surface blocking (by 2-mercaptoethanol and 1 mg/mL BSA, see MNP preparation part) on the assay specificity for the DNA target detection has been investigated.

Specifically, 20 μg MNP-cDNA1 (either before or after blocking) was mixed with HRP-sDNA1 (10 nM, final concentration) and with or without target DNA1 (100 pM, final concentration) in 500 μL PBS buffer. After incubation for 1 h and washing with PBS buffer, the resulting MNP-DNA-enzyme sandwich was subjected to 1 hr enzyme amplification and the absorbance at 571 nm of each sample was recorded and is shown in Figure 4.7.

As indicated in Figure 4.7, the grey and **red** bars show the assay prior to and after the blocking (by 2-mercaptoethanol and 1 mg/mL BSA, see MNP preparation part), respectively. The signal/background ratio for 5 fmol DNA1 target increases from ~4.4 (before blocking) to ~62 after blocking, confirming surface blocking is essential to achieve high signal/background ratio. Therefore all cDNA-MNPs have been blocked by 2-mercaptoethanol and BSA before being used.

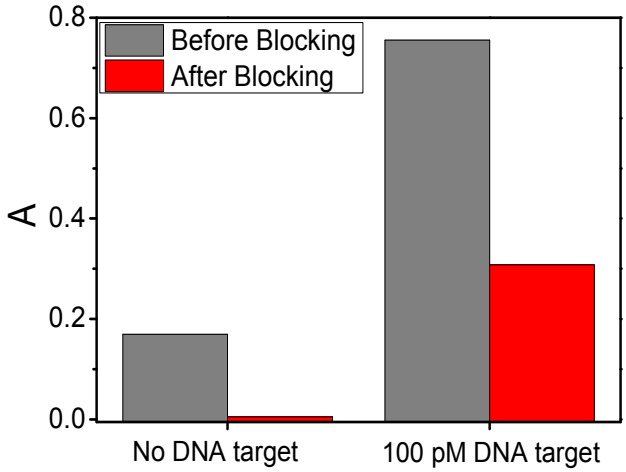

Figure 4.7 Effect of cDNA-MNP surface blocking on the assay specificity for DNA target detection. . (Reprinted by permission of the Royal Society Chemistry)[32]

4.5.1.2 Evaluation of the effect of MNP amount

Evaluation of the effect of MNP amount on the assay sensitivity has been carried out by using various amounts (0-40 μg) of MNP-cDNA1 with a fixed amount of 5 pmol HRP-sDNA to detect DNA1 (200 pM, final concentration) in PBS 7.4 buffer. After 1 h incubation and washing, 40 mins enzyme amplification was carried out and the absorbance of each sample was recorded. In the mean time, the mixtures of various amounts of MNP-cDNA with 5 pmol HRP-sDNA without target DNA were also prepared and tested as controls.

Figure 4.8 shows the effect of the cDNA-MNP amount on the signal response for detecting 5 fmol DNA target: **red dots●** show the assay without the DNA target (background due to non-specific adsorption), and **black squares■** show the assay with 5 fmol DNA target, and **blue triangles▲** (**black squares■ - red dots●**) show the net contribution from the DNA target.

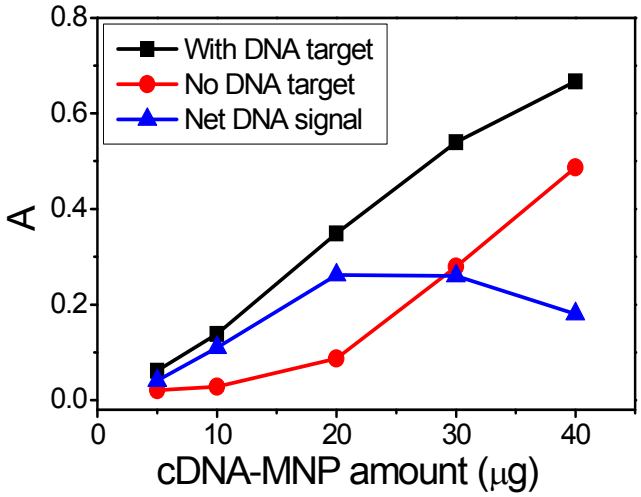

Figure 4.8 Absorbance of samples using different amounts of cDNA-MNPs to detect 200 pM (5 fmol) DNA1 and corresponding blank controls. . (Reprinted by permission of the Royal Society Chemistry)[32]

Although 2-mercaptoethanol and BSA were used to treat the MNPs to reduce the non-specific absorption, this cannot eliminate the non-specific adsorption of the enzyme completely. A small amount of the HRP-NAV can still absorb on the MNPs surface non-specifically, contributing to some background signal. As displayed in Figure 4.8, although increasing the amount of MNP-cDNA used in the assay produced a stronger signal, indicating more efficient target capture, however, the background due to enzyme nonspecific absorption also increased significantly. As a result, the net contribution from the DNA target only (**black – red**) actually decreased when the amount of MNPs was over 20 μg. Therefore, 20 μg cDNA-MNP was found to be optimum here because it gave the maximum net signal from the DNA target. Thus 20μg MNP-cDNA was employed for the later experiments.

4.5.1.3 Evaluation of temperature effect

Temperature is an important environmental factor for biosensing because it could affect specific recognition kinetics and moreover the enzyme activity. Herein, the dependence on temperature was assessed.

20 µg MNP-cDNA3 were mixed with 20 µL HRP-sDNA3 (0.25 µM) and target DNA3 of various concentrations. The final volume of each sample is 500 µL in PBS buffer (containing 1 mg/mL BSA). Four sets of samples as described above were prepared and incubated for 1 h at 4 different temperatures (4 °C, 15 °C, 24 °C, 37 °C). After this, all of the samples were washed to remove unbound target DNA and HRP-sDNA, and finally the UV spectra of all the supernatants of samples were recorded after 1 h enzymatic amplification at room temperature.

As shown in Figure 4.9, temperature does affect the sensitivity of the assay. Specifically, in the tested temperature range, as temperature goes up, the sensitivity (slope of the calibration curve) increases correspondingly and reaches its maximum value at 24 °C. As the temperature increases further to 37 °C, the sensitivity is maintained almost the same as that at 24 °C (roughly about room temperature. Therefore all assays were subsequently carried out at room temperature without specific temperature controls. Here, the sensitivity reflects the combined effects of the enzyme activity and the DNA hybridization efficiency (*e.g.* capture efficiency).

HRP was reported to be reasonably thermal stable, its tertiary structure melted at ~45 °C to be a pre-molten globule form.[49-50] Its optimum activity temperature was reported to be 45 °C-50 °C according to the product introduction from invitrogen. The depletion of the heme catalytic centre from the cavity in HRP structure takes place at ~74 °C.[50] The DNA hybridization melting temperature was evaluated using the “Sci tool” on “integrated DNA technologies” website to

be ~52 °C. However, in this experiment, since the concentration of the target DNA sequences used here is much lower (down to ~pM range, with the cDNA and sDNA concentration of ~10 nM), the melting temperature of the resulting nicked dsDNA structure would be much lower than 52 °C.

At lower temperature (for instance 4 °C), the DNA hybridization is facilitated, while the enzymatic activity is severely hampered. As the temperature goes up to 37 °C, which is still below the optimum activity temperature of HRP, [49-50] the catalytic reactivity of HRP is assumed to be increasing accordingly. However, the similar sensitivity of the assay observed at 24 °C and 37 °C may suggest that the DNA hybridization efficiency is reduced as temperature is increased from 24 to 37 °C.

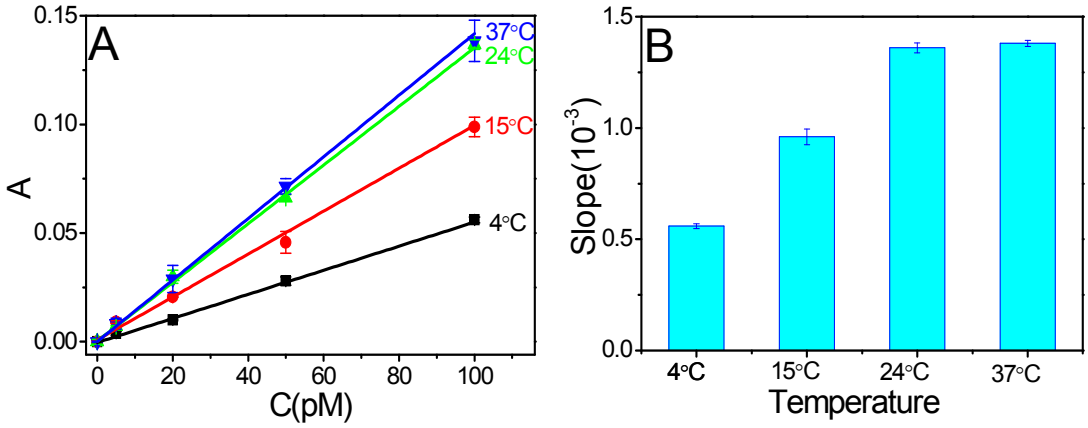

Figure 4.9 Effects of temperatures on DNA sensing ability.

(A) Absorbance responses of DNA titrations at different testing temperatures. **(B)** Slopes (sensing sensitivity) of each linear curve of DNA titrations at different temperatures.

Inspection of the temperature dependence of the sensing system indicates that this sensing platform can work over a wide temperature range (4 - 37 °C) although its sensitivity varies with temperature. Therefore, all of the subsequent

experiments are carried out at room temperature (~24 °C) for convenience and optimum results.

4.5.1.4 Evaluation of cDNA loading amounts on MNPs

The loading amounts of cDNA3 on the MNP surface could also affect the sensing ability of the system. 20 µg MNPs conjugated with different amounts of cDNA3 were mixed with 20 µL HRP-sDNA3 (0.25 µM) and target DNA3 of various concentrations in 500 µL PBS buffer (all containing 1 mg/mL BSA). After 1 h incubation and washing process, enzymatic amplification (1 h) was carried out. Finally the UV spectra of all the samples were recorded.

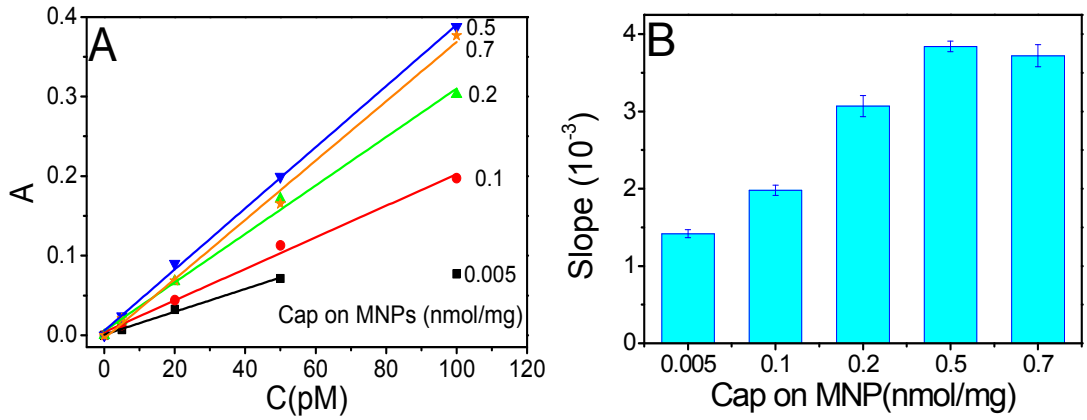

Figure **4.10** Effect of cDNA loading amounts on the MNP on the capture efficiency (assay absorbance response).

(A) Absorbance responses of DNA titrations by MNPs with different cDNA loading amounts. **(B)** Slopes (sensing sensitivity) of each linear curve of DNA titrations by MNPs with different cDNA loading amounts. . (Reprinted by permission of the Royal Society Chemistry)[32]

As shown in Figure 4.10A, for the MNP loaded with the lowest amount of cDNA (0.005 nmol cDNA per mg MNP, **Black squares■**, total cDNA on 20 µg MNP

was 100 fmol), the absorbance increases linearly with the increasing target DNA3 concentration initially, but becomes quickly saturated at 50 pM (25 fmol in 500 µL). This result seems to suggest that not all MNP immobilised cDNAs can hybridize to (capture) the target DNA, and its maximum capture (hybridization) efficiency here is found to be ~25% (25/100).

Moreover, as the loading amounts of the capture DNA on MNPs increase, the sensitivity of the sensor (slope of the sensing curve) increases at first, but achieves a maximum value at ~0.5 nmol/mg. Therefore this loading is determined as optimum, and is used for all subsequent assays.

4.5.2 Wide range DNA titrations using optimized experimental conditions

Using the optimized experimental conditions, a wider target DNA concentration range was implemented as follows to demonstrate the dynamic range of the sensing system.

Specifically, 20 µg MNPs loaded with ~10 pmol cDNA were mixed with 5 pmol HRP-sDNA3 and various amounts of target DNA3 (0 - 0.5 pmol). The final volume of each sample was 500 µL in PBS buffer (containing 1 mg/mL BSA). After 1 h incubation at room temperature, a washing process was carried out to remove any unbound species. Then the MNP-dsDNA-HRP sandwiches were subjected to enzymatic amplification for 1 h. After which, 20 µL NaN_3 (1 M) was added into each sample to stop the enzymatic assay and the UV spectra of all the supernatants of samples were recorded.

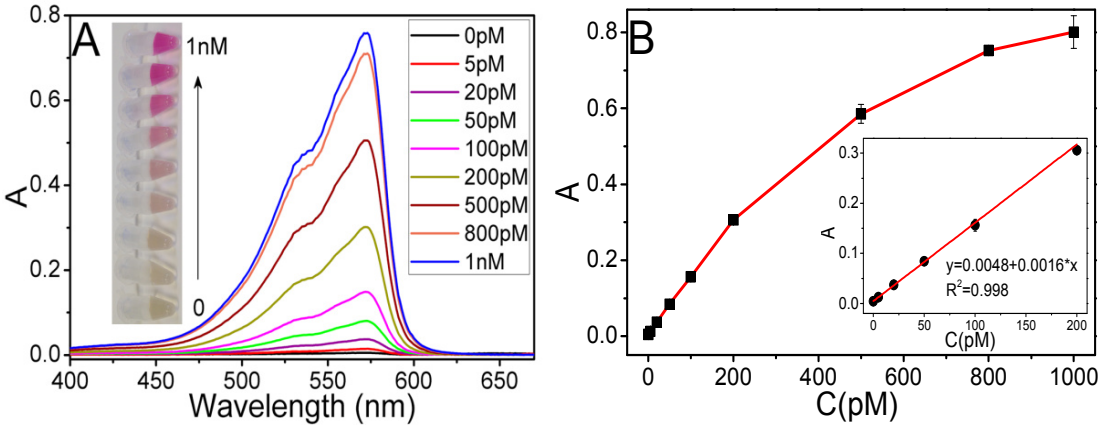

Figure 4.11 Wide range DNA quantification using HRP as signal reporter.

(A) Absorption spectra with inset: sample photo; **(B)** calibration curve for quantification of DNA with Inset: linear fitted amplified region over 0-200 pM DNA target.

Figure 4.11 demonstrates the absorption spectra and calibration curve for DNA titration. Like other typical enzymatic reactions, the absorbance initially displayed a rapid and linear increase with the increasing target DNA concentration up to 200 pM (Figure 4.11B). As the target DNA concentration is increased further, the absorbance-concentration relationship deviates from linear and gradually becomes saturated (see Figure 4.11B data points for 0.5 - 1 nM). This may be attributed to the depletion of amplex red concentration at higher target DNA (hence HRP) concentrations. The initial low target DNA concentration parts (data points for 0 - 200 pM) of the calibration curve showed a good linearity (R^2 = 0.998, see Figure 4.11B inset).

4.5.3 Kinetic studies for DNA titrations and HRP activities

This MNP-enzyme sandwich assay for DNA detection is based upon the conversion of the target DNA strands into MNP-dsDNA-HRP sandwiches for target DNA detection. Thus the amount of enzyme HRP bound on the MNPs

represents the target DNA conjugation efficiency. To investigate the target capture efficiency of this proposed system, kinetic studies of both HRP of different concentration and DNA titrations have been carried out.

For the HRP activity assay, solutions with different amounts (0 - 7.5 fmol) of HRP-NAV were prepared in 1300 µL PBS buffer (containing 1g/L BSA). The enzymatic activity assay was triggered by the addition of 200 µL substrates (containing amplex red and H_2O_2, 150 µM each in PBS buffer), and real-time absorbance changes were monitored by UV-Vis spectroscopy (see Figure 4.12A).

Similarly, for kinetics studies of DNA titrations, 20 µg cDNA3-MNPs were mixed with 5 pmol HRP-sDNA3 and target DNA3 of various amounts (0 - 150 fmol) in 500 µL PBS 7.4 buffer (containing 1 mg/mL BSA). After 1 h incubation and washing processes, the MNP sandwiches were dispersed in 1300 µL PBS 7.4 buffer (containing 1 mg/mL BSA), the enzymatic assay was initiated by the addition of 200 µL substrates (containing amplex red and H_2O_2, 150 µM each in PBS 7.4 buffer), and real-time absorbance changes were monitored (see Figure 4.12B).

Here, it is assumed that the free HRP in solution and bound HRP on MNPs have the same enzymatic activities. By carefully examining the correlations between the kinetic results of these two sets of experiments, the capture efficiency and theoretical detection limit are deduced. Using the fitted function for pure HRP activity ($y*10^5=3.01+14.6*x$, from Figure 4.12C), the conjugated HRP amounts on the MNPs through each individual MNP- dsDNA-HRP activity rate were calculated. Then, a plot demonstrating the correlation between the amount of target DNA and corresponding conjugated HRP on the MNP was obtained (see Figure 4.13). Since each conjugated HRP molecule on the MNP

indicates one target DNA mediated sandwich formation (assuming no dehybridisation of the MNP-dsDNA-HRP sandwich during the washing step), the successful target capture efficiency could be demonstrated by the ratio of conjugated HRP molecules to total target DNA amounts.

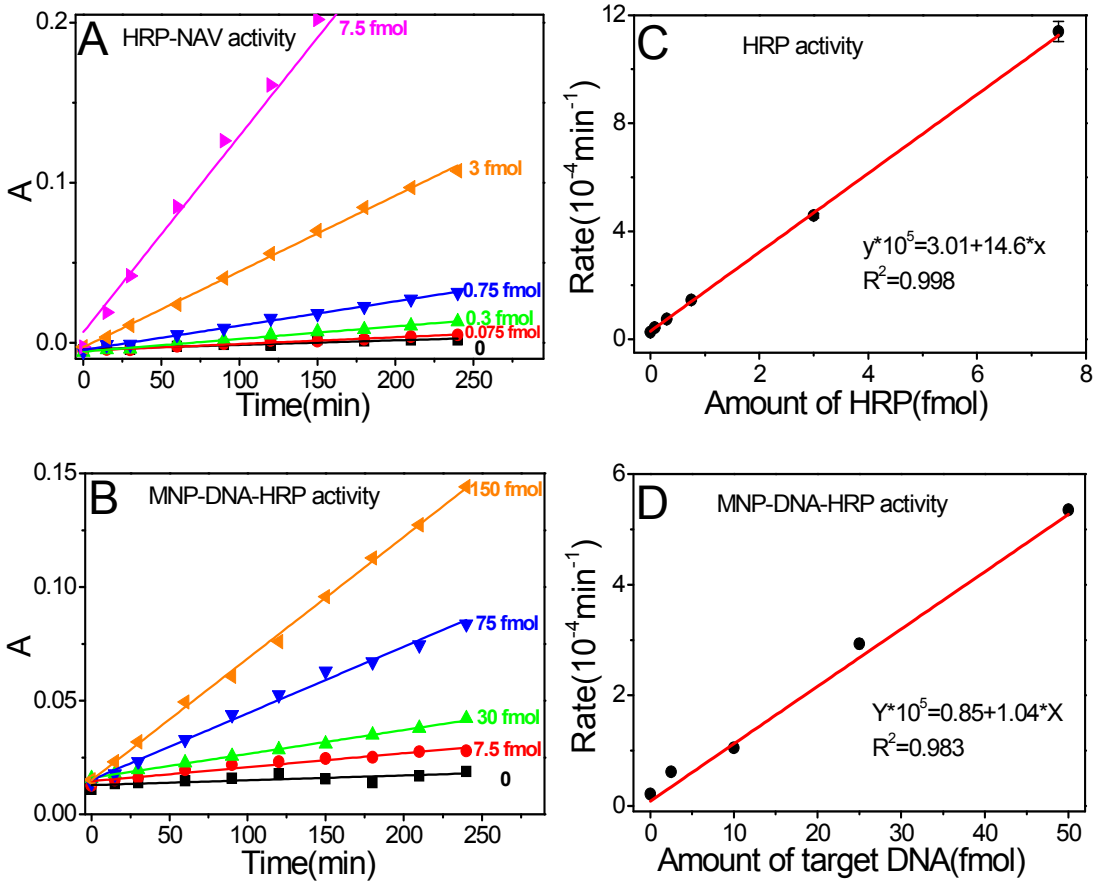

Figure 4.12 The results for both sets (HRP only and MNP-DNA-HRP complex) of kinetic studies.

Real time enzymatic kinetic curves for the HRP only (**A**) and MNP-DNA-HRP complex (**B**) reactions are displayed. The relationship between the catalytic reaction rates and HRP amount **(C)** and total target DNA amounts **(D)** were fitted to a linear relationship.

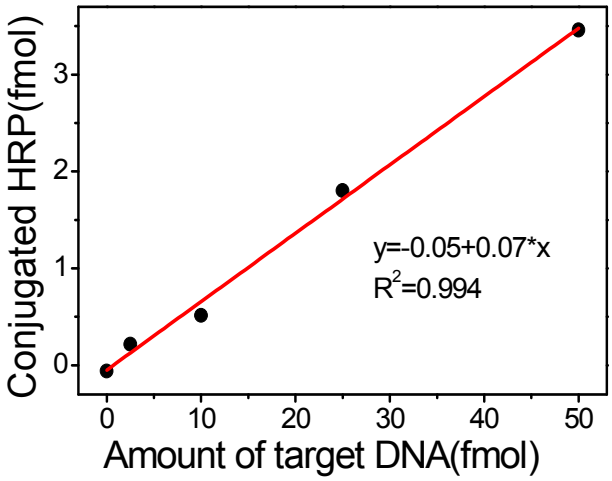

Figure 4.13 Correlation between the total amount of target DNA and conjugated HRP on the MNPs mediated by target DNA.

According to the fitted linear function, target DNA strands which lead directly to HRP conjugation on the MNP surface were only 7% of the total target DNA amounts, suggesting a successful DNA conversion rate of 7% using current experimental conditions. It should be possible to improve this by reducing the washing time (reducing the possible DNA loss from dsDNA dehybridisation), and also minimizing the loss of MNP during washing (it is unavoidable that a small fraction of the MNPs will be lost in each washing step). In the absence of target DNA strands (*e.g.* x = 0), the background signal is negative (-0.05), which might be caused by the scattering effect of MNPs in the suspension. On the other hand, this indicates the background of this sensing system is ultralow.

As shown in Figure 4.12A (time traces of HRP activity), the HRP with concentration down to 50 fM (0.075 fmol) is clearly detectable, from which the theoretical detection limit of this sensing platform is estimated as ~715 fM (50 fM/0.07) by this simple absorption assay. It may be concluded from the above kinetics results of HRP only and MNP-dsDNA-HRP complex, that increasing the target DNA conversion to MNP-linked HRP would be an important factor for

further sensitivity improvement. This issue may be solved by introducing a DNA ligase which could ligate the two probes to reduce the possible loss of conjugated HRP during the washing procedures. Otherwise, an enzyme with a higher activity is necessary to lower the detection limit. Seeking for enzymes that possesses higher catalytic activities is important to further improve the sensitivity of this assay. Nevertheless, even using current experimental condition without further optimization, a sub-pM level theoretical detection limit without DNA target amplification is already competitive in the DNA sensing field.

In addition, DNA titrations subjected to different enzymatic amplification times were examined and the results are displayed in Figure 4.14. Over the whole DNA concentration range (0 - 1 nM), the titration curves show linearity in between 0 - 120 mins enzymatic amplification time. As the amplification time further extends to 180 mins (magenta plots) and 300 mins (dark yellow plots), the titration curves tend to deviate from linearity. These results indicate that the linear dynamic range is being narrowed down as the enzymatic time increasing. If examined more carefully over the lower DNA concentration range (see Figure 4.14B), all of the titration curves over the 0 – 100 pM concentration range are of good linearity, while their slopes which represent sensitivities are enhanced proportionally as the enzymatic amplification time increase (see Figure 4.14C).

The dynamic range is an important factor to evaluate an assay's feasibility in real sample applications. By carefully tuning the enzymatic amplification time, the dynamic range could be adjusted correspondingly. For example, the dynamic range could be enlarged by reducing the enzymatic amplification time. On the other hand, increasing the amplification time can offer higher signal to background ratio thus enhancing sensitivity. Moreover, the MNPs could easily be retrieved by using an external magnet, thus the species of interest bound onto the MNPs could be easily concentrated or diluted where required, which

can be further combined with the adjustment of enzymatic amplification time to achieve the desired dynamic range to suit the specific assay needs.

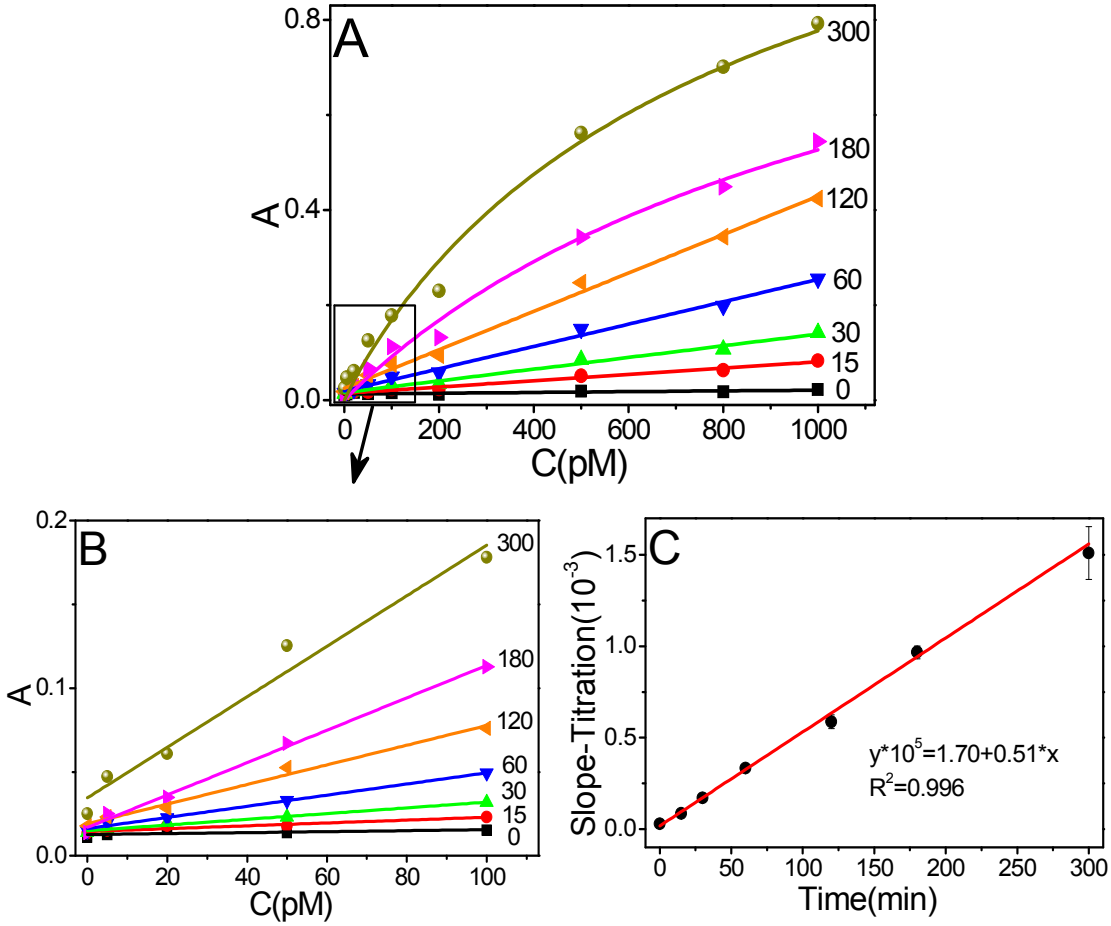

Figure 4.14 DNA titration studies subjected to different enzymatic amplification times.

(A) DNA titration curves corresponding to different enzymatic amplification times (0 - 300 mins, the amplification times are indicated on each curve). **(B)** The enlarged region over 0 - 100 pM DNA target. **(C)** The relationship between the corresponding slopes of curves in (B) and amplification times.

4.5.4 Generality and stability of MNP-cDNA

A major challenge of the proposed protocol is to apply the method for the detection of target DNAs in real biological samples, which are complex media. To test its feasibility, DNA samples in diluted human serum (10% in PBS buffer) were analyzed.

Specifically, 20 µg cDNA3-MNPs were mixed with 5 pmol HRP-sDNA3 and target DNA3 of various amounts (0 -50 fmol). The final volume of each sample is 500 µL in 10% (v/v) human serum /PBS buffer. After incubation and washing processes, the MNP sandwiches were subjected to enzymatic amplification for 1 h followed by stopping the amplification by addition of 20 µL NaN_3 (1 M). The UV-Vis absorption spectra of the supernatants of all samples were recorded.

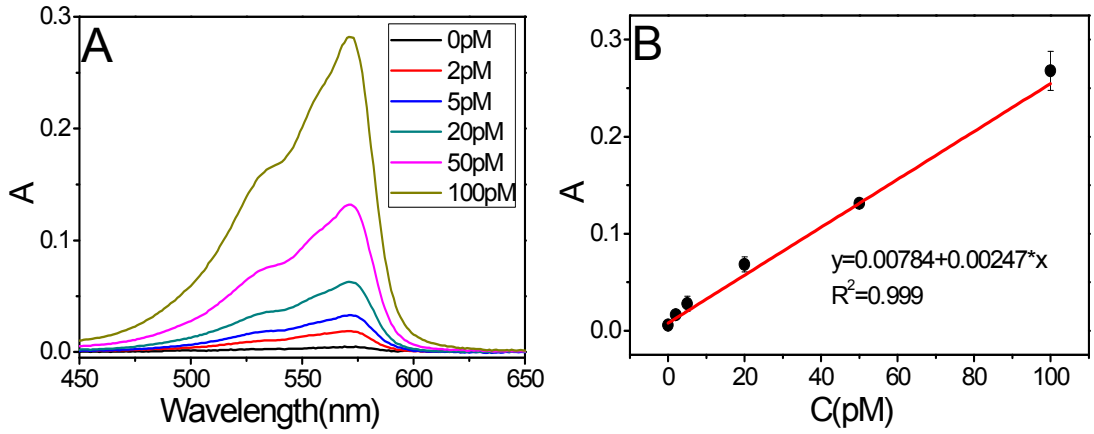

Figure 4.15 Absorbance spectra and calibration curve for DNA titrations in diluted human serum (10% in PBS 7.4 buffer).

As shown in Figure 4.15, a good linear relationship between target concentration and absorbance has been obtained, which indicates this sensing platform also worked in human serum media. This is attributed to the robust surface modification and functionalisation of the MNPs, which minimized non-specific adsorption and the interference from serum proteins. The higher sensitivity of this experiment in the serum than that in PBS buffer (slopes of the

calibration curves are 0.0025 and 0.0016, respectively) may be attributed to the batch-to-batch variations of the HRP activities.

The stability of the MNP-cDNA is another important issue in developing practical and commercial assays, which often require the reagents to have a long shelf-life. To address this challenge, the MNP-cDNA probe suspension (in pure water) was examined after 5 months storage time in a fridge (4 °C).

20 µg cDNA2-MNPs (either freshly prepared or 5 months old) were mixed with 5 pmol HRP-sDNA2 and target DNA2 of various amounts (0 -100 fmol) in 500 µL PBS buffer. After incubation and washing processes, the MNP sandwiches were subjected to enzymatic assays in PBS buffer for 1 h. Finally, the amplification assay was stopped by addition of 20 µL NaN_3 (1 M) and the UV-Vis absorbance spectra of the supernatants of all the samples were recorded.

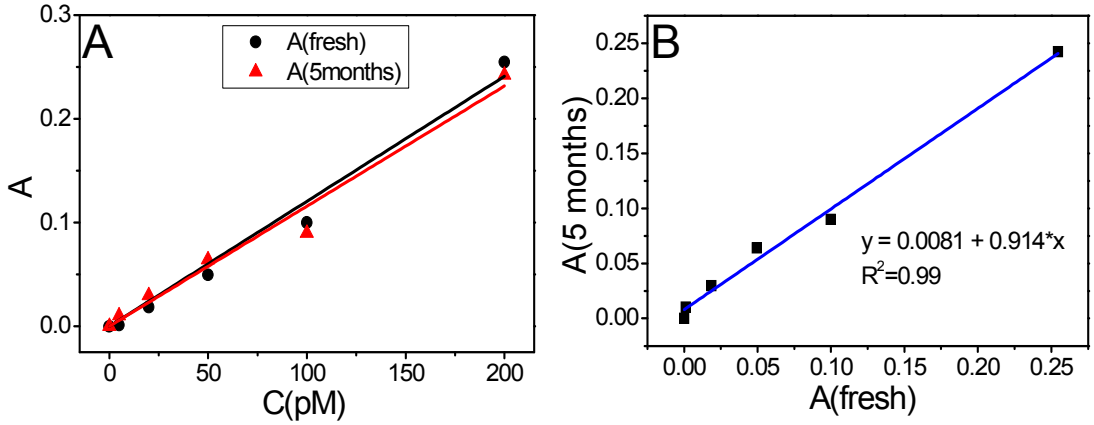

Figure 4.16 Target DNA titration studies using freshly prepared and 5 months old cDNA-MNP.

As shown in Figure 4.16, DNA quantitation has been realized by using the 5 month old cDNA-MNPs with similar sensitivity to that using freshly prepared

MNP-cDNA. The 5 month old cDNA-MNPs not only remain magnetically responsive, but also exhibit reasonable good sensing ability. In this designed system, the synthesized and cDNA conjugated MNPs are stable due to a dense silica coating shell which can effectively protect the Fe_3O_4 core from further oxidation or etching caused by its environment. Besides, the PEG linker between the cDNA and MNP surface allows the necessary distance and repulsion between particles which avoids aggregation issues.

4.6 DNA detection using ALP as signal reporter

To further demonstrate the generality of the MNP-enzyme based sandwich assay for DNA detection, ALP was further used to substitute HRP in detecting a different DNA target. Because inorganic phosphate could effectively inhibit the enzymatic ability of ALP,[47] Tris buffer (pH 8.5) was employed instead of PBS buffer in preparing the samples, washing and signal amplification procedures.

For single DNA detection using ALP as signal amplifier, ALP-NAV was conjugated to biotin-sDNA first by 1 to 1 ratio for further use in the same way as that used for HRP. Then MNP-cDNA2 (20 μg) was mixed with 20 μL ALP-sDNA2 (0.25 μM) and target DNA2 of various concentrations ranging from 0 - 200 pM. The final volume of each assay was also 500 μL in Tris buffer (containing 1 mg/mL BSA). After 1 h incubation at room temperature, all the samples were washed with 500 μL Tris buffer once, Tris buffer (containing 0.1% Tween-20) twice, and Tris buffer once again to remove any unbound species. Then the MNP-dsDNA-enzyme sandwiches were dispersed in 430 μL Tris buffer, and then each was mixed with 50 μL FDP (0.2 mM) to initiate the enzymatic amplification assay. After 1 h, 20 μL PBS buffer was added to stop

the enzymatic reaction, and the UV spectra of all the supernatants of samples were recorded.

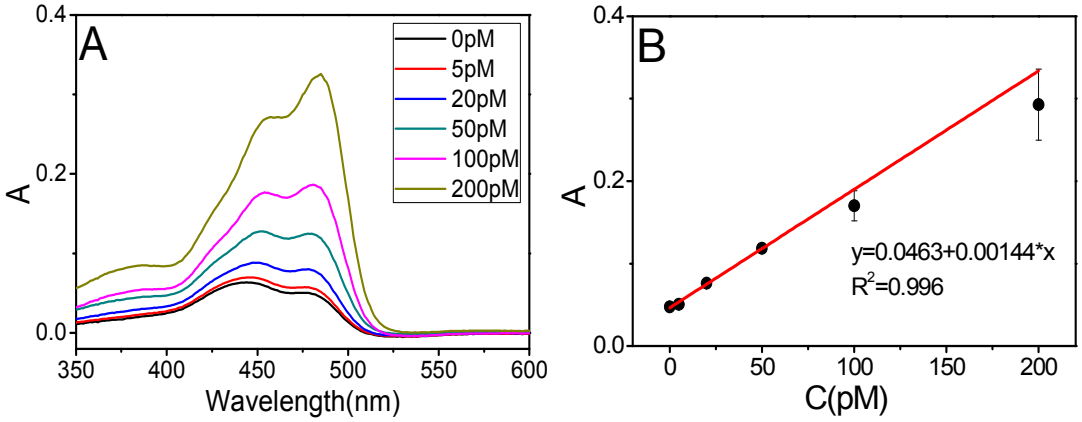

Figure 4.17 DNA detection using ALP as signal amplifier.

(A) Absorption spectra of samples with different concentrations of target DNA2. **(B)** The linear relation between concentration of target and absorbance at 485 nm.

ALP also has efficient catalytic properties which can turnover colorless molecules, FDP, into a highly coloured (and fluorescent) product, fluorescein which has its maximum absorption at 485 nm. The DNA sensing ability of this system involving ALP as signal amplifier has been tested (see Figure 4.17), where a good linear relationship (R^2 = 0.994) between the absorbance and target DNA concentration over the 0 - 200 pM range was also obtained. The results clearly show that ALP is as just powerful as HRP in terms of substrate turnover (signal amplification) efficiency. As a result, after converting the target DNA into an ALP *via* the sandwich binding, it can also turnover hundreds of thousands non-coloured FDP molecules into strongly coloured product molecules, thus offering great signal amplification.

4.7 Simultaneous quantifications of two DNA targets

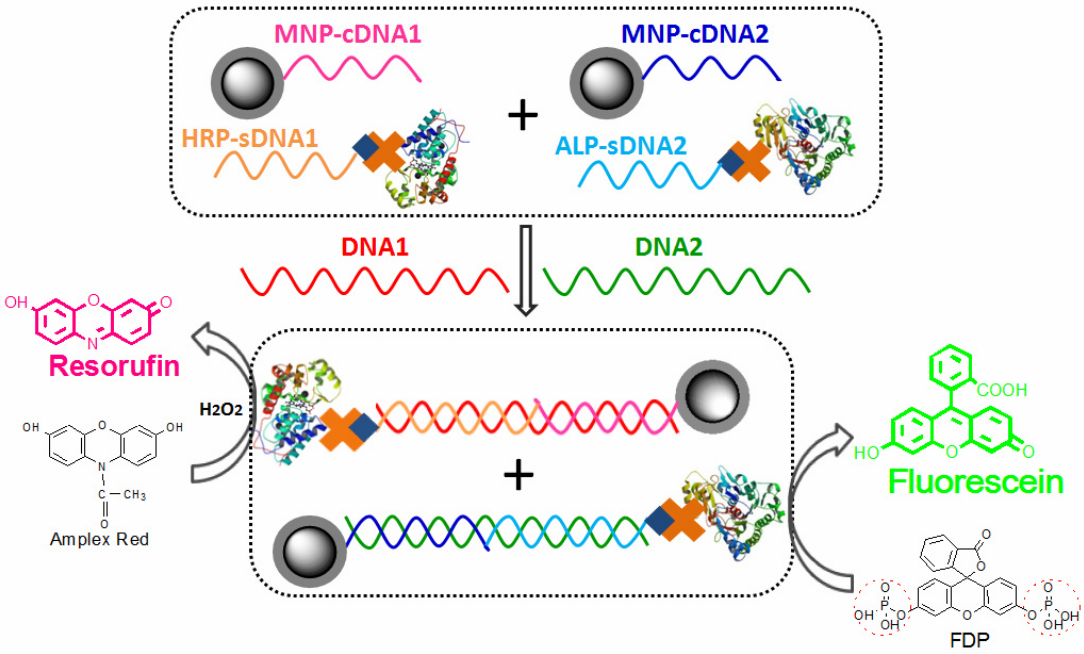

Figure 4.18 Illustration for simultaneous two target DNA detection principle.

Two types of MNPs each modified by a unique cDNA, were mixed with two different signal probes conjugated with either ALP or HRP. Upon addition of specific DNA targets, two different MNP-dsDNA-enzyme sandwiches are formed specifically, allowing specific detection of two different DNA targets via their respective enzymatic amplified signals, where absorbance from resorufin (λ_{abs} maximum at 571 nm) and fluorescein (λ_{abs} maximum at 485 nm) represent DNA1 and DNA2 respectively.

The ability of detection of multiple DNA biomarkers simultaneously opens new opportunities for understanding the disease, molecular diagnosis and new drug discovery.[51] It is therefore critical to develop robust, sensitive, and simple detection methods that can perform multiple DNA targets analysis.

Compared to PCR, which have a limited multiplex ability and often offer false-positive results due to target variations,[52] this proposed approach based on the

MNPs and enzyme probes is simple, highly sensitive, selective, and possesses DNA multiplexing capacity. The large surface to volume ratio of MNPs and magnetic retrieval properties allows the efficient capture and separation of several DNA strands simultaneously, and DNA targets may be detected in the same solution by combining different enzymes. The principle of simultaneous detection of double DNA targets *via* sandwich assays is shown in Figure 4.18. cDNA1 modified MNPs and HRP-sDNA1 are mixed with cDNA2 modified MNPs and ALP-sDNA2 conjugates. Then in the presence of target DNA1, HRP would be bound to MNP-cDNA1 surface through specific DNA hybridizations. Likewise, target DNA2 mediated sandwich formation would link ALP to the MNP-cDNA2, effectively converting target DNA1 and DNA2 into HRP and ALP, respectively. Thus the two HRP and ALP catalyzed enzymatic assays can be used to amplify the target DNA1 and DNA2 signal, respectively. Through UV-vis evaluation, the absorbance from the produced resorufin (λ_{abs} maximum at 571 nm) and fluorescein (λ_{abs} maximum at 485 nm) can be used to quantify the concentration of DNA1 and DNA2, respectively.

Detailed experimental procedures are as described above in the experimental methods, and UV spectra of all the supernatants of samples were recorded and are shown in Figure 4.19.

As shown in Figure 4.19, the absorbance signals from resorufin (at 571 nm) and fluorescein (at 485 nm) represent DNA1 and DNA2, respectively. And the correlations between absorbance intensities and target DNA concentrations are demonstrated in Figure 4.19B. The linear dynamic range is 0 - 500 pM for both plots with similar slope (assay sensitivities). The absorption spectrum with 5 pM target DNA is clearly distinguishable from the background only (see Figure 4.19B inset), the detection limit here for both DNA target is therefore estimated as 5 pM.

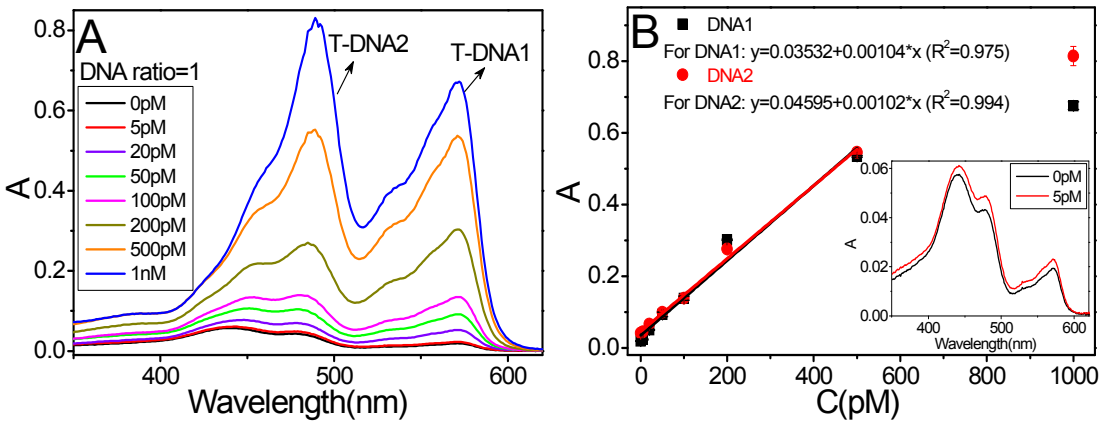

Figure 4.19 Multiplex DNA detection.

(A) Absorption spectra of the samples with various DNA concentrations (the two DNA targets are of the same concentrations). **(B)** The resulting calibration curves of the two different DNA targets, linear fits over the 0-500 pM range for both DNA targets are given. The inset in (B) shows the zoomed spectra of samples without target (0 pM, background) and with 5 pM target.

These results presented here thus established a simple, versatile, multiplexed DNA sensing technique by simply using a set of unique MNP-cDNA and enzyme-sDNA probes that can form sequence-specific dsDNA sandwiches in the presence of the specific DNA target. An advantage of the approach here is the use of MNPs as nanoscale carriers to template the cDNA/target/sDNA sandwich formation, allowing for rapid, efficient target capture in a homogeneous solution and followed by convenient magnetic separation of unwanted species. Moreover, a large excess of the MNP-cDNA and enzyme-sDNA probes can be used to push the equilibrium of the target toward the captured state, allowing detection of target well-below its thermal dynamic dissociation constant K_d.[18, 53-56] Alternative approaches using a solid support to capture and separate the ligated products can suffer from low hybridization efficiency and slow binding kinetics, as a result, they require a longer assay time and often exhibit lower sensitivity (see Table 4.2).[57]

Table 4.2 Comparison of the sensing performances of several recently reported DNA assays.

Sensing method	No.*	LOD (pM)	S/N	Reference
MNP-enzyme sandwich assay	2	5	~27	This work
Photonic crystal hydrogel beads	2	0.66	~18	60
Electrochemical detection based on bar-coded GNPs	2	~4	~12	23
MNP-dye sandwich assay	2	100	~90	61
Au particle-on-wire Surface-Enhanced Raman Scattering (SERS) sensor	4	10	~88	62
Fluorescence based on Ag@Poly(m-phenylenediamine) Nanoparticles	3	250	~8.8	63
chemiluminescence resonance energy transfer (CRET) between QD and DNAzyme	1	10000	~14	64
Graphene quenched fluorescence	3	1000	~13	28
Graphene-Based High-Efficiency Surface-Enhanced Raman Scattering (SERS)	2	10	~22	65
Zn(II)-protoporphyrin IX/G-quadruplex complex with Exo III-assisted analyte recycle	1	200	~15	66
MNP-enzyme probe via personal glucose meter detection	1	40	~60	67

*(No. = number of target detected; LOD = limit of detection; S/N = signal to noise ratio)

Both enzymes employed here allow for sensitive detection of DNA target, because they both offer highly efficient enzymatic turnover rates. The MNP-enzyme sandwich binding format can effectively convert each captured DNA target into a specific enzyme. During the 1 h amplification time, each enzyme can turnover more than 200,000 colorless substrates into strongly coloured product (see the calculated turnover rate of the HRP and ALP from Figure 4.5), allowing sensitive, simple colorimetric detection of target DNA.[58-59] Besides, the enzymatic products (fluorescein from FDP by ALP and resorufin from amplex red by HRP) have distinct absorption spectra which have hardly any overlap, and thus the signal outputs for each of the two different target DNAs could be easily distinguished and analyzed.

Moreover, another advantage of this approach is its general applicability: it can effectively target any DNA of interest by simply changing the sequences of the cDNA-/sDNA- probe pair. Compared to other reported DNA detection methods, this sensing method is simple to operate, having really low background interference, and more importantly can offer superior sensitivity and specificity to many other recently reported multiplexed DNA assays (see Table 4.2 for detailed comparison).

4.8 Conclusions

In summary, a simple, sensitive and quantitative DNA detection methodology has been successfully developed using MNP-cDNA and enzyme-sDNA probes in a sandwich binding format. This assay combines the advantages of the MNP based efficient target capture and easy magnetic separation, delicate MNP surface coating and blocking for greatly reduced background, together with the

great efficiency of enzyme based signal amplification, allowing low pM sensitivity for specific DNA. Such a low detection limit is better than or comparable with the other recently reported sensitive DNA sensors. Moreover, this assay also works equally efficiently even in complex media, such as 10% human serum, implying it has good potential for specific target DNA detection in real clinical samples. More importantly, this method also has the capability of detecting two different DNA targets in a homogenous phase simultaneously. Therefore it is believed that the sensing platform developed herein should have great potential for a wide range of DNA based multiplexed biosensing and disease diagnostic applications.

Nevertheless, there are several strategies that can be used to address some of the issues related to the current assay format and further improve its sensitivity. First, the possible positive signal loss during the washing process due to the dissociation of the dsDNA sandwich format, which results in the detachment of enzymes from MNPs, is a limitation of this system (*e.g*. a target DNA to HRP enzyme conversion rate of ~7% was determined in Figure 4.13). This issue can be addressed by introducing a DNA ligase that can ligate the two probes templated by target DNA, making the signal DNA (hence enzyme) covalently bound to the MNPs and preventing signal loss during the washing process due to dsDNA dehybridisation. Second, this sensor could be further optimized by using more efficient alternative enzymes as the signal reporter and amplifier to improve the sensitivity. Furthermore, the use of multiple enzymes in one target recognition will offer greater signal amplification power and hence further sensitivity enhancement.

4.9 References

1. S. Song, Z. Liang, J. Zhang, L. Wang, G. Li and C. Fan, *Angew. Chem. Int. Ed.*, 2009, **48**, 8670-8674.
2. R. Köppel, J. Ruf and J. Rentsch, *Eur. Food Res. Technol.*, 2011, **232**, 151-155.
3. R. Yamashige, M. Kimoto, T. Mitsui, S. Yokoyama and I. Hirao, *Org. Biomol. Chem.*, 2011, **9**, 7504-7509.
4. L. Bonel, J. C. Vidal, P. Duato and J. R. Castillo, *Biosens. Bioelectron.*, 2011, **26**, 3254-3259.
5. Y. Du, B. Li, S. Guo, Z. Zhou, M. Zhou, E. Wang and S. Dong, *Analyst*, 2011, **136**, 493-497.
6. Q. Zhao, X.-F. Li and X. C. Le, *Anal. Chem.*, 2011, **83**, 9234-9236.
7. X. Chen, X.-E. Zhang, Y.-Q. Chai, W.-P. Hu, Z.-P. Zhang, X.-M. Zhang and A. E. G. Cass, *Biosens. Bioelectron.*, 1998, **13**, 451-458.
8. C. Ding, Y. Ge and S. Zhang, *Chemistry-A European Journal*, 2010, **16**, 10707-10714.
9. H. Yang, *Curr. Opin. Chem. Biol.*, 2012, **16**, 422-428.
10. A. E. Cass, G. Davis, G. D. Francis, H. A. O. Hill, W. J. Aston, I. J. Higgins, E. V. Plotkin, L. D. Scott and A. P. Turner, *Anal. Chem.*, 1984, **56**, 667-671.
11. L.-Q. Chen, X.-E. Zhang, W.-H. Xie, Y.-F. Zhou, Z.-P. Zhang and A. E. Cass, *Biosens. Bioelectron.*, 2002, **17**, 851-857.
12. Y. Xiao, F. Patolsky, E. Katz, J. F. Hainfeld and I. Willner, *Science*, 2003, **299**, 1877-1881.
13. G. Liu, Y. Wan, V. Gau, J. Zhang, L. Wang, S. Song and C. Fan, *J. Am. Chem. Soc.*, 2008, **130**, 6820-6825.
14. Y. Zhang, Z. Tang, J. Wang, H. Wu, A. Maham and Y. Lin, *Anal. Chem.*, 2010, **82**, 6440-6446.
15. F. Patolsky, A. Lichtenstein, M. Kotler and I. Willner, *Angew. Chem. Int. Ed.*, 2001, **40**, 2261-2265.
16. M. Kaatz, H. Schulze, I. Ciani, F. Lisdat, A. R. Mount and T. T. Bachmann, *Analyst*, 2012, **137**, 59-63.
17. J. M. Nam, C. S. Thaxton and C. A. Mirkin, *Science*, 2003, **301**, 1884-1886.

18. Y. Zhang and D. Zhou, *Expert Rev. Mol. Diagn.*, 2012, **12**, 565-571.

19. A. H. Lu, E. L. Salabas and F. Schüth, *Angew. Chem. Int. Ed.*, 2007, **46**, 1222-1244.

20. I. J. Bruce and T. Sen, *Langmuir*, 2005, **21**, 7029-7035.

21. Y.-F. Huang, Y.-F. Wang and X.-P. Yan, *Environ. Sci. Technol.*, 2010, **44**, 7908-7913.

22. Y. Deng, D. Qi, C. Deng, X. Zhang and D. Zhao, *J. Am. Chem. Soc.*, 2007, **130**, 28-29.

23. D. Zhang, M. C. Huarng and E. C. Alocilja, *Biosens. Bioelectron.*, 2010, **26**, 1736-1742.

24. http://www.cancer.gov/cancertopics/factsheet/detection/tumor-markers.

25. R. S. Gaster, D. A. Hall, C. H. Nielsen, S. J. Osterfeld, H. Yu, K. E. Mach, R. J. Wilson, B. Murmann, J. C. Liao, S. S. Gambhir and S. X. Wang, *Nat Med*, 2009, **15**, 1327-1332.

26. B. Dubertret, M. Calame and A. J. Libchaber, *Nat. Biotechnol.*, 2001, **19**, 365-370.

27. S. He, B. Song, D. Li, C. Zhu, W. Qi, Y. Wen, L. Wang, S. Song, H. Fang and C. Fan, *Adv. Funct. Mater.*, 2010, **20**, 453-459.

28. M. Zhang, B. C. Yin, W. Tan and B. C. Ye, *Biosens. Bioelectron.*, 2011, **26**, 3260-3265.

29. C. Hui, C. M. Shen, T. Z. Yang, L. H. Bao, J. F. Tian, H. Ding, C. Li and H. J. Gao, *J. Phys. Chem. C*, 2008, **112**, 11336-11339.

30. Z. L. Lei, Y. L. Li and X. Y. Wei, *J. Solid State Chem.*, 2008, **181**, 480-486.

31. Z. Lei, X. Pang, N. Li, L. Lin and Y. Li, *J. Mater. Process. Technol.*, 2009, **209**, 3218-3225.

32. Y. Zhang, Y. Guo, P. Quirke and D. Zhou, *Nanoscale*, 2013, **5**, 5027-5035.

33. W. Stober, A. Fink and E. Bohn, *J. Colloid Interface Sci.*, 1968, **26**, 62-69.

34. E. P. Plueddemann, ed., *Silane coupling agents*, Plenum Press, New York, 1991.

35. M. Ohmori and E. Matijevic, *J. Colloid Interface Sci.*, 1993, **160**, 288-292.

36. S. Wang, H. Cao, F. Gu, C. Li and G. Huang, *J. Alloys Compd.*, 2008, **457**, 560-564.

37. S. Kralj, M. Drofenik and D. Makovec, *J. Nanopart. Res.*, 2011, **13**, 2829-2841.

38. L. M. Shannon, E. Kay and J. Y. Lew, *J. Biol. Chem.*, 1966, **241**, 2166-2172.

39. S. Deshpande, *Enzyme immunoassays: from concept to product development*, Springer, 1996.

40. R. John, Totowa: Humana Press, 1995.

41. M. Zhou, Z. Diwu, N. Panchuk-Voloshina and R. P. Haugland, *Anal. Biochem.*, 1997, **253**, 162-168.

42. H. Zollner, *Handbook of enzyme inhibitors*, Wiley Online Library, 1993.

43. L. Tamás, J. Huttová, I. Mistrík and G. Kogan, *Chem. Pap*, 2002, **56**, 326-329.

44. M. Besman and J. E. Coleman, *J. Biol. Chem.*, 1985, **260**, 11190-11193.

45. R. Morton, *Biochem. J*, 1955, **61**, 232.

46. R. Morton, *Biochem. J*, 1955, **61**, 240.

47. H. D. Hill, G. K. Summer and M. D. Waters, *Anal. Biochem.*, 1968, **24**, 9-17.

48. K. L. Prime and G. M. Whitesides, *J. Am. Chem. Soc.*, 1993, **115**, 10714-10721.

49. Z. S. Farhangrazi, M. E. Fossett, L. S. Powers and W. R. Ellis Jr, *Biochemistry*, 1995, **34**, 2866-2871.

50. K. Chattopadhyay and S. Mazumdar, *Biochemistry*, 2000, **39**, 263-270.

51. H. Dong, J. Zhang, H. Ju, H. Lu, S. Wang, S. Jin, K. Hao, H. Du and X. Zhang, *Analytical Chemistry-Columbus*, 2012, **84**, 4587.

52. J.-M. Nam, S. I. Stoeva and C. A. Mirkin, *J. Am. Chem. Soc.*, 2004, **126**, 5932-5933.

53. F. Patolsky, Y. Weizmann, E. Katz and I. Willner, *Angew. Chem. Int. Ed.*, 2003, **42**, 2372-2376.

54. S. Bi, L. Li and S. Zhang, *Anal. Chem.*, 2010, **82**, 9447-9454.

55. C. Shi, Y. Ge, H. Gu and C. Ma, *Biosens. Bioelectron.*, 2011, **26**, 4697-4701.

56. X. Chen, A. Ying and Z. Gao, *Biosens. Bioelectron.*, 2012, **36**, 89-94.

57. X. Xue, W. Xu, F. Wang and X. Liu, *J. Am. Chem. Soc.*, 2009, **131**, 11668-11669.

58. J. Garcia, Y. Zhang, H. Taylor, O. Cespedes, M. E. Webb and D. Zhou, *Nanoscale*, 2011, **3**, 3721-3730.

59. Zhou, A. Bruckbauer, Ying, C. Abell and D. Klenerman, *Nano Lett.*, 2003, **3**, 1517-1520.

60. J. Hu, X. W. Zhao, Y. J. Zhao, J. Li, W. Y. Xu, Z. Y. Wen, M. Xu and Z. Z. Gu, *J. Mater. Chem.*, 2009, **19**, 5730-5736.

61. H. Liu, S. Li, L. Liu, L. Tian and N. He, *Biosens. Bioelectron.*, 2010, **26**, 1442-1448.

62. T. Kang, S. M. Yoo, I. Yoon, S. Y. Lee and B. Kim, *Nano Lett.*, 2010, **10**, 1189-1193.

63. Y. Zhang, L. Wang, J. Tian, H. Li, Y. Luo and X. Sun, *Langmuir*, 2011, **27**, 2170-2175.

64. R. Freeman, X. Liu and I. Willner, *J. Am. Chem. Soc.*, 2011, **133**, 11597-11604.

65. S. He, K.-K. Liu, S. Su, J. Yan, X. Mao, D. Wang, Y. He, L.-J. Li, S. Song and C. Fan, *Anal. Chem.*, 2012, **84**, 4622-4627.

66. Z. Zhang, E. Sharon, R. Freeman, X. Liu and I. Willner, *Anal. Chem.*, 2012, **84**, 4789-4797.

67. Y. Xiang and Y. Lu, *Anal. Chem.*, 2012, **84**, 1975-1980.

Chapter 5
Sensitive single nucleotide polymorphism (SNP) discrimination and DNA detection

5.1 Introduction

Single-point mutations (SPMs) or SNPs in genetics are associated with numerous important human diseases, such as cancer, diabetes, vascular disease, and some forms of mental illness, etc. Therefore, the sensitive detection of specific SPMs and SNPs in particular genes has considerable value in disease diagnosis, and prediction of patients' responses to treatment, risk of relapse of disease and outcomes.[1-4] However, the inherent small difference in thermodynamic stability from a single-base mismatch between the perfect-match and its SNP targets makes it challenging to be able to achieve both high SNP discrimination and sensitivity. Over the past decade, several different approaches capable of SNP discrimination have been reported, such as high resolution DNA melting analysis (~μM level sensitivity),[5-9] single molecule fluorescence (*via* different annealing and melting kinetics between the perfect- and SNP- targets);[10] molecular beacon,[11-13] hybridization chain reaction,[14] surface enhanced Raman scattering[15] and electrochemical chemical detection.[16] Despite such developments, most methods reported so far displayed relatively low SNP discrimination ratios (*ca.* < 20 fold) and/or limited sensitivity, and can also suffer from poor fidelity when analyzing samples with large excesses of DNA contaminants.

More recently, several enzyme based approaches have been developed to improve SNP detection and discrimination. For example, nicking

endonucleases,[17] and restriction enzymes[2] have been used to discriminate SNPs from perfect-match target *via* the specific enzyme restriction sites. Nevertheless, these approaches are only suitable for detection of SNPs containing the enzyme recognition sequences, limiting their application scope. Whereas enzymes, such as S1 nuclease, endonuclease (I, III and IV) and λ exonuclease, are suitable for all DNA sequences with delicate designs, and therefore can be used as a general method for SPM/-SNP detection. However, the poor SNP discriminating ability of these enzymes means they have to be combined with other more specific enzymes to achieve the desired SNP discrimination, such as the combined use of endonuclease IV and λ exonuclease in a recent SNP detection system.[18] DNA Polymerase, widely used in PCR for DNA target amplification, possesses high specificity and is also suitable for SNP detection.[16, 19]

On the other hand, the ligation reaction based on Taq DNA ligase is general, and can be applied to any target of interest. Moreover, it has high selectivity in ligating two nicked DNA strands hybridised to a full-complementary DNA template over those having a single-base mismatch at the nicking site. It is therefore well-suited for sensitive SNP and point-mutation detections.[20-21] Indeed, a few sensitive, specific assays that may be suitable for genotyping and point-mutation detection have been realized with ligase-based approaches,[22-27] such as the combination of the ligation chain reaction (LCR) and conjugate polymer based FRET,[22] and GNP based colorimetric assay[23] for sensitive SNP detection. The ligation reaction has also been combined with other signal amplification strategies, *e.g.* RCA,[24-26] and polymerase mediated target displacement,[27] to further enhance sensitivity. Despite these, the development of simple, sensitive diagnostic assays suitable for rapid detection of SNPs and point mutations associated with specific diseases remains a challenge. Herein, a novel, general and highly sensitive approach for specific, label-free detection of SNPs is developed using the KRAS somatic mutations (codons 12/13) that

are widely found in several human cancers (*e.g.* colorectal, pancreas, ductal and lung) as the model cancer DNA targets. This sensor can detect as little as 30 amol of unlabelled DNA targets, and can offer high discrimination, up to > 380 fold after background correction, between the full-match and the SNP targets. It can quantitate the KRAS cancer SNP mutant in large excesses of coexisting wild-type DNA target down to 0.75% level (*e.g.* < 1% of the DNA targets being the SNP cancer mutant).

5.2 Design principle

Figure 5.1 shows this approach schematically. Two short ssDNA probes, each complementary to one half of the DNA target, are designed. The two probes are modified with a 5'-biotin (blue, for signal amplification) and 5'-phosphate (green, for magnetic capture of ligated product, see later), respectively. First, the two probes are hybridised to a ssDNA target, forming a nicked dsDNA at annealing temperature (45 °C). The two probes hybridised to a full-complementary DNA target are subsequently ligated by the Taq DNA ligase at 45 °C, producing a covalently ligated DNA product with a terminal biotin (the ligated product). Whereas a single-base mismatch in the probes/SNP target duplex at the nick site can prevent such ligation, so the two probes remain unlinked. Upon heating to denaturation temperature (95 °C), the DNA targets are dehybridised (released) from the ligated products (or un-ligated probes), which are subsequently used to template the ligation of a 2nd pair of biotin-/phosphate- probes as temperature is reduced to 45 °C. In this way, the DNA target is recycled, and hence this process is named as target-recycled ligation (TRL). Excess biotin-/phosphate- probes over the target DNA are used to minimize the re-hybridisation of the target to the ligated products. Repeating the denaturation, annealing and ligation process thus recycles the DNA target, producing a

ligated product during each cycle, leading to accumulation of the ligated products as the number of thermal cycles is increased.

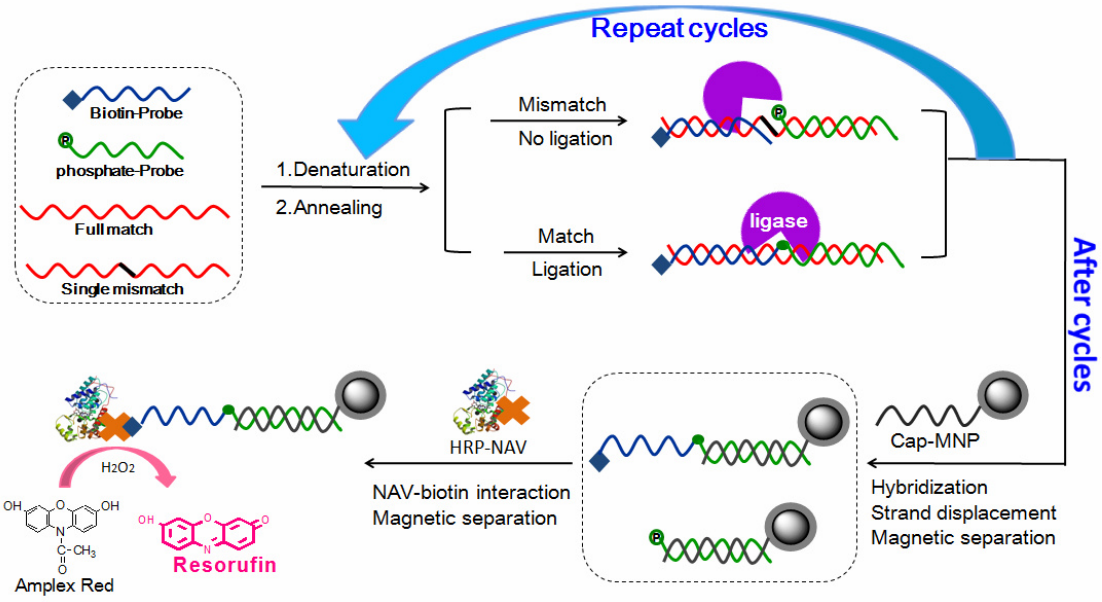

Figure 5.1 Schematic illustration of this strategy to specific SNP DNA detection. A biotin-probe (blue) and a phosphate-probe (green) are hybridized to each half of a complementary DNA target, which are then ligated by the Taq DNA ligase if the sequences between the probes and target are fully complementary, but not for those having a single-base mismatch (ca. SNP) at the nicking site. The system is then subjected to multiple cycles of denaturation, annealing and ligation, where each full-match template produces a ligated product in each cycle. A capture-DNA modified MNP (note hundreds of capture-DNA strands are linked to each MNP, only one is shown here for simplicity) is added to capture the ligated products, and followed by magnetic separation. Finally, a NAV conjugated HRP (NAV-HRP) is bound to the MNP, allowing for sensitive detection of the full-match DNA target via the HRP catalysed enzymatic assay. (Reprinted by permission of the Royal Society Chemistry)[28]

After 5-30 thermal cycles, a capture-DNA (with sequence complementary to the phosphate-probe section and in large excess) modified MNP (Cap-MNP) is then added to capture the free ligated products *via* hybridization. For ligated products pre-hybridised to the DNA targets, the capture-DNAs may displace the DNA

targets *via* a toehold mediated strand displacement. A large excess of the Cap-MNP over the target DNA is used here (>100 fold) to ensure efficient target capture and strand-displacement. After that, a magnetic separation followed by several rounds of washing is applied to separate the MNP-captured ligated products from unbound free species. The MNPs (with the captured products) are subsequently treated with a NAV conjugated HRP (NAV-HRP), converting each captured DNA product (with a terminal biotin) into an HRP enzyme *via* the strong, biospecific biotin-NAV interaction.[29-30] This allows for sensitive detection of the ligated product (from the templated ligation by the full-match DNA target) *via* the efficient HRP catalysed conversion of a non-fluorescent substrate, amplex red, into a strongly fluorescent product, resorufin,[29, 31] for the real-time fluorescence monitoring on a conventional 96 well fluorescence plate reader. An advantage here is general applicability: it can target any DNA of interest by simply changing the sequences of the phosphate-/biotin- probe pair. In practice, a common phosphate-probe and a specific biotin-probe (P2 or P3) are employed to detect each of the two KRAS mutants (T2 or T3, see Table 5.1) that are associated with the human colorectal cancer.

The stringent matching requirement of the Taq DNA ligase for ligating the two probes at the nick site[20-21] enables this approach to be highly specific for the perfect-match over the SNP target(s). To separate the ligated products from other species after ligation, gel electrophoresis is commonly used, but it has poor sensitivity, often at μM level.[32] Alternative approaches using a solid support to capture and separate the ligated products can suffer from low hybridization efficiency and slow kinetics, limiting their sensitivity.[33] MNPs are highly attractive here because of their tiny particle sizes and super-paramagnetic properties, allowing the formation of a stable, uniform dispersion in the media for rapid, homogeneous target capture without an applied magnetic field, while still being readily retrievable upon applying an external magnetic field.[25, 27, 34-36] Here, the Cap-MNP is employed to capture the ligated products

via strand displacement, where a ssDNA hybridises to a short complementary toehold first, leading to progressive displacement of the pre-hybridised strands.[37] Its kinetics can be regulated by tuning the length of toeholds. Strand displacement is widely used in designing DNA nanomachines[38], logic circuits[39], hybridization chain reaction[40], DNA-templated synthesis,[41] as well as DNA detection and point-mutation discrimination,[42-45] but is rarely used for DNA capture and separation. In this design, a large excess of the Cap-MNPs (100-100,000 fold excess over the full-match target) are used here to hybridise to the overhang toeholds in phosphate-probe/ligated product(s) and to displace pre-hybridised target strands. More-over, the capture and displacement efficiency also benefits from the enhanced affinity of the Cap-MNPs for the ligated products *via* polyvalent binding similar to those observed for multivalent DNA-GNP conjugates: where 2 orders of magnitude higher binding affinity for the same DNA target has been reported for multivalent DNA-GNP conjugates over the corresponding doubled-stranded DNA in solution.[46-47]

5.3 Experimental section

5.3.1 Materials and reagents

Taq DNA ligase and 10 × ligation buffer (200 mM Tris-HCl, 250 mM potassium acetate, 100 mM magnesium acetate, 10 mM NAD, 100 mM dithiothreitol and 1.0 % Triton X-100, pH 7.6) were purchased from New England Biolabs (UK). All DNA probes and target strands were purchased commercially from the IBA GmbH (Germany). They were all HPLC purified by the supplier and their sequences are summarised in Table 5.1.

Table 5.1 The DNA sequences and their abbreviations used in this study. (Reprinted by permission of the Royal Society Chemistry)[28]

DNA code	DNA Sequences
Phosphate-probe	PO_4^--5'-T GGC GTA GGC AAG AGT ACG ACA-3'
Biotin-probe 1 (P1)	Biotin-5'-TTT TTT GTG GTA GTT GGA GCT G**G**-3'
Biotin-probe 2 (P2)	Biotin-5'-TTT TTT GTG GTA GTT GGA GCT G**A**-3'
Biotin-probe 3 (P3)	Biotin-5'-TTT TTT GTG GTA GTT GGA GCT G**T**-3'
Biotin-probe 4 (P4)	Biotin-5'-TTT TTT GTG GTA GTT GGA GCT G**C**-3'
Wild-type target (T1)	3'-CAC CAT CAA CCT CGA C**C**A CCG CAT CCG TTC TCA-5'
Mutant target 2 (T2)	3'-CAC CAT CAA CCT CGA C**T**A CCG CAT CCG TTC TCA-5'
Mutant target 3 (T3)	3'-CAC CAT CAA CCT CGA C**A**A CCG CAT CCG TTC TCA-5'
Mutant target 4 (T4)	3'-CAC CAT CAA CCT CGA C**G**A CCG CAT CCG TTC TCA-5'
Capture DNA	3'-A CCG CAT CCG TTC TCA TGC TGT TTT TTT TTT-5'-C_6SH

HRP-NAV and amplex red were purchased from Thermo Scientific (UK) and Invitrogen Life Technologies (UK), respectively. All other chemicals and reagents were purchased from Sigma-Aldrich (UK) and used without further purification unless otherwise stated. PBS buffer (137 mM NaCl, 10 mM

Na_2HPO_4, 2.7 mM KCl, 1.8 mM KH_2PO_4, pH 7.4) was made with ultra-pure MilliQ water (resistance > 18 $M\Omega.cm^{-1}$). The MNPs were in house synthesized and modified as described in chapter 4.

5.3.2 Experimental methods

Typically, TRL reaction was performed in 50 µL 1 × ligation buffer containing the Taq DNA ligase (25 units), biotin-probe and phosphate-probe (1 pmol each), and the various concentrations of mutant or/and wild-type DNA targets. Certain thermal cycles were carried out, with each cycle consisting of a 2 min denaturation at 95 °C and 5 min annealing/ligation. After the final cycle, the Taq ligase was inactivated by addition of EDTA (8 µL, 50 mM).

Subsequently, the capture DNA modified MNPs (Cap-MNP, 20 µg, loaded with ~10 pmol of the capture DNA) were added to initiate strand displacement and ligated product capture at room temperature overnight, although incubation for 1 hour was found just as effective as for overnight. After magnetic separation, the MNPs with bound ligated products were dispersed in 200 µL PBS 7.4 buffer (containing 1 mg/mL BSA) and incubated with HRP-NAV (1 pmol) for 0.5 h. The MNPs were then magnetically separated (assisted with a brief ~30 s centrifugation) and then washed once with PBS 7.4 buffer, twice with PBS 7.4 buffer containing 0.1% Tween-20 and once more with PBS 7.4 buffer.

The MNPs (with bound enzymes) were subsequently transferred to a 96 well plate for high throughput screening where different sensing conditions were evaluated simultaneously. The enzymatic assay was triggered by the addition of amplex red and H_2O_2 (2 µM each, final concentration) in PBS 7.4 buffer (200 µL final assay volume), and real-time fluorescence changes were monitored on an

Envision plate reader using BODIPY TMR FP 531 as excitation filter and Cy3 595 as emission filter.

5.4 Detection of perfectly matched target

This approach is first used to detect one of the KRAS cancer mutants T2 (25 fmol) as the perfect-match target using the biotin-probe 2 (P2) and phosphate-probe (1 pmol each). Taq DNA ligase was used to ligate the two probes templated by T2 (25 fmol). 30 thermal cycles were carried out, with each cycle consisting of a 2 min denaturation at 95 °C and 5 min annealing/ligation at 45 °C. After the final cycle, the Taq ligase was inactivated followed by addition of the Cap-MNPs to initiate strand displacement and ligated product capture at room temperature overnight. After magnetic separation, the produced MNPs conjugates were incubated with HRP-NAV (1 pmol) for 0.5 h. Then after magnetic separation and washing process, the MNPs were subsequently transferred to a 96 well plate. The enzymatic assay was triggered by the addition of amplex red and H_2O_2 and real-time fluorescence changes were monitored on an Envision plate reader. Besides, a set of control experiments were implemented for comparison.

Figure 5.2 reveals that the rate of fluorescence increase for the sample containing both the T2 and ligase (**e**) is much greater than that of the controls either containing no ligase (**d,** 79(±12) fold) or T2 (**C,** 87(±13) fold). This result clearly demonstrates that the fluorescence response observed herein is due to the T2 templated ligation only, with almost no contribution from non-specific adsorption of the NAV-HRP. The negligible false positive for controls without either the ligase or T2 (**c** or **d**) confirms the success and excellent specificity of this approach for target DNA detection.

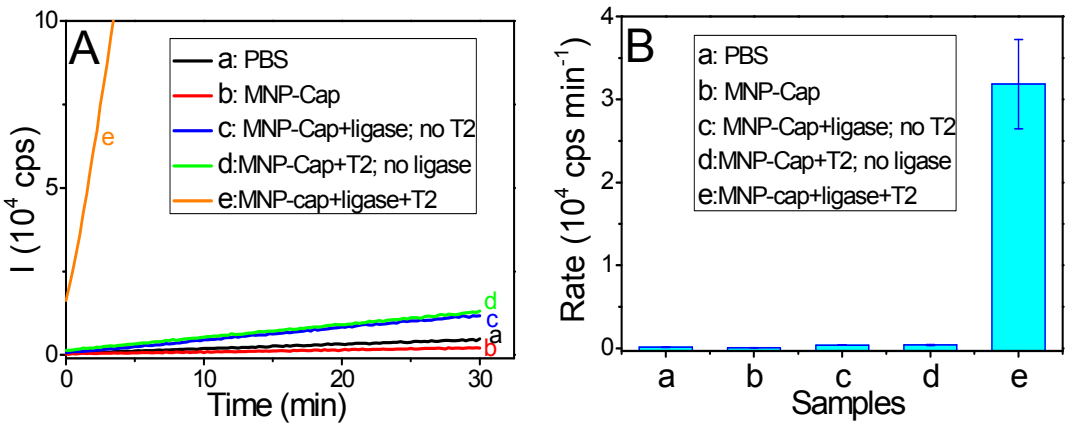

Figure 5.2 (A) Real time fluorescence response and **(B)** rate of Fluorescence increase for different samples.

All samples are subjected to identical thermal cycle treatments and contain the same amount of amplex red (2 μM) and H_2O_2 (2 μM). The samples are: (**a**) PBS, (**b**) cDNA-MNP in PBS, (**c**) cDNA-MNP + ligase but no T2; (**d**) cDNA-MNP + T2 but no Taq ligase; and (**e**) cDNA-MNP + T2 + Taq DNA ligase. (Reprinted by permission of the Royal Society Chemistry)[28]

Prior to using the approach to quantitate target DNA, the effect of the number of thermal cycles on the specific DNA signal has been examined. Biotin-probe4 (P4) and phosphate-probe (1 pmol each) were used to detect 100 fmol fully-matched mutant DNA target (T4). The TRL was subjected for specific thermal cycles (0 - 30 cycles), with each cycle consisting of a 2 min denaturation at 95 °C and 5 min annealing/ligation at 45 °C. The experimental procedures otherwise were the same as described above.

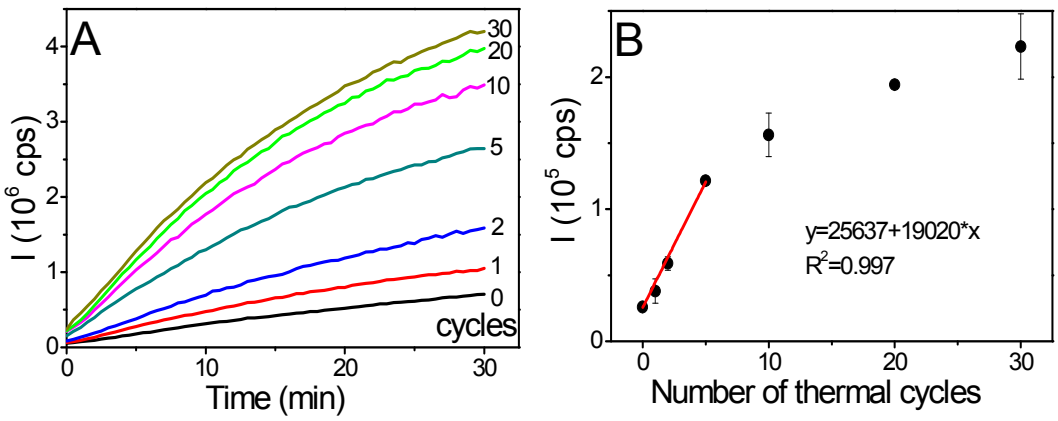

Figure 5.3 Effect of thermal cycle number on the rate of fluorescence increase.

(A) Real time-dependent fluorescence responses for samples subjected to different thermal cycles (cycle numbers are indicated on each curve). **(B)** The corresponding correlation between fluorescence increasing rate and thermal cycle numbers. The initial part of the plot is fitted to a linear function. (Reprinted by permission of the Royal Society Chemistry)[28]

As shown in Figure 5.3, the signal increases linearly during the first 5 cycles (indicating linear amplification), but the rate of increase gradually levels off as more thermal cycles are used (due to depletion of the DNA probes, a 10 fold DNA probes to target DNA ratio is used here). Nevertheless, the assay with 30 thermal cycles gives the highest signal, being 8.6 times that without thermal cycle, confirming the success of the TRL for signal amplification. 30 thermal cycles are therefore used in all assays to enhance signals unless otherwise noted.

Quantification of target T2 (0 - 25 fmol) was carried out by using perfect matched biotin probe2 (P2) and phosphate probe (1 pmol each). 30 thermal cycles with each cycle consisting of a 2 min denaturation at 95 °C and 5 min annealing/ligation at 45 °C were carried out. The experimental procedures otherwise are the same as described above.

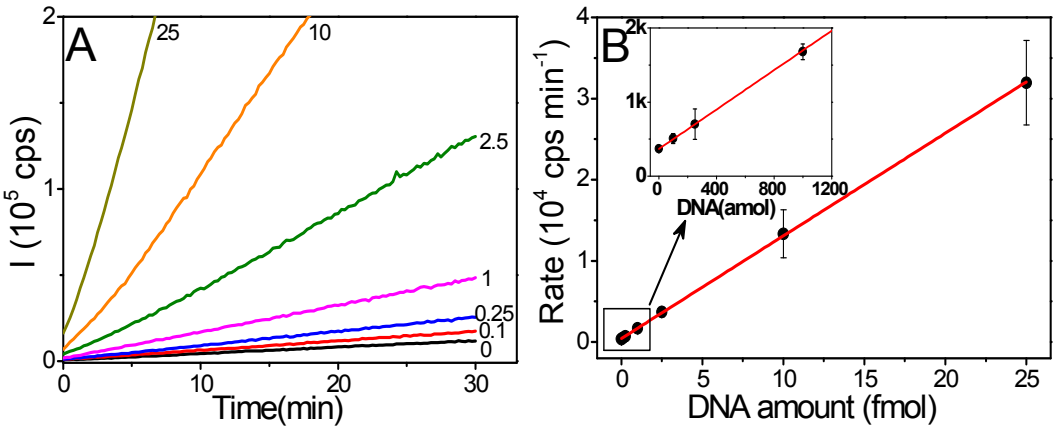

Figure 5.4 Full complementary DNA target quantification.

(**A**) Real time-dependent fluorescence responses for samples containing different amounts (0-25 fmol, the amounts are indicated on each curve) of the full-match DNA target, T2. (**B**) The corresponding correlation between the rate of fluorescence increase and amounts of the T2 target, fitted to a linear function (y = 368.8 + 65.2*x, R^2 = 0.9997). Inset: amplified region over 0 -1200 amol T2 range. (Reprinted by permission of the Royal Society Chemistry)[28]

Figure 5.4A shows the time-dependent evolution of fluorescence intensity at different amounts of the perfect-match target, T2, which clearly show that the rate of resorufin production increases with the increasing amount of the target DNA. The relationship between target DNA amount and the rate of fluorescence increase is found to be highly linear over the 0 - 25 fmol range (R^2 = 0.9997), suggesting that this approach can offer excellent target DNA quantitation accuracy. The LOD based on 3σ/slope is estimated as 30 amol (600 fM in 50 μL).[48] The LOD here is comparable to or better than several recently reported sensitive DNA assays (Table 5.3). This high sensitivity is attributed to the great signal amplification power of the enzyme (where each NAV-HRP can turnover several hundred thousand non-fluorescent amplex red substrates into strongly fluorescent resorufin products over a 30 min assay period), [29] efficient target capture and magnetic separation, and the careful optimisation of the Cap-MNP probe which leads to negligible nonspecific adsorption of the enzyme, and hence greatly reduced background. In addition, the magnetic capture and

separation process was also carefully arranged (see experimental section 5.3.2): the Cap-MNP was added after the thermal cycles to avoid the aggregation of the MNPs at high temperatures. I found MNP aggregation can lead to decreased target capture efficiency and significantly increased background.

5.5 Mimicking DNA melting assay

The melting temperature (T_m) of nucleic acids is the temperature at which half of dsDNAs are dehybridised into ssDNA structures. The melting is typically considered as dissociation of the two strands in a dsDNA into two single stranded states, where intermediate states are often ignored.[9] In this approach, a pair of the biotin-/ phosphate- probes are first hybridised to target DNA (mutant or wild-type), forming a probes/target duplex with a nick site, which are then ligated by the ligase to form a covalently linked product. At high annealing temperatures, few probes can form stable sandwiches with the target DNA, leading to a decrease of the ligated products. Therefore the ligation efficiency (enzymatic activity after NAV-HRP binding) is a useful indication of the probes/target sandwich formation, which may be controlled by the annealing/ligation temperature.

The effect of annealing temperature on the detection of the full-match target T2 (100 fmol) using the phosphate-/biotin-probe 2 (1 pmol) was tested. In this mimicking DNA melting assay, the experimental procedures were similar to those described above, except only 5 thermal cycles were used. Each cycle included a 2 min denaturation at 95 °C and a 5 min annealing/ligation at specific temperatures shown in Figure 5.5.

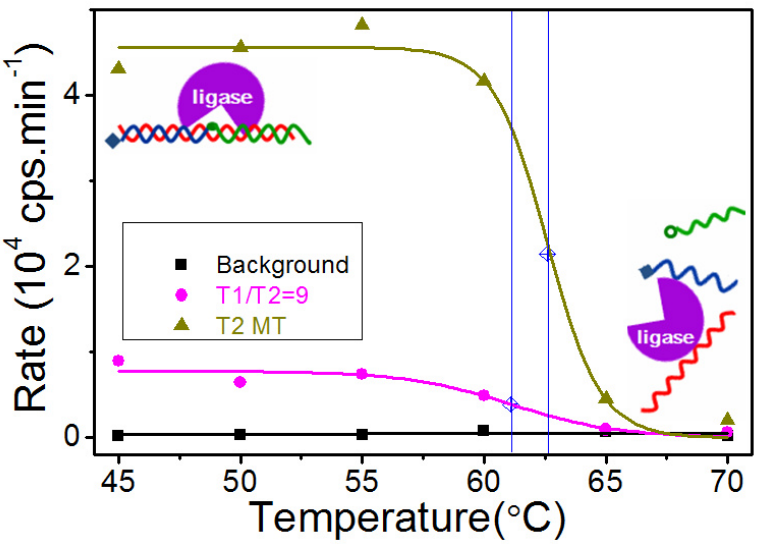

Figure 5.5 Relationship between the rate of fluorescence increase and ligation temperatures.

According to the fitted melting curves, T_ms were calculated and are indicated by blue solid lines crossing blue diamonds. (Reprinted by permission of the Royal Society Chemistry)[28]

The signal obtained from the SNP target only (*e.g.* 100 fmol T1) was found indistinguishable from the background (no target), due to the high specificity of this assay. Therefore two samples with the identical amount of total DNA (100 fmol), one containing the T2 only and the other being a T2/T1 mixture (molar ratio = 1/9), were studied and the results were shown in Figure 5.5.

The relationship between the annealing temperature and the fluorescence change rate (which is positively correlated to the amount of ligated products) closely resembles a typical DNA melting assay (see Figure 5.5). At low annealing/ligation temperatures (*e.g.* 45 - 55 °C), the fluorescence signal was constant, suggesting the probes/target sandwich was stable over this temperature range and hence efficiently ligated. As the temperature was increased further, the signal decreased sharply, implying the dissociation of the probes/target sandwich under such elevated temperatures. The data can be

fitted by a sigmoidal function to extract the mimicked T_m of each DNA sample.[8-9, 49]

$$y(T) = \frac{a}{1+e^{k*(Tm-T)}} \qquad (5.1)$$

The fluorescence increase rate *versus* ligation temperature can be fitted well by the above equation (with R^2 = 0.99 and 0.91), yielding T_m values of 62.6 and 61.1 °C for the pure T2 and 1:9 molar mixed T2:T1 targets, respectively (Figure 5.5). The presence of 9-fold excess of the SNP target T1 led to ~1.5 °C decrease of the effective T_m. This is not unexpected because a fixed amount of total DNA (T1 + T2) was used, so the T2 concentration in the later was only 10% that of the former (T1 could not contribute to positive ligation, see the previous paragraph). The maximum fluorescence response for the (T1 + T2) mixture was ~15% that of the pure T2 sample, which is likely due to competition of T1 in forming unligatable probes/T1 duplex, reducing the chances of forming ligatable probes/T2 duplex.

Recently, a colorimetric detection of low abundance mutants with excellent specificity has been reported by Zu *et al*. using the sharp melting behaviour of nanoparticle-immobilised target DNAs.[50] However, this assay required stringent temperature adjustment according to specific target sequences and mutant concentration. In addition, it only gave nM levels of absolute sensitivity. The approach here, having fM sensitivity together with excellent SNP discrimination ability *via* both the inferred T_m and fluorescence response, appears to be well-suited for accurate SNP and point-mutation detection.

5.6 SNP discrimination

5.6.1 Detection of SNPs

I further evaluated the potential of this approach in specific detection of the SNPs in the KRAS gene that are associated with many human cancers (*e.g.* colorectal, pancreas, ductal and lung).

In this regard, four DNA targets (100 fmol each) are used in these experiments: the wild-type T1 (counting from 5', base 17=**C**), two cancer mutants: T2 (17C→T), T3 (17C→A), and T4 (17C→ G, a cancer irrelevant mutation but is used here to demonstrate the general applicability of this sensor), which can be detected by their full-match biotin-probes, P1, P2, P3, and P4, respectively. 30 thermal cycles with each cycle consisting of a 2 min denaturation at 95 °C and 5 min annealing/ligation at 45 °C were carried out. The experimental procedures otherwise are the same as described in 5.3.2.

Typical time-dependent assay fluorescence responses using P2 to detect such DNA targets were shown in Figure 5.6A. The full-match P2/T2 clearly exhibited much greater fluorescence signal than those containing a single-base mismatch, *i.e.* this sensor is highly specific. In fact, this high level of full-match target specificity was achieved throughout the whole probe/target combinations: greatly increased signals were only observed for the full-match probe/target combinations (*e.g.* P1/T1; P2/T2; P3/T3 or P4/T4), but not for those containing a single mismatch (*e.g.* P1/T2-T4; P2/T1, P2/T3-T4; P3/T1-T2, P3/T4 or P4/T1-T3, see Figure 5.6B).

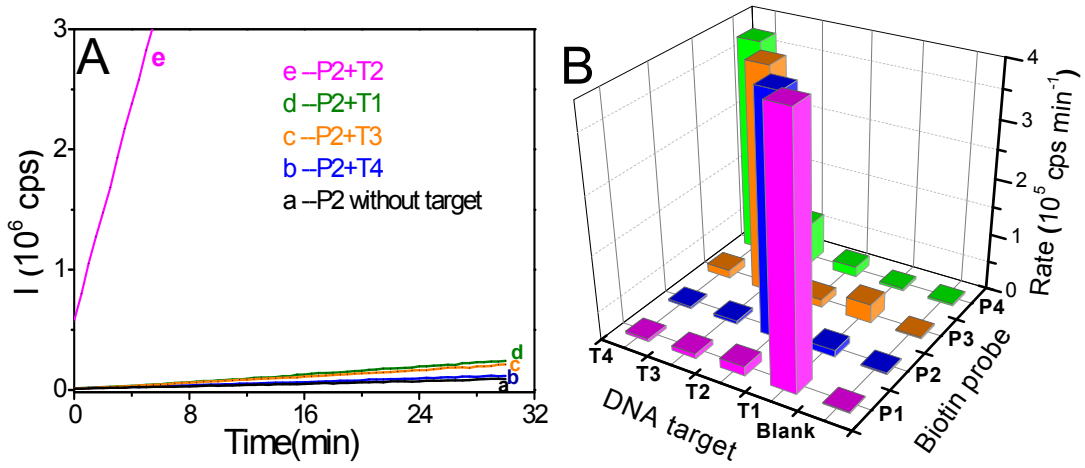

Figure 5.6 Specificity of the sensor in discriminating the full-match against other single-base mismatch DNA targets.

(**A**) Typical time-dependent fluorescence assay curves of using the P2 (perfect-match to T2) to detect other different SNP targets. (**B**) Comparison of the average fluorescence increase rates (slopes of fluorescence response curves as shown in Figure 5.6A) for different target/probe combinations (n = 3). (Reprinted by permission of the Royal Society Chemistry)[28]

Figure 5.6 revealed that the fluorescence signals of the latter were typically comparable to blank controls, ranging from 0.81 ± 0.09% (for P2/T4) to 4.6±1.0% (P4/T2) that of their respective full-match samples before background correction (BC, except for P3/T1 or P4/T3, which was 8.3 ± 0.9% or 19 ± 4.0% that of the P3/T3 or P4/T4 signal, respectively). The detailed discrimination ratios (DRs) between the full-match P*n*/T*n* (*n* = 1 - 4) samples over their corresponding single-base mismatch P*n*/T*m* ($n \neq m$; *n*/*m* = 1 - 4) samples are summarised in Table 5.2. Impressive SNP DRs of up to 121(± 14) fold before background correction (P2/T2 over P2/T4) were obtained, which further increased to up to 383(± 45) fold after BC. This level of SNP discrimination ratio is among the highest reported in the literature (see Table 5.3).

Table 5.2 The discrimination ratios (DRs) of specific biotin-probes for their respective full-match over other SNP DNA targets.

The data shown in the brackets are after background correction, error bars are the standard deviations of 3 parallel samples. DR is defined as signal ratio of the full-match target, P*n*/T*n*, over their respective SNP targets, P*n*/T*m* (where $n \neq m$). (Reprinted by permission of the Royal Society Chemistry)[28]

Target (base 17)\Probe	**P1 (G)**	**P2 (A)**	**P3 (T)**	**P4 (C)**
T1 (C)	1 (1)	35 ± 4.1 (43 ± 5.1)	12 ± 0.4 (13 ± 0.4)	91 ± 6.2 (298 ± 20)
T2 (T)	53 ± 15 (70 ± 20)	1 (1)	30 ± 1.1 (36 ± 1.2)	21 ± 1.4 (25 ± 1.7)
T3 (A)	57 ± 16 (78 ± 22)	76 ± 8.9 (133 ± 16)	1(1)	5.2 ± 0.4 (5.4 ± 0.4)
T4 (G)	96 ± 27 (176 ± 50)	121 ± 14 (383 ± 45)	27 ± 1.0 (32 ± 1.1)	1(1)
Blank	212 ± 60 (–)	175 ± 21 (–)	162 ± 5.8 (–)	130 ± 9 (–)

Moreover, two DNA targets T1 and T2 at low concentration (5 fmol each) were discriminated by using biotin probe P2 and phosphate probe (1 pmol each) subjected to 5 thermal cycles (each cycle contains a 2 min denaturation at 95 °C and 5 min annealing/ligation at 45 °C). The experimental procedures otherwise are the same as described in 5.3.2.). This experiment shows that even at relatively low target abundance (*e.g.* 5 fmol), this approach could offer a

SNP discrimination ratio of > 3 fold before background correction, increasing to 13.5 fold after BC (see Figure 5.7).

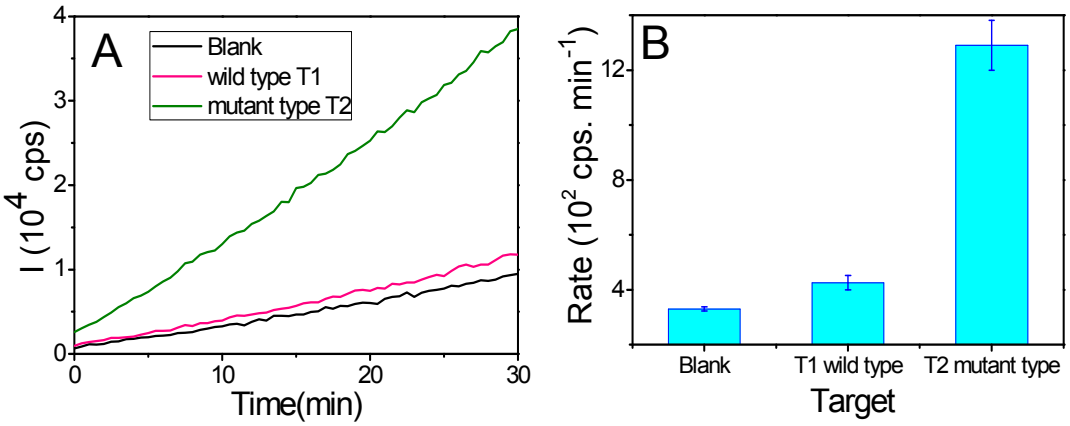

Figure 5.7 Discrimination between the full-match (T2) and single mismatch target (wild-type T1) at low target abundance (5 fmol).

Five thermal cycles with an annealing temperature of 45 °C were used. (**A**) Time-dependent fluorescence intensity change for the blank control (**black**), SNP target T1 (**red**) and perfect-match target T2 (**green**). **(B)** The corresponding fluorescence rate changes of the three samples. The discrimination ratio between the full-match T2 and the SNP target T1 was determined as ~3.03 fold before background correction, which was increased to ~13.5 fold after background correction (*e.g.* Blank control background signal was subtracted from the T2 and T1 signals). (Reprinted by permission of the Royal Society Chemistry)[28]

All these results confirm the excellent specificity of this approach in SNP detection. It is also noteworthy that all of the perfect-match P*n*/T*n* samples here gave > 130 fold greater absolute signals over their respective blank controls, which is considerably higher than most other ultra-sensitive DNA sensors reported recently (see Table 5.3 for details). For biosensing, a high absolute signal-to-background ratio (S/B) is highly advantageous because not only can this increase the accuracy of target quantification, but it can also simplify the data analysis by eliminating any requirement of background correction.

Table 5.3 Comparison of the sensing performances of several recently reported, sensitive SNP assays. (Reprinted by permission of the Royal Society Chemistry)[28]

Sensing Method	LOD* for target DNA/RNA	SNP* DR	S/B*	LOD for rare alleles	Reference
Target-recycled ligation + MNP capture + enzymatic amplification	30 amol (0.6 pM)	121 383(BC)	130-212	0.75%	This work
Taq DNA Polymerase + conjugated polymer FRET	?	~8	~8	2%	4
Multi-colour molecular beacons + GNP	~500 pM	~2.5-10	~5.2-30	?	11
Molecular beacon probe + enzymatic amplification	1000 pM (RNA)	~7	~10	10%	13
Pyrene excimer probes + hybridization chain reaction	0.26 pM	~10	~32	?	14
Endonuclease IV + lambda exonuclease	1 fmol	~2.2-3	~6	0.5%¶	18
LCR + exonuclease + conjugated polymer FRET	1 fM	~3	~6	1%	22
LCR + gold nanoparticle	20 aM	?	?	~0.1%	23
Nanoparticles+ ligation + silver amplification	~1 pM	~20-30	~29	?	33
Ligation mediated strand displacement + DNAzyme signal amplification	0.1 fM	106	108	?	42

*LOD = limit of detection, where for the full-match DNA/RNA target, this value is given in total DNA amount and/or concentration; BC = background correction; SNP DR: discrimination ratio between full-match and SNP target; S/B: absolute signal-to-blank background ratio.

¶ The 0.5% LOD for rare allele here referred to the SNP over 1,3-double mismatch target, not the full-match target.

5.6.2 Quantification of rare DNA allele frequency

The high sensitivity and excellent SNP detection specificity make this assay well-suited for quantification of low abundance alleles. To evaluate this potential, a series of samples containing different amounts of the cancer mutant T2 (*e.g.* 0-50 fmol) mixed with large excess of the wild-type T1 (fixed at 500 fmol) were detected using the biotin probe P2. 30 thermal cycles with each cycle consisting of a 2 min denaturation at 95 °C and 5 min annealing/ligation at 45 °C were implemented. The experimental procedures otherwise are the same as described in 5.3.2. The results are shown in Figure 5.8.

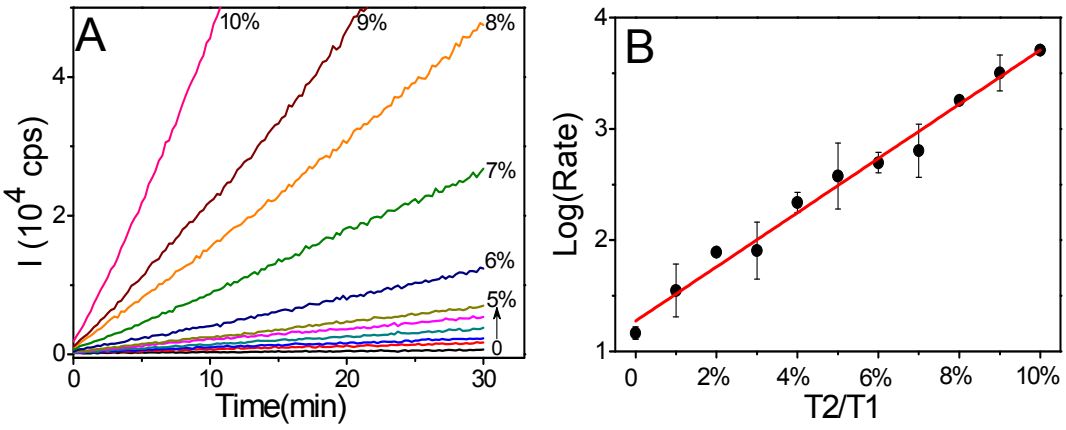

Figure 5.8 Quantification of the DNA target T2 (KRAS cancer mutant) in the presence of a large excess the wild type SNP target T1.

(A) Time-dependent fluorescence responses of samples with different ratios of T2 to T1, with fixed amount of T1 (500 fmol). **(B)** Relationship between the logarithmic rate of increase of fluorescence increase rate and the allele frequency, the data were fitted to a linear function (R^2 = 0.98). (Reprinted by permission of the Royal Society Chemistry)[28]

Figure 5.8A revealed that the rate of fluorescence increase initially showed a gradual increase with the increasing T2/T1 (full-match /SNP) ratio over 0-5%.

As the T2/T1 ratio was further increased, the rate of fluorescence response was greatly enhanced: the signal for the 10% T2/T1 sample was a massive 345 fold higher than that for the 0% T2/T1 sample. Moreover, the log (fluorescence increase rate) was found to increase roughly linearly (R^2 = 0.98) with the increasing T2/T1 ratio (Figure 5.8B), where an allele frequency down to as low as 1% was clearly detectable. The estimated theoretical LOD of the allele frequency was 0.75% based on 3σ/slope.[48] Therefore, quantification of the low abundant KRAS 12 cancer specific SNP mutant (T2) can be realized in even > 100-fold excesses of the wild-type target T1. This result is comparable to or better than most other recently reported, sensitive SNP detection techniques (see Table 5.3 for details). Furthermore, the LOD for a low level SNP cancer mutant in a large excess of coexisting wild-type target here is also comparable to the high resolution melting or gene sequencing technique (LOD: 0.1 - 1%) developed in the Makrigiorgos group, one of the most sensitive SNP detection techniques.[51-52] Therefore, this approach appears to be well-placed for sensitive detection of rare point mutations associated with important human diseases (*e.g.* cancer, diabetes, and cardiovascular diseases) as well as studying the SNP-disease correlations.

5.7 Conclusions

In summary, this chapter has demonstrated a highly sensitive, specific DNA detection approach which combines TRL, strand displacement, MNP mediated target capture/separation, efficient enzymatic signal amplification, and the high efficiency and SNP discrimination ability of the Taq DNA ligase. This approach can quantitate amol levels of unlabelled target DNA with excellent discrimination ratio, up to 121 fold before background correction (increasing to >380 fold after background correction), between the full-match and SNP target. It can quantitate trace amounts of single point cancer mutants in large excesses of

wild-type targets with an LOD down to 0.75%. This assay can also mimic DNA melting behaviours, making SNP detection highly reliable. Moreover, it is also general, and can be readily extended to other DNA targets of interest by simply changing the biotin-probes used (*e.g.* P1 for T1, P2 for T2; P3 for T3; P4 for T4 here) and/or other nanoparticle systems.

5.8 References

1. J. G. Hacia, L. C. Brody, M. S. Chee, S. P. A. Fodor and F. S. Collins, *Nat. Genet.*, 1996, **14**, 441-447.
2. F. S. Santiago, A. V. Todd, N. J. Hawkins and R. L. Ward, *Mol. Cell. Probes*, 1997, **11**, 33-38.
3. M. K. Halushka, J. B. Fan, K. Bentley, L. Hsie, N. Shen, A. Weder, R. Cooper, R. Lipshutz and A. Chakravarti, *Nat. Genet.*, 1999, **22**, 239-247.
4. X. Duan, Z. Li, F. He and S. Wang, *J. Am. Chem. Soc.*, 2007, **129**, 4154-4155.
5. G. H. Reed, J. O. Kent and C. T. Wittwer, *Pharmacogenomics*, 2007, **8**, 597-608.
6. J. T. Ney, S. Froehner, A. Roesler, R. Buettner and S. Merkelbach-Bruse, *Archives of Pathology & Laboratory Medicine*, 2012, **136**, 983-992.
7. U. Malapelle, C. Carlomagno, M. Salatiello, A. De Stefano, C. De Luca, R. Bianco, R. Marciano, C. Cimminiello, C. Bellevicine and S. De Placido, *Br. J. Cancer*, 2012, **107**, 626-631.
8. C. J. Wienken, P. Baaske, S. Duhr and D. Braun, *Nucleic Acids Res.*, 2011, **39**, e52-e52.
9. S. Sorgenfrei, C. Chiu, R. L. Gonzalez Jr, Y. J. Yu, P. Kim, C. Nuckolls and K. L. Shepard, *Nat. Nanotechnol.*, 2011, **6**, 126-132.
10. I. I. Cisse, H. Kim and T. Ha, *Nat. Struct. Mol. Biol.*, 2012, **19**, 623-627.
11. S. Song, Z. Liang, J. Zhang, L. Wang, G. Li and C. Fan, *Angew. Chem. Int. Ed.*, 2009, **48**, 8670-8674.

12. M. You, Y. Chen, L. Peng, D. Han, B. Yin, B. Ye and W. Tan, *Chemical Science*, 2011, **2**, 1003-1010.

13. Y. Song, W. Zhang, Y. An, L. Cui, C. Yu, Z. Zhu and C. J. Yang, *Chem. Commun.*, 2012, **48**, 576-578.

14. J. Huang, Y. Wu, Y. Chen, Z. Zhu, X. Yang, C. J. Yang, K. Wang and W. Tan, *Angew. Chem. Int. Ed.*, 2011, **50**, 401-404.

15. D. Graham, B. J. Mallinder, D. Whitcombe, N. D. Watson and W. E. Smith, *Anal. Chem.*, 2002, **74**, 1069-1074.

16. F. Patolsky, A. Lichtenstein and I. Willner, *Nat. Biotechnol.*, 2001, **19**, 253-257.

17. W. Xu, X. Xue, T. Li, H. Zeng and X. Liu, *Angew. Chem. Int. Ed.*, 2009, **48**, 6849-6852.

18. X. Xiao, C. Zhang, X. Su, C. Song and M. Zhao, *Chem. Sci.*, 2012, **3**, 2257-2261.

19. X. Duan, L. Liu, F. Feng and S. Wang, *Acc. Chem. Res.*, 2009, **43**, 260-270.

20. J. Kim and M. Mrksich, *Nucleic Acids Res.*, 2010, **38**, e2-e2.

21. F. Barany, *Proc. Natl. Acad. Sci.*, 1991, **88**, 189-193.

22. Y. Cheng, Q. Du, L. Wang, H. Jia and Z. Li, *Anal. Chem.*, 2012, **84**, 3739-3744.

23. W. Shen, H. Deng and Z. Gao, *J. Am. Chem. Soc.*, 2012, **134**, 14678-14681.

24. J. Li and W. Zhong, *Anal. Chem.*, 2007, **79**, 9030-9038.

25. S. Bi, L. Li and S. Zhang, *Anal. Chem.*, 2010, **82**, 9447-9454.

26. H. Dong, C. Wang, Y. Xiong, H. Lu, H. Ju and X. Zhang, *Biosens. Bioelectron.*, 2013, **41**, 348-353.

27. C. Shi, Y. Ge, H. Gu and C. Ma, *Biosens. Bioelectron.*, 2011, **26**, 4697-4701.

28. Y. Zhang, Y. Guo, P. Quirke and D. Zhou, *Nanoscale*, 2013, **5**, 5027-5035.

29. J. Garcia, Y. Zhang, H. Taylor, O. Cespedes, M. E. Webb and D. Zhou, *Nanoscale*, 2011, **3**, 3721-3730.

30. Zhou, A. Bruckbauer, Ying, C. Abell and D. Klenerman, *Nano Lett.*, 2003, **3**, 1517-1520.

31. S. Rauf, D. Zhou, C. Abell, D. Klenerman and D. J. Kang, *Chem. Commun.*, 2006, 1721-1723.

32. C. J. Pachuk, M. Samuel, J. A. Zurawski, L. Snyder, P. Phillips and C. Satishchandran, *Gene*, 2000, **243**, 19-25.

33. X. Xue, W. Xu, F. Wang and X. Liu, *J. Am. Chem. Soc.*, 2009, **131**, 11668-11669.

34. F. Patolsky, Y. Weizmann, E. Katz and I. Willner, *Angew. Chem. Int. Ed.*, 2003, **42**, 2372-2376.

35. X. Chen, A. Ying and Z. Gao, *Biosens. Bioelectron.*, 2012, **36**, 89-94.

36. Y. Zhang and D. Zhou, *Expert Rev. Mol. Diagn.*, 2012, **12**, 565-571.

37. D. Y. Zhang and G. Seelig, *Nature chem.*, 2011, **3**, 103-113.

38. J. Bath and A. J. Turberfield, *Nat. Nanotechnol.*, 2007, **2**, 275-284.

39. G. Seelig, D. Soloveichik, D. Y. Zhang and E. Winfree, *Science*, 2006, **314**, 1585-1588.

40. R. M. Dirks and N. A. Pierce, *Proc. Natl. Acad. Sci. USA*, 2004, **101**, 15275.

41. Y. He and D. R. Liu, *J. Am. Chem. Soc.*, 2011, **133**, 9972-9975.

42. H. Q. Wang, W. Y. Liu, Z. Wu, L. J. Tang, X. M. Xu, R. Q. Yu and J. H. Jiang, *Anal. Chem.*, 2011, **83**, 1883-1889.

43. A. X. Zheng, J. Li, J. R. Wang, X. R. Song, G. N. Chen and H. H. Yang, *Chem. Commun.*, 2012, **48**, 3112-3114.

44. D. Wang, W. Tang, X. Wu, X. Wang, G. Chen, Q. Chen, N. Li and F. Liu, *Anal. Chem.*, 2012, **84**, 7008-7014.

45. D. Y. Zhang, S. X. Chen and P. Yin, *Nature chem.*, 2012, **4**, 208-214.

46. A. K. Lytton-Jean and C. A. Mirkin, *J. Am. Chem. Soc.*, 2005, **127**, 12754-12755.

47. N. L. Rosi, D. A. Giljohann, C. S. Thaxton, A. K. Lytton-Jean, M. S. Han and C. A. Mirkin, *Science*, 2006, **312**, 1027-1030.

48. Y. Xiang and Y. Lu, *Anal. Chem.*, 2012, **84**, 1975-1980.

49. J. L. Mergny and L. Lacroix, *Oligonucleotides*, 2003, **13**, 515-537.

50. Y. Zu, A. L. Ting and Z. Gao, *Small*, 2011, **7**, 306-310.

51. J. Li, L. Wang, H. Mamon, M. H. Kulke, R. Berbeco and G. M. Makrigiorgos, *Nat. Med.*, 2008, **14**, 579-584.

52. C. A. Milbury, J. Li and G. M. Makrigiorgos, *Clin. Chem.*, 2009, **55**, 2130-2143.

Chapter 6
Overall conclusions and future directions

6.1 overall conclusions and future directions

This thesis includes two parts: Part I is based on the FRET studies between small-molecule ligands capped QD and his-tag appended FPs; Part II is the development of a sensitive and selective DNA sensing platform by combining magnetic capture/separation and enzymatic signal amplifcation.

The FRET between a CdSe/ZnS core/shell QD capped with three different small-molecule ligands (MPA, GSH, DHLA) and a His_6-tagged FP (mCherry) has been studied. The Förster radius (R_0) and corresponding donor-acceptor distances (r) for each of the QD-FP FRET systems were evaluated by using the Förster dipole-dipole interaction formula. Interestingly, both the FRET efficiency (E) and r were found to be strongly dependent on the capping small-molecule ligands on the QD surface. Two kinds of molecular models were proposed to explain the possible reasons behind these observations. The dissociation constants (K_ds) and kinetics of the self-assembled QD-FP systems were also evaluated. Results demonstrate that the QD-FP self-assembly interaction is fast and strong, which can complete in minutes at low nM concentration, suggesting that the QD-His_6-tagged biomolecule self-assembly is an effective strategy for prepare compact QD-bioconjugates which may have a wide range of sensing and biomedical applications.

The QD-His-tag self-assembly process can be extended to other systems for biosensing, imaging *etc*. Future efforts could focus on the investigation of the affinities between proteins and their specific recognizing molecules such as sugars, aptamers, and antigens based on FRET studies at SM levels. Moreover, the development of biosensors (DNA sensors, aptasensors, and antigen sensors) for ultrasensitive and specific disease diagnostics based on single molecule fluorescence is also a promising topic, because SM fluorescence possesses unique capabilities of detecting static conformational heterogeneity and dynamic conformational changes of single biological molecules that are not detectable at the bulk level both in solution and immobilized to surfaces.[1-3]

Moreover, a facile, rapid, and sensitive DNA sensor has been developed by combining the efficient MNP-based target capture and magnetic separation together with the highly efficient signal amplification power of enzymes to achieve ultra-sensitivity. This sensor shows similar sensing ability in both pure buffer and complex media (such as 10% human serum in buffer) and demonstrates excellent linear correlations between signals and target concentrations. Moreover, this developed strategy is able to quantitate two distinct DNA strands in a homogenous phase simultaneously with a detection limit of ~5 pM. Therefore, the MNP-enzyme sandwich sensor is anticipated to have excellent potential for a wide range of DNA based multiplexed biosensing and diagnostic applications.

In future work, the sensing platform developed here will be extended to detect low-abundant disease biomarkers (such as specific cells, small molecules, enzymes, antigens or hormones) using specific nucleic acid aptamers. [4-5] Moreover, the use of sensitive DNA amplification strategies (*e.g.* nanoparticle barcode assay[6], RCA[7]) could be introduced for greater sensitivities. The advantages of using nucleic acid aptamers such as high chemical/thermal

stability, cheap production *via* completely *in vitro* processes without using animals, no batch-to-batch variation, and ease of site-specific incorporation of bespoke labels and functional groups, make the MP-aptamer biosensors extremely attractive and powerful in broad biosensing and biodiagnostic applications.

In addition, a novel, highly sensitive and selective approach for label-free DNA detection and SNP discrimination has been developed by combining TRL, MNP assisted target capture/ separation, and efficient enzymatic amplification.

This approach shows a detection limit of 600 fM for unlabelled single-stranded DNA targets detection. The SNP discrimination ratio between a perfect-match cancer specific mutant and its single-base mismatch (wild-type) DNA target achieved by this approach (up to 380 fold with background correction) is among the highest reported in the literature. In addition, this assay consistently yields a high signal to background (S/B) ratio of >100, which can effectively eliminate the need for background correction and is advantageous for accurate target quantitation. More importantly, it can quantitate a rare cancer mutant (KRAS codon 12) in large excess of coexisting wild-type DNAs down to 0.75%. This sensor offers one of the best SNP discrimination and S/B ratios among recently reported sensitive DNA sensors. As a result, this sensor appears to be well-suited for sensitive SNP detection and a wide range of DNA mutation based diagnostic applications.

Although this assay has demonstrated excellent sensitivities in detecting cancer specific SNPs (KRAS codon12/13) against the wild type non-cancerous target that makes it highly useful for early cancer diagnosis, it still remains at the proof-of-principle stage where all the experiments were carried out using synthetic DNAs rather than the clinical targets. Moreover, its absolute sensitivity

still remains at sub-pM level, and therefore a PCR amplification may still be needed for clinical application. Therefore, further efforts should focus on developing more specific, effective signal amplification strategies (for instance, by introducing LCR[8-9] or RCA[10-11]) to further improve the assay sensitivity and extending its application to real clinical samples without PCR pre-amplification.

6.2 References

1. X. S. Xie and J. K. Trautman, *Annu. Rev. Phys. Chem.*, 1998, **49**, 441-480.
2. S. Weiss, *Science*, 1999, **283**, 1676-1683.
3. T. Ha, I. Rasnik, W. Cheng, H. P. Babcock, G. H. Gauss, T. M. Lohman and S. Chu, *Nature*, 2002, **419**, 638-641.
4. C.-H. Leung, D. S.-H. Chan, H.-Z. He, Z. Cheng, H. Yang and D.-L. Ma, *Nucleic Acids Res.*, 2012, **40**, 941-955.
5. Y. Xiang and Y. Lu, *Nat Chem*, 2011, **3**, 697-703.
6. N. L. Rosi and C. A. Mirkin, *Chem. Rev.*, 2005, **105**, 1547-1562.
7. C. Ma, W. Wang, Q. Yang, C. Shi and L. Cao, *Biosens. Bioelectron.*, 2011, **26**, 3309-3312.
8. Y. Cheng, Q. Du, L. Wang, H. Jia and Z. Li, *Anal. Chem.*, 2012, **84**, 3739-3744.
9. W. Shen, H. Deng and Z. Gao, *J. Am. Chem. Soc.*, 2012, **134**, 14678-14681.
10. J. Li and W. Zhong, *Anal. Chem.*, 2007, **79**, 9030-9038.
11. S. Bi, L. Li and S. Zhang, *Anal. Chem.*, 2010, **82**, 9447-9454.